UNIVERSITAT
POLITÈCNICA
DE VALÈNCIA

Acoustic System Development for Neutrino Underwater Detectors

María Saldaña Coscollar

Tesis Doctoral

Director: Miquel Ardid Ramírez
Co-director: Juan A. Martínez Mora

Junio 2017

Contents

Resumen

El objetivo principal de esta investigación es el diseño y desarrollo de dos tipos de emisores acústicos diferentes para ser utilizados en el telescopio submarino de neutrinos KM3NeT, en concreto, uno como emisor en el sistema de posicionamiento acústico (APS) y otro para la calibración de la detección acústica de neutrinos. El proyecto KM3NeT es un telescopio óptico de neutrinos, que actualmente está en fase de construcción, y está ubicado en las profundidades del mar. Los objetivos principales del telescopio son el descubrimiento y la observación de las fuentes que originan los neutrinos de alta energía en el universo y la determinación de la jerarquía de masas de los neutrinos. Los detectores de KM3NeT consisten en conjuntos tridimensionales de módulos de sensores de luz distribuidos en grandes volúmenes de agua en las profundidades del mar Mediterráneo. Los módulos de sensores ópticos registran el tiempo de llegada de la luz y el brillo de la luz para reconstruir la dirección y la energía del neutrino. Con objeto de lograr una implementación correcta de las estructuras mecánicas y una reconstrucción precisa de los eventos del neutrino, el telescopio incluye el APS como subsistema necesario para proporcionar la posición exacta de las estructuras mecánicas en tiempo real. Además, el APS puede ser una herramienta excelente para estudiar la viabilidad de un detector de neutrinos acústico y de una posible correlación entre la señal acústica y óptica. El nuevo detector KM3NeT es una oportunidad para continuar con el estudio de detección acústica de neutrinos. La detección acústica permitiría la combinación de las dos técnicas de detección de neutrinos para un telescopio submarino de neutrinos híbrido, y más aún, teniendo en cuenta que el telescopio óptico necesita de sensores acústicos para monitorizar la posición de los sensores.

En esta tesis, por un lado, se ha desarrollado un emisor acústico (AB) como parte del APS de KM3NeT. Previamente, se desarrolló el primer prototipo del emisor acústico, el cual se instaló en anteriores telescopios de neutrinos, concretamente en ANTARES y NEMO, con el fin de comprobar su funcionamiento in situ. Como parte de la tesis, se realizaron los análisis de las pruebas in situ y los resultados obtenidos mostraron que cumplía los requisitos del sistema de posicionamiento, únicamente se necesitaron algunas mejoras para la versión final. La versión final del AB está compuesta por un transductor piezo-cerámico y una placa electrónica integrado en una sola pieza en un recipiente cilíndrico de aluminio anodizado. El diseño y el trabajo realizado para una calibración precisa de laboratorio se llevó a cabo, logrando resultados óptimos en todos los aspectos requeridos. El nivel de presión sonora (SPL) obtenido con el AB final varía entre 174 dB y 194 dB re 1 µPa@1m en el rango frecuencial de 20 kHz a 50 kHz, respectivamente. El sistema final es capaz de emitir señales acústicas de alta intensidad en una gama de frecuencia amplia y de soportar condiciones de alta presión en el agua. Un total de dieciocho unidades del AB fueron satisfactoriamente

producidas en colaboración con MSM SLL, y fueron entregadas a KM3NeT. A finales de 2015, dos unidades del AB se integraron en el detector ARCA en la primera campaña marina. Los emisores se probaron in situ a principios de 2016 y los datos grabados se analizaron para extraer algunas conclusiones de la funcionalidad del APS. Además, se realizó un estudio a través de simulaciones, con objeto de seleccionar las posiciones óptimas para la integración de los ABs en el APS de los detectores ARCA y ORCA. La configuración óptima de las posiciones de los ABs fue seleccionada en base a conseguir la distribución más equitativa de la presión acústica en el campo de los detectores.

El segundo trabajo principal desarrollado en esta tesis consistió en el diseño de un array paramétrico de transductores capaz de imitar la señal acústica generada por la interacción del neutrino de ultra-alta energía (UHE) en el agua. La primera parte de su diseño se centró en el desarrollo de un transductor individual capaz de emitir paramétricamente la señal acústica del neutrino. El transductor completo se constituyó por una cerámica piezoeléctrica cilíndrica con un material en el interior del cilindro, llamado backing, y una capa de adaptación exterior que la recubre, llamada heading o matching layer, estas produjeron un incremento en la sensibilidad de emisión en comparación con lo obtenido únicamente con la cerámica. La generación paramétrica de la señal del pulso bipolar del neutrino se validó satisfactoriamente con el transductor individual. Posteriormente, se realizó el diseño del array completo compuesto por varias unidades del transductor diseñado, con el objeto de lograr un pulso bipolar más enérgico y directivo. Se eligió una solución flexible para la su mecánica con la que poder cambiar la distancia entre emisores y comprobar diferentes configuraciones del mismo y así optimizarlo según lo obtenido experimentalmente. Por último, el array calibrador se caracterizó para una de las configuraciones óptimas obtenidas en la simulación, basada en tres emisores separados 14 cm entre sí. La caracterización se realizó tanto para el haz primario (lineal) como para el haz secundario (paramétrico). Debido a las cortas distancias de la piscina aún se observó el efecto de la interferencia de la emisión de cada transductor del array, pero mediante la comparación de las medidas experimentales con las simulaciones se pudo concluir que el array es capaz de reproducir la señal acústica del neutrino utilizando la técnica paramétrica. Se obtuvó una directividad similar para el haz primario y el secundario, demostrando que se consiguió el objetivo de alcanzar una directividad final de unos pocos grados con la señal de pulso bipolar.

Resum

L'objectiu principal d'esta investigació és el disseny i desenvolupament de dos tipus d'emissors acústics diferents per a ser utilitzats en el telescopi submarí de neutrins KM3NET, en concret, ú com emissor en el sistema de posicionament acústic (APS) i altre per a la calibració de la detecció acústica de neutrins. El projecte KM3NET és un telescopi òptic de neutrins, que actualment està en fase de construcció, i està ubicat en les profunditats del mar. Els objectius principals del telescopi són el descobriment i l'observació de les fonts que originen els neutrins d'alta energia en l'univers i la determinació de la jerarquia de masses dels neutrins. Els detectors de KM3NET consisteixen en conjunts tridimensionals de mòduls de sensors de llum distribuïts en gran volums d'aigua en el Mediterrani. Els mòduls de sensors òptics registren el temps d'aplegada de la llum i la intensitat de la llum per a reconstruir la direcció i l'energia del neutrí. Com objectiu d'aconseguir una implementació correcta de les estructures mecàniques i una reconstrucció precisa dels events del neutrí, el telescopi inclou l'APS com subsistema necessari per a proporcionar la posició exacta de les estructures mecàniques en temps real. A mes, l'APS pot ser una ferramenta excel·lent per a estudiar la viabilitat d'un detector de neutrins acústic i d'una possible correlació entre el senyal acústic i òptic. El nou detector KM3NET és una oportunitat per a continuar en l'estudi de detecció acústica del neutrí. La detecció acústica permetria la combinació de les dos tècniques de detecció de neutrins per a un telescopi submarí de neutrins híbrid, i més encara, tenint en compte que el telescopi òptic necessita de sensors acústics per a monitoritzar la posició dels sensors.

En aquesta tesis, per un costat, s'ha dissenyat un emissor acústic (AB) com part de l'APS de KM3NET. Prèviament, se desenvolupà el primer prototip de l'emissor acústic, el qual s'instal·là en anteriors telescopis de neutrins, concretament en ANTARES i NEMO, amb el fi de comprovar-se el seu funcionament *in situ*. Com part de la tesis, es realitzaren els anàlisis de les proves *in situ* i els resultats obtinguts mostraren que complia els requisits del sistema de posicionament, únicament necessitant-se d'algunes millores per a la versió final. La versió final de l'AB està composta per un transductor piezo-ceràmic i una placa electrònica integrats en una sola peça en un recipient cilíndric d'alumini anoditzat. El disseny i el treball realitzat per a una calibració precisa de laboratori es va dur a terme, aconseguint resultats òptims en tots els aspectes requerits. El nivell de pressió sonora obtingut en l'AB final varia entre 174 dB i 194 dB re 1 µPa@1m en el rang freqüencial de 20 kHz a 50 kHz, respectivament. El sistema final es capaç d'emetre senyals acústics d'alta intensitat en una gama ampla de freqüència i de suportar condicions d'alta pressió en l'aigua. Un total de díhuit unitats de l'AB foren satisfactòriament produïdes en col·laboració amb MSM SLL, i foren entregades a KM3NET. A finals de 2015, dos unitats de l'AB s'integraren en el detector ARCA en la primera campanya marina. Els emissors es provaren *in situ* a principis de 2016 i els senyals enregistrats s'analitzaren per a extraure algunes conclusions de la funcionalitat de l'APS. A més, es realitzà un estudi

a través de simulacions, amb l’ objectiu de seleccionar les posicions òptimes per a la integració dels ABs en l'APS dels detectors ARCA i ORCA. La configuració òptima de les posicions dels ABs fou seleccionada en base a aconseguir la distribució més equitativa de la pressió acústica en el camp dels detectors.

Com segon treball principal desenvolupat en esta tesis, s'ha dissenyat un array paramètric de transductors capaç d'imitar el senyal acústic generat per l'interacció del neutrí d'ultra-alta energia (UHE) en l'aigua. La primera part de disseny es centrà en el desenvolupament d'un transductor individual capaç d'emetre paramètricament el senyal acústic del neutrí. El transductor complet està constituït per una ceràmica piezoelèctrica cilíndrica amb un material en l'interior del cilindre, anomenat *backing,* i una capa d’adaptació exterior que la recobreix, anomenada *heading* o *matching layer*, estes produïren un increment en la sensibilitat d’emissió en comparació amb allò obtingut únicament amb la ceràmica. La generació paramètrica de la senyal del pols bipolar del neutrí es va validar satisfactòriament en el transductor individual. Posteriorment, es va realitzar el disseny de l'*array* complet compost per varies unitats del transductor dissenyat, amb l'objectiu d’aconseguir un pols bipolar més energètic i directiu. Es va triar una solució flexible per a la mecànica de l'*array,* en la que poder canviar la distancia entre emissors i comprovar diferents configuracions del mateix i així optimitzar-ho experimentalment. Per últim, l'*array* calibrador es va caracteritzar per a una de les configuracions òptimes obtingudes en la simulació, basada en tres emissors separats 14 cm entre sí. La caracterització es va realitzar tant per al feix primari (lineal) com per al feix secundari (paramètric). Degut a les curtes distàncies de la piscina encara s'observà l'efecte de la interferència de l’emissió de cada transductor de l'*array*, tanmateix mitjançant la comparació de les mesures experimentals amb les simulacions fou possible concloure que l'*array* es capaç de reproduir el senyal acústic del neutrí utilitzant la tècnica paramètrica, obtenint-se una directivitat similar per al feix primari i el secundari, i per tant, demostrant que l'objectiu de tindre una directivitat final d'uns pocs graus en el senyal de pols bipolar s’ha aconseguit.

Abstract

The main objective of this research is the design and development of two different underwater acoustic emitters aimed to the deep-sea KM3NeT neutrino telescope, more specifically for the Acoustic Positioning System (APS) and for the calibration of the acoustic neutrino detection technique. The KM3NeT project is a new optical-based deep-sea neutrino telescope, currently under construction. The main objectives of the KM3NeT telescope are the discovery and observation of high-energy neutrino sources in the Universe and the determination of the mass hierarchy of neutrinos. The KM3NeT detectors consist of three-dimensional arrays of light sensor modules distributed over large volumes of the transparent water in the deep Mediterranean Sea. The sensor modules register the time of arrival of the light and the brightness of the light to reconstruct the direction and energy of the neutrino. In order to achieve an accurate deployment of the mechanical structures and a precise reconstruction of neutrino induced events, the telescope includes an APS as mandatory sub-system that provides an accurate position of the mechanical structures in real time. Additionally, the APS could also be an excellent tool to study the feasibility of an acoustic neutrino detector and a possible correlation between acoustic and optical signals. The new detector KM3NeT is an excellent opportunity to continue with the study of the acoustic neutrino detection. The acoustic detection would allow the combination of the two neutrino detection techniques for a hybrid underwater neutrino telescope, especially considering that the optical based telescope needs acoustic sensors to monitor the position of the sensors.

An Acoustic Beacon (AB) as part of the APS of KM3NeT has been developed in this thesis. Previously, the first emitter prototype was developed and it was installed in previous neutrino telescopes, such as ANTARES and NEMO, in order to be tested in situ. The analyses of the in situ test with the prototypes were performed as part of this thesis. The results obtained from the tests showed that the requirements for the positioning system are accomplished, just needing few improvements for the final version. The final version of the AB is composed by a piezo-ceramic transducer and an electronic board integrated in a single piece in a cylindrical hard-anodized aluminium vessel. The design and the work done for a precise laboratory test was performed achieving optimal results in all aspects. The sound pressure level obtained with the final AB varies from 174 dB to194 dB re 1 µPa@1m in the 20 kHz to 50 kHz frequency range, respectively. The final system was able to emit very intense acoustic signals in a broad frequency range and support high pressure conditions in water. In cooperation with MSM SLL, a total of eighteen AB units were satisfactorily developed and delivered to KM3NeT. By the end of 2015, two units of the AB were integrated at ARCA detector through the first sea campaign. They were tested *in situ* in the beginning of 2016 and the recorded data was analysed in order to extract some conclusions of the APS functionality. In addition, the selection of the optimal

positions for integrating the ABs in the APS of both ARCA and ORCA detectors was performed through simulations. The position configuration was chosen according to the most equitable distribution of the sound pressure in the field of the detectors.

As second main work performed in this thesis, a parametric transducer array able to mimic the acoustic signal generated by Ultra-High Energy (UHE) neutrino interaction in water was designed and developed. The first part was designing a single transducer able to emit parametrically the acoustic neutrino signal. The single transducer was constituted by a cylindrical piezo-ceramic designed with a backing and heading material that increased the emission sensitivity in comparison with the bare ceramic. The parametric generation of the neutrino bipolar pulse signal was satisfactorily validated for the single transducer. Afterwards, the design of the complete array system composed of few units was performed in order to achieve a more energetic and directional bipolar pulse. A flexible mechanical array solution was chosen which allowed to change the distance between emitters in order to test different interesting array configurations and being able to optimise it experimentally. Finally, the line-array calibrator was characterized for one of the optimal configurations obtained in simulation, the one based on three emitter transducers separated 14 cm. The characterization was performed for the primary beam (linear) and for the secondary beam (parametric). Although for the distances of the pool, the effect of the interference from the emission of each transducers of the array was still observed, by comparing with simulations of the measurements it was possible to conclude that the array is able to reproduce the acoustic neutrino-like signal using the parametric technique. A similar directionality was obtained for both primary and secondary beams, proving that the goal of having a final directionality of a few degrees for the bipolar pulse signal was reached.

Introduction

Over the last decades astrophysical neutrino detection has become of great interest in the observation and study of the Universe. The neutral electrical and low matter interaction properties of the neutrino particle makes it as an ideal messenger from Cosmos. Since neutrinos can reach the Earth from sources unperturbed by magnetic fields and almost without energy losses and absorption, they are an optimal probe to observe high energy astrophysical phenomena. Due to its properties, neutrinos bring a unique way to obtain certain astrophysical information and to understand some particle physics principles. For the neutrino detection, large scale instrumented detection volumes in dense media (water, ice) are used. In this media, when the neutrino interaction is produced, charged particles are produced generating Cherenkov light. This radiation is detected by an array of optical sensors that form the detector. Cherenkov neutrino detectors have been developed in both ice and water media to investigate more about the neutrino physics and the Universe.

Currently, a new optical-based deep-sea neutrino telescope is under construction, the KM3NeT telescope, which will have a volume of several cubic kilometres. The main objectives of the KM3NeT Collaboration are the discovery and observation of high-energy neutrino sources in the Universe and the determination of the mass hierarchy of neutrinos. The KM3NeT detectors consists of three-dimensional arrays of light sensor modules distributed over large volumes of the transparent water in the deep Mediterranean Sea. The sensor modules register the time of arrival of the light and the brightness of the light to reconstruct the direction and energy of the neutrino. The KM3NeT neutrino research infrastructure will comprise two types of neutrino detectors: the detectors of the ARCA (KM3NeT-It) telescope, in the Italian site, that will be optimised to register the highest energy neutrinos, while the geometry of the ORCA detector (KM3NeT-Fr), in France site, is optimal for the registration of lower energy neutrinos, necessary for the determination of the neutrino mass hierarchy.

In parallel to the optical system the Acoustic Positioning System (APS) is a mandatory sub-system of KM3NeT that must provide the position of the telescope's mechanical structures in a geo-referenced coordinate system. The APS is important for a safe and accurate deployment of the mechanical structures and, for precise reconstruction of neutrino induced events. In addition to these functionalities referred to the detector positioning, the APS could also be an excellent tool to study the feasibility of an acoustic neutrino detector and observe a possible correlation between acoustic and optical signals. Previous work has been done in acoustic neutrino detection but this detection technique is still under study. The new detector KM3NeT is an excellent opportunity to continue with the investigation. Measuring acoustic pressure pulses in underwater acoustic arrays is a promising approach for the detection of cosmic neutrinos with energies exceeding 100 PeV. Acoustic detection of Ultra-High Energy (UHE) neutrinos is based on the thermo-acoustic effect. Basically, when a UHE neutrino interacts with a nucleus in water, its energy is released in a volume of about a centimetre in radius and several meters in length. This phenomenon induces a local heating in a very short period of time leading to a short pressure pulse signal with bipolar shape in time and a very directional pattern (pancake-like), being emitted mainly in the perpendicular plane of the shower axis. The acoustic detection would allow the combination of those two neutrino detection techniques for a hybrid underwater neutrino telescope, especially considering that the optical neutrino detection technique needs acoustic sensors to monitor the position of the optical sensors.

The framework of the thesis is the KM3NeT experiment, focused on the acoustics aspects of the telescope, which are the APS and the acoustic neutrino detection. The work performed in the thesis is mainly centred on the design, development and characterization of the Acoustic Beacon (AB) for the APS and on the design and development of a transducer array able to calibrate the acoustic neutrino detection technique. The progress of the thesis involved the development and application of innovative techniques on data processing analysis, simulation, instrumentation, measuring strategies and design. Chapter 1 explains the fundamentals of the thesis, they help to contextualize, hence to understand the thesis progress and its contents. The principal concepts of underwater acoustics are introduced; the acoustic wave propagation, transducing, parametric generation and acoustic positioning. The acoustics associated to neutrino astronomy detection in underwater environments are introduced. Firstly, the characteristics of the neutrino particle are introduced and its detection principles. Next, the principal neutrino telescopes are presented, in particular, the KM3NeT as outline of the thesis. The importance of the APS in the telescope is stated and its particularities are detailed. Then, the acoustic neutrino detection is presented as other effective way of studying the neutrino interaction. The previous work done in acoustic neutrino detection is introduced and the next possibilities of studying and testing this technique are exposed. The new detector KM3NeT could be an excellent opportunity to continue with this investigation.

It is noteworthy that the thesis work has been developed within the framework of two international collaborations: ANTARES and KM3NeT, with the support of European and National funds. This has allowed, besides the training and research in the areas and techniques described in the thesis, acquiring transversals abilities, knowledge and skills: teamwork, international stays, English communication skills, astroparticles knowledge, software techniques, data analysis, instrumentation etc.

An important objective of the thesis is centred on the developing of the ABs (emitters) as part of the KM3NeT APS, which is described in Chapter 2. Firstly, the previous work performed on developing the first emitter prototype is introduced. This prototype was installed in previous neutrino telescopes, such as ANTARES and NEMO, in order to be tested in situ. The analyses and results obtained from the tests showed that it accomplished the requirements for the positioning system, just needing few improvements for the final version. The final version of the AB is composed by a piezo-ceramic transducer and an electronic board integrated in one single piece in a cylindrical hard-anodized aluminium vessel. The design and the work done for a precise laboratory test are detailed in this chapter. The AB showed optimal results in all aspects; acoustics, electronics, mechanics and functionality. The final system was able to emit very intense signals in a broad frequency range and support high pressure conditions in water. In cooperation with MSM SLL, a total of eighteen AB units were satisfactorily developed and provided to the KM3NeT project in 2015. By the end of 2015, two units of the AB were integrated at ARCA detector through the first sea campaign. They were tested *in situ* in the beginning of 2016 and the recorded data was analysed in order to extract some conclusions of the APS functionality. The integration and *in situ* tests result are presented. In addition, the selection of the optimal positions for integrating the AB in the APS of both ARCA and ORCA detectors was performed through simulation. The position configuration was chosen according to the most equitable distribution of the sound pressure along the field of the detectors. This study is described at the end of Chapter 2.

The second main objective of the thesis is focused on the development of a parametric array transducer able to mimic the acoustic signal generated by UHE neutrinos on its interaction in water, this work is shown in Chapter 3. The acoustic neutrino detection could be implemented in the new optical neutrino telescope KM3NeT. In order to study the viability of the acoustic detection, it was decided to work on the design of an acoustic array calibrator able to imitate the bipolar pulse signal as part of this thesis. The acoustic neutrino signal presents the peculiarity of having a cylindrical symmetry with tight directionality, short and low frequency components in the tens of kHz range. The generation of the signal was performed by using parametric generation, which allows to generate low frequency signals with similar directivities to the emitted signal at high frequency, which is easier to get directional beams. In a first stage, a single transducer able to emit parametrically the acoustic neutrino signal was designed validating the parametric generation of the neutrino bipolar pulse signal. After the design of the single transducer, the design of the complete array system composed of few units was performed in order to achieve a more energetic and directional bipolar pulse. This is obtained by the interaction, at long distances, of the parametric beam generated for each array element. The array design involved the use of simulation methods which helped to select an appropriate array configuration. Afterwards, a mechanical array solution with a flexible design was created, in order to find the best configuration following the experimental results. Finally, with the complete array finished, the characterization was performed for the primary beam (linear range) and for the secondary beam (parametric range). The results showed that the array is able to reproduce the acoustic neutrino-like signal using the parametric technique, showing favourable results. All the steps performed on the array design and the results obtained in the characterization are detailed in Chapter 3. The last chapter of the thesis summarises the main results and conclusions.

1 Acoustics in Underwater Neutrino Telescopes

This chapter introduces the acoustics associated to neutrino particle detection in underwater environments. Firstly, an introduction of the neutrino particle characteristics and its detection is presented. The main projects involved on its detection and study are introduced. In particular, as outline of the thesis, the optical cubic kilometre neutrino telescope KM3NeT is described in more detail, emphasizing on its Acoustic Positioning System (APS). After acquiring significant experience with previous detectors, especially with ANTARES, the KM3NeT system is currently under deployment as a powerful and improved detector. It will be the biggest neutrino telescope in the northern hemisphere. The main objectives of the telescope, the infrastructures and present status are presented in this chapter. The importance of the APS in the telescope is stated. Before explaining the KM3NeT APS, the fundamentals of underwater acoustics are described, highlighting the parts involved on the thesis development. This part will help to contextualize the thesis contents. In succession, the APS methodology, its components, data acquisition system and data processing techniques are detailed, since an important part of the thesis development is done for the positioning system. On the other hand, the acoustic neutrino detection is presented as other effective way of studying the neutrino interaction. The acoustic neutrino effect in water and its detection procedure are explained. The previous work done in acoustic neutrino detection is introduced and the next possibilities of studying and testing this technique are exposed, showing that the new detector KM3NeT could be an excellent opportunity to continue with this investigation.

1.1 Introduction to Neutrino Telescopes

The observation of Universe had provided relevant information about the physical and chemical processes that occur at the energy sources of the Universe. During last decades, most of the information and knowledge of the Universe was deduced from the observation of photons and cosmic rays (Rossi 1964). However, some information that could be carried by photons does not reach the Earth since they interact with matter and are affected by background radiation. On the other hand, the observation of proton component of the cosmic rays can also provide valuable information about the energy sources, but due to its charge, some of them are affected by the galactic magnetic fields, therefore directional information can be lost. Due to these limitations, the search of other messengers that could be used for studying astrophysical sources, with neutral electrical properties and low matter interaction led to the neutrino particle, the only candidate known at this moment with these properties (Close 2010).

1.1.1 Neutrino Particle

Neutrinos are weakly-interacting elementary particles that have no electric charge and have an extremely small mass. These properties makes that the neutrino is not affected by the electromagnetic or strong nuclear forces, however it is affected by the weak nuclear and gravitational forces. Neutrinos are produced from high-energy collisions and they are able to pass through the ordinary matter almost without perturbation, since its interaction with the other particles is insignificant. For these reasons, the neutrinos particle can carry information from the high-energy processes of the Universe. Neutrinos belong to the lepton family of matter and are classified in three types related to the charge: the electron neutrino ν_e, muon neutrino ν_μ and tau neutrino $\nu_{\tau.}$ They are included in the Standard Model of particle physics (Fig. 1.1), which explain the elementary particles and the three fundamental forces involved (Ho-Kim & Pham 1998).

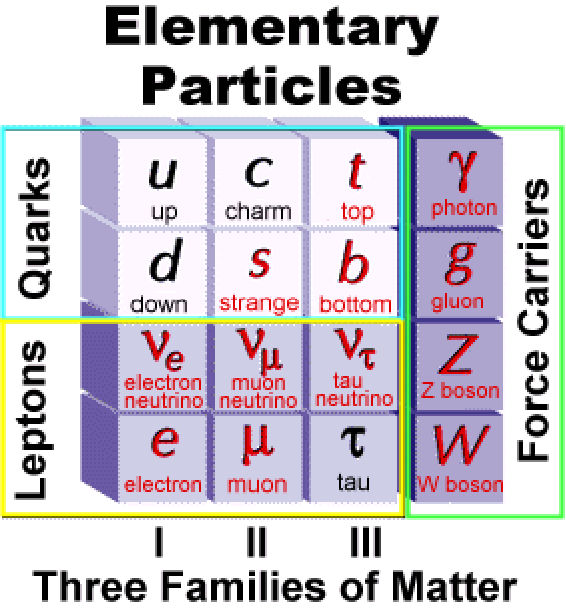

Fig.1.1. The particles in Standard Model (From SLAC National Accelerator Laboratory website).

1.1.2 Neutrino Detection and Neutrino Astronomy

Neutrino astronomy is a promising method to observe the Universe. The low interaction with matter of the neutrino makes it a complementary way to extract information from Cosmos (Ageron 2011). There are different techniques to detect high energy neutrinos, the Cherenkov light detection in large volumes of water or ice is the method most used for the energy range of interest from 10^{11} to 10^{16} eV. When neutrinos interact with atomic nuclei, it produces charged leptons which emit Cherenkov radiation in water and ice media. From the radiation pattern of the Cherenkov light it is possible to deduce direction, energy, and flavour information from the neutrino event.

A neutrino telescope is composed of an array of optical detectors with photomultiplier tubes (PMTs) hosted inside of pressure-resistant glass spheres called optical modules (OMs). The arrival times of the light detected by optical detectors is used to reconstruct the muon trajectory, and also that of the neutrino (Fig. 1.2). The accuracy of reconstruction of the muon track depends on knowing the position of the optical sensors at any moment. Since the detection lines move with sea current, a precise positioning system is used in order to achieve good angular resolution. The measurement of the amount of light detected help to estimate the neutrino energy and improve the quality of the muon track reconstruction.

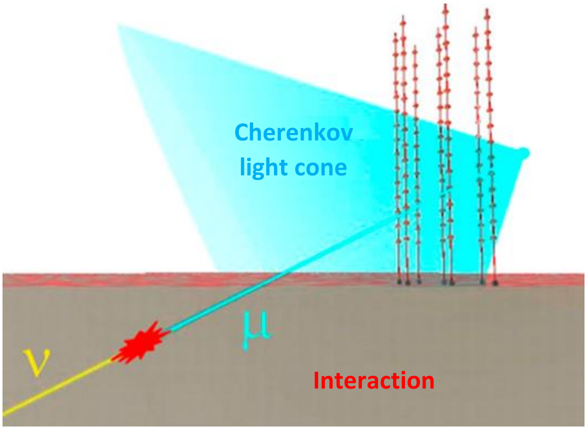

Fig. 1.2. Principle of detection of high energy muon neutrino in an underwater neutrino telescope.

In 1930 Wolfgang Pauli postulated a new particle, called neutrino, so to keep the energy-momentum conservation in beta decays of nuclei. The neutrino was firstly observed experimentally in 1956 (Reines & L.Cowan 1956) and in 1962 it was discovered that there were more types of neutrinos when the interactions of the muon neutrino were detected. Then DUMAND (Bosetti 1988) was the pioneering project for detecting neutrinos through the Cherenkov radiation method, however, then the technology was limited to achieve the issues of the detector and the project was not finished. In 1987 the Kamiokande detector observed neutrinos from Supernova

1987A. Later, the detection of the tau neutrino interaction was announced in 2000 by the DONUT Collaboration at Fermilab. On the other hand, the BAIKAL (Belolaptikov 1997) and AMANDA detector (Andrés 2001) were developed as detector systems in ice and water. Then, in 2002, after the completion of AMANDA, the collaboration started with the construction of a much larger detector, the IceCube telescope, located at the South Pole. Recently, IceCube discovered high-energy astrophysical neutrinos (Icecube Collaboration 2013). Besides IceCube, the existing neutrino telescopes are the NT200+ in Lake Baikal (Aynutdinov 2008), and deep sea neutrino telescope by ANTARES (Ageron 2011), NEMO (Sapienza 2006), NESTOR (NESTOR Collaboration 2006). Furthermore, a new optical-based deep-sea neutrino telescope is under construction, the KM3NeT telescope (Adrian-Martinez 2016), which will have a volume of several cubic kilometres.

1.1.3 ANTARES

The ANTARES (Astronomy with a Neutrino Telescope and Abyss environmental RESearch) Collaboration built and is operating a neutrino telescope in the deep Mediterranean Sea (in the coast of France) for detecting the Cherenkov light of muons coming from high-energy astrophysical neutrinos (Ageron 2011). It was completed in May 2008. It is the largest neutrino telescope in the Northern hemisphere and the first one in deep sea. The detector is composed of 12 vertical detection lines with 25 storeys, arranged at equal distances of 14.5 m along the line. The distance between lines is about 70 m. Each storey holds OMs and a container, called Local Control module that holds the electronics. An additional line, Instrumentation Line (IL), is equipped with instruments for monitoring the environment and for Earth-Sea science studies. The principal objective of ANTARES is the observation of astrophysical high-energy neutrinos in cosmic accelerators such as gamma ray bursts, active galactic nuclei, micro-quasars, supernova remnants. Other main goal is the indirect search for Dark Matter (DM) through neutrinos produced in annihilation or decays of DM particles accumulated either in the Sun, Galactic Centre or Earth.

Another detection technique is being tested in ANTARES in order to complement the optical detection. This is the acoustic detection of Ultra High Energy (UHE) neutrinos, based on the detection of the thermo-acoustic pulse produced after the UHE neutrino interaction (see section 1.4). For this purpose, the AMADEUS (ANTARES Modules for the Acoustic DEtection Under the Sea) system was installed in the general infrastructure to study the viability of the acoustic (Aguilar 2011). The AMADEUS system consists of 36 acoustic sensors in six storeys and includes time synchronization and a continuous monitoring.

1.1.4 NEMO

The NEMO (NEutrino Mediterranean Observatory) Collaboration was set up in 1998 with the objective to research and validate towards the future large neutrino telescope. The detection principle of NEMO is also based on the measurement of the Cherenkov light coming from the neutrino. The installation of the detector started at the end of 2006 so-called NEMO Phase I (Migneco 2006) and was successfully operated until May 2007 (Amore et al. 2009). In 2013, the NEMO Phase 2 tower (the prototype of the KM3NeT tower in Italy) was installed in the Capo Passero site and interesting results were obtained from data taking (Chiarusi et al. 2014), such as the optical rates. These features revealed the optimal nature of the Capo Passero abyssal site to host a km^3-sized Neutrino Telescope.

1.1.5 KM3NeT

KM3NeT is a new Cherenkov optical-based deep-sea neutrino telescope under construction in the Mediterranean Sea (Adrian-Martinez 2016) which will have some cubic kilometres of volume, an artistic view of the telescope is shown in Fig. 1.3. Two recent important discoveries, which are the high-energy astrophysical neutrino signal reported by IceCube (Aartsen et al. 2014) and the sizeable contribution of electron neutrinos to the third neutrino mass eigenstate as reported by Daya Bay, Reno and others (An 2012) (Seon-Hee 2014) influenced the main goals of KM3NeT Collaboration which are the observation of high-energy neutrino sources in the Universe and the determination of the mass hierarchy of neutrinos.

KM3NeT is now in the first phase of construction, namely KM3NeT Phase-I. By the end of 2015, the first sea campaign of KM3NeT-It was performed. Two Junction Boxes and the first Detection Unit (DU) were satisfactorily installed during the deployment and tested in the beginning of 2016. After the first phase of construction, the detector will consist of 24 Detection Units (DUs) deployed off-shore KM3NeT-IT and 7 DUs, deployed off-shore KM3NeT-FR. The infrastructure in Phase II, KM3NeT 2.0, will consist of three so-called building blocks and each building block comprises a 3-dimensional array of photo sensors A building block consist of 115 DUs, each DU, holds 18 Digital Optical Modules (DOMs) and each DOM hold 31 PMTs (Fig. 1.5).

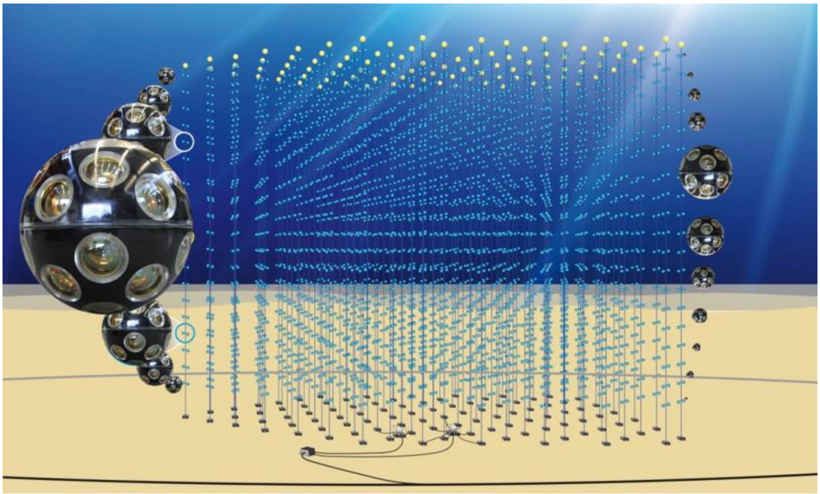

Fig. 1.3. Artistic view of the KM3NeT neutrino telescope array.

There are three off-shore deep-sea sites selected for the full KM3NeT project which are Toulon (France), Capo Passero (Sicily, Italy) and Pylos (Peloponnese, Greece). For KM3NeT Phase-2.0, three building blocks are planned to be developed: two KM3NeT-It/ARCA (Astroparticle Research with Cosmics in the Abyss) blocks will be installed at the Capo Passero site (Italy), with a large spacing between DOMs to target astrophysical neutrinos at TeV energies and above exploring the IceCube signal; and one KM3NeT-Fr/ORCA (Oscillation Research with Cosmics in the Abyss) block in a denser DOM configuration (see Fig. 1.4) will be installed at the Toulon site (France), to target atmospheric neutrinos in the few-GeV range and to precisely measure atmospheric neutrino oscillations and determine the mass hierarchy of neutrinos.

The deep-sea sites are linked to shore with a network of electro-optical cables for electrical power and high-bandwidth data communication. On site, shore stations are equipped to provide power, computing and a high-bandwidth internet connection to the data repositories.

The detection of neutrinos is based on the detection of Cherenkov light produced by relativistic particles emerging from a neutrino interaction. The PMTs and the readout electronics are hosted within pressure-resistant glass spheres, so called Digital Optical Modules (DOMs). The DOMs must be synchronized at the nanosecond level, while the position and orientation of the photo-sensors must be monitored to a few centimetres and few degrees precision, respectively. The DOMs are distributed along flexible strings, anchored to the sea floor and being held close to vertical by a submerged buoy. The concept of strings is modular by design. The construction and operation of the research infrastructure thus allows for a phased and distributed implementation. A collection of 115 strings forms a single KM3NeT building block.

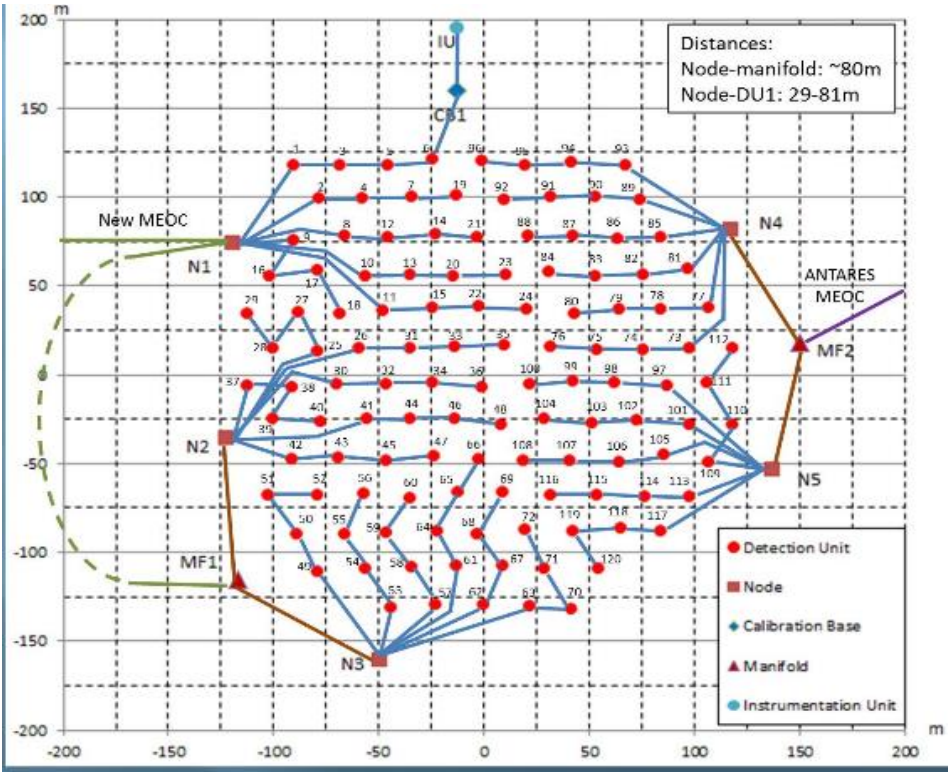

Fig. 1.4. Layout of the KM3NeT-ORCA array. Located on the Mediterranean Sea South from Toulon, France.

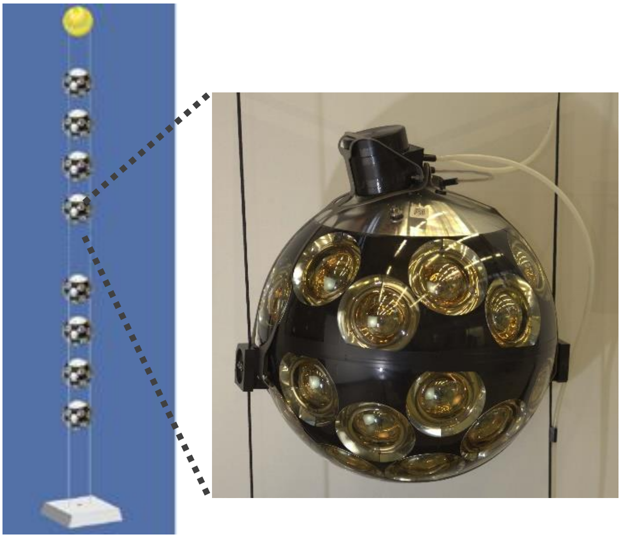

Fig. 1.5. KM3NeT Detection Unit and photograph of DOM

The design of the DOM has some advantages compared to the old-style optical modules that used single large PMT, the new design provides almost a uniform angular coverage. Moreover, more than one photon can be detected at the same arrival time at the DOM with good efficiency. On the other hand, the directional information improves the optical background rejection.

In parallel to the optical data, the data from the Acoustic Positioning System (APS) is processed and represents a data volume of about one third of that of the optical data. The APS is a mandatory sub-system of KM3NeT that must provide the position of the telescope's mechanical structures in a geo-referenced coordinate system. The APS is important for a safe and accurate deployment of the mechanical structures and, for the sake of science, for precise reconstruction of neutrino induced events. Since data are continuously transmitted to shore and distributed to the local data acquisition network at the shore station, acoustic data are also available for Earth and Sea science users. Section 1.3 describes the features of the KM3NeT APS.

This thesis has been developed in collaboration with the KM3NeT experiment, focused on the acoustics aspects of the telescope, which are the APS and the acoustic neutrino detection. The work performed in the thesis is mainly centred on the design, development and characterization of the Acoustic Beacons (AB) for the APS and on the design and development of a transducer array able to calibrate the acoustic neutrino detection, which are detailed in Chapter 2 and 3, respectively.

After introducing to the neutrino particle detection and before describing the KM3NeT APS in Section 1.3 and the neutrino acoustic detection in Section 1.4 the main aspects of underwater acoustics are described in the following section, emphasizing in the main points related to the thesis development. This will help to better understand the next thesis contents.

1.2 Fundamentals of Underwater Acoustics

In this section the main concepts of underwater acoustics used in the thesis are introduced: transducers, parametric generation and acoustic positioning. They will help to understand the thesis progress and the contents. Firstly, the characteristics of the acoustic wave and its propagation in water will be explained. Then the piezoelectric transducer mechanisms and its calibration will be described. Afterwards, the acoustic parametric effect will be detailed. And finally, a brief introduction to acoustic underwater positioning will be presented. In the next chapters, these points will be described more specifically for its application in the development of the acoustic beacons and the neutrino array calibrator as part of the underwater neutrino telescopes.

1.2.1 The Acoustic Wave

Acoustic waves constitute one kind of pressure fluctuation that can exist in a compressible fluid. In practice the acoustic pressure is the most often used quantity in underwater acoustics. The acoustic pressure is expressed in Pascals (Pa) or microPascals (µPa). Background noise measured in a narrow frequency band under quiet conditions may be only few tens of µPa, whereas the sound level close to a high-power source may reach 10^{12} µPa which is more than 10 orders of magnitude higher. This justifies using logarithmic notation.

Normally, the useful acoustic signals are not instantaneous perturbations, they are maintained oscillations characterized by their frequency *f* which is the number of elementary oscillations per second. The frequency is expressed in Hertz (Hz) and by the period T which is the duration of an elementary oscillation cycle being $T=1/f$. The wavelength λ is the spatial correspondence to time periodicity, it means the distance travelled by the wave for one period with velocity *c*.

Acoustic waves in viscid fluids exhibit fewer constraints to deformations than do solids. The restoring forces responsible for propagating a wave are the pressure changes that occur when the fluid is compressed or expanded. Acoustic waves propagating in gases and liquids follow the laws of fluid mechanics (Kinsler et al 1999). Their propagation is described by the wave equation:

$$\frac{\partial^2 p}{\partial x^2}+\frac{\partial^2 p}{\partial y^2}+\frac{\partial^2 p}{\partial z^2}-\frac{1}{c^2(x,y,z)}\frac{\partial^2 p}{\partial t^2}=0 \tag{1.1}$$

where *p* is the acoustic pressure of a wave propagating in the space *(x, y, z)* as a function of time *t* and *c (x, y, z)* is the local sound velocity. For a sinusoidal wave of frequency f_0 the wave equation becomes the *Helmholtz equation*:

$$\Delta p + k^2(x,y,z)p = 0 \tag{1.2}$$

where Δ is the Laplacian operator and $k\ (x, y, z) = 2\pi f_0/c(x, y, z)$ is the wave number, $w=2\ \pi f_0$ the angular frequency or pulsation. For a constant velocity, $c\ (x, y, z) = c$, and propagation restricted to one single direction *x*, last equation becomes:

$$\frac{\partial^2 p}{\partial x^2}+\frac{\omega^2}{c^2}p=0 \tag{1.3}$$

The solution of which is a pressure wave of the type:

$$p(x,t)=p_0\exp\left(jw\left(t-\frac{x}{c}\right)\right)=p_0\exp(j(\omega t-kx)) \tag{1.4}$$

with a constant amplitude p_0, and a phase depending on a single Cartesian space coordinate x and the time t. The constant phase surfaces associated to this wave, named wavefronts, are planes orthogonal to direction of propagation *x*. This type of wave is therefore called plane wave. The expressions of corresponding particle displacement velocity *v (x, t)* and displacement *a (x, t)* are identical, replacing modulus p_0 by respectively v_0 and a_0. For a plane wave propagating in the x direction, the last equation provides a simple relation between amplitudes of acoustic pressure p_0, speed of sound in the fluid *c* and velocity:

$$\frac{\partial p}{\partial x} = -\rho \frac{\partial v}{\partial t} \rightarrow p_0 = \rho_0 c v_0 = \rho_0\, c\, \omega\, a_0 \tag{1.5}$$

where $\omega=2\,\pi f_0$ inks the displacement a to its time-derivative, the fluid velocity v.

The specific acoustic impedance is defined as the ratio of acoustic pressure to velocity of particle in media:

$$z = \frac{p}{v} \tag{1.6}$$

For plane waves is named the characteristic acoustic impedance of the propagation medium is $\rho_0\, c$. The SI-related unit for acoustic impedance is (Pa·s/m) or Rayl. In a high-impedance medium like water ($z=\rho_0\, c \sim 1.5 \cdot 10^6$ Rayl).

When considering the propagation in the three spatial directions of an isotropic medium, the solution to the wave equation for a point source is a *spherical wave*:

$$p(r,t) = \frac{p_0}{r} \exp\left(j\omega\left(t - \frac{r}{c}\right)\right) = \frac{p_0}{r} \exp(j(\omega t - kr)) \tag{1.7}$$

The space variable considered here is the radial distance r from the source. The wave fronts are now spheres centred on the source located at r = 0, and the pressure amplitude decreases $1/r$, from its value p_0 conventionally considered 1 meter away from source.

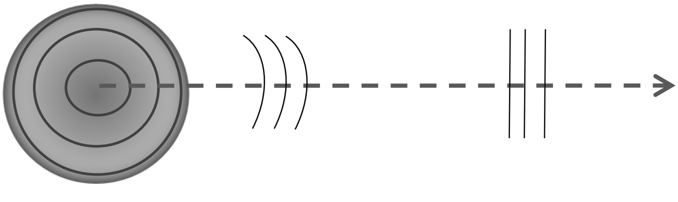

Fig. 1.6. Spherical and plane waves: the wavefront curvature is an important physical feature close to the source (geometrical structure, amplitude loss), and can be neglected at larger ranges, where the wave may be considered as plane (locally constant amplitude)(Lurton 2010).

Plane and spherical waves are the two basic tools for modelling the propagation of acoustic waves (Fig. 1.6). Plane waves are the easiest to handle; they are used when the amplitude can be approximated to a constant, and the wave fronts show a negligible curvature. These conditions are satisfied far away enough from the sound source, in general when condition $k\,r >> 1$ is satisfied, for the modelling of local processes. Spherical waves are descriptive of a field transmitted at short range by a point-like source (i.e. sufficiently small compared to the wavelength), and the amplitude decreasing with propagation from the source must be accounted.

1.2.2 The Acoustic Wave Propagation in Seawater

Although many factors limit the transmission of sound through seawater, acoustics is far superior to electromagnetism and light for transmitting energy through the oceans since in comparison its attenuation over long distances is quite lower (Lurton 2010). When acoustic waves propagate, the most evident effect is their loss of intensity, because of geometric spreading (divergence effect) and absorption of acoustic energy by the propagation medium itself. This propagation loss (or transmission loss) is a key parameter for acoustic systems, since it constrains the amplitude of the signal received, hence the reception performance, directly dependent on the signal-to-noise ratio. As energy is conserved, the intensity will decrease proportionally to the inverse of the surface, this process is known as geometric spreading loss.

The simplest case is the homogeneous, infinite medium, with a small-dimension source radiating in all directions (point source). The energy transmitted is conserved, but it is spread over spheres of larger radius (Fig. 1.7)

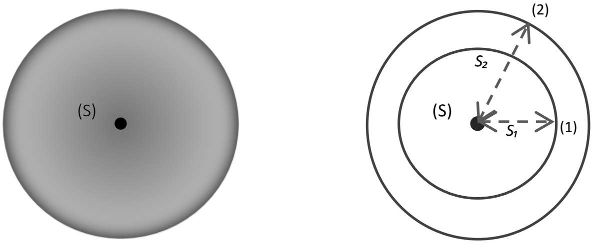

.

Fig. 1.7. Spherical spreading: the acoustic intensity decreases with distance from the source, in inverse proportion to the sphere surface.(Lurton 2010).

The decrease in local acoustic intensity between points (1) and (2) is then inversely proportional to the ratio of the surfaces S_1 and S_2 of the spheres:

$$\frac{I_2}{I_1} = \frac{S_1}{S_2} = \frac{4\pi r_1^2}{4\pi r_2^2} = \left(\frac{r_1}{r_2}\right)^2 \qquad (1.8)$$

where r_1 *and* r_2 are the radial distances from the source. Hence intensity decreases in $1/r^2$, and pressure in $1/r$. This is the amplitude dependence in range for spherical waves. The spreading transmission loss, considered from the reference unit distance ($r_{1m}=1m$) can be expressed in dB as:

$$TL = 20\log\left(\frac{r}{r_{1m}}\right) \qquad (1.9)$$

Sea water is a dissipative propagation medium; it absorbs a part of the transmitted wave energy, which is dissipated through viscosity or chemical reactions (thermal conduction being weak in water). The local amplitude decrease is proportional to the amplitude itself; hence the acoustic pressure decreases exponentially with distance. This will add to spreading losses. For a spherical wave, the pressure becomes:

$$p(r,t) = \frac{p_0}{r}\exp(-\gamma r)\exp\left(j\omega\left(t - \frac{r}{c}\right)\right) \tag{1.10}$$

Attenuation is here quantified by the absorption parameter γ (expressed in Neper/m). The exponential decrease of pressure gives a loss in dB proportional to propagation range: this is conveniently expressed through an attenuation coefficient α in decibels per meter, related to γ by $\alpha\ (dB/m) = 20\,\gamma \log e \approx 8.686\,\gamma\ (Np/m)$. Note that, in practice, attenuation of sound in seawater is best-dimensioned in dB/km. The pressure amplitude of a damped spherical wave is:

$$P(r) = \left(\frac{A}{r}\right)e^{-\alpha(r-1)} \tag{1.11}$$

The most important phenomenon that alters the spherical spreading of sound in the ocean is the refraction that results from spatial variations in the sound speed induced by inhomogeneity in temperature, salinity, and pressure. The acoustic ray is bended in a medium where refraction exist. Variations in the speed of sound with depth are quite small, and variations in speed for changes in temperature are larger. The speed of sound in seawater can be measured directly as a function of temperature, salinity and pressure (depth). A reasonably accurate approximation for calculating c is to use equation (Kinsler 1999):

$$\begin{aligned} c(T,S,P) = {} & 1449.08 + 4.57Te^{-\left[\frac{T}{86.9}+\left(\frac{T}{360}\right)^2\right]} \\ & + 1.33(S-35)e^{-\frac{T}{120}} \\ & + 0.1522Pe^{\left[\frac{T}{1200}+(S-35)/400\right]} + 1.46 \\ & \times 10^{-5}P^2e^{-\left[\frac{T}{20}+(S-35)/10\right]} \end{aligned} \tag{1.12}$$

where c is the speed of acoustic wave in m/s, T the temperature in degrees Celsius, S the salinity in parts per thousand (ppt), and P the pressure in atmospheres.

Absorption is often the most limiting factor in acoustic propagation. Its amount depends strongly on the propagation medium and the frequency. The absorption attenuation in seawater is caused by pure water viscosity, which effect increases with squared frequency. For the frequency range of 1-100 kHz absorption is mainly caused by a chemical relaxation process that is connected with the association-dissociation

of magnesium sulphate ($MgSO_4$) ions. Below 1 kHz, a similar mechanism involving boric acid ($B(OH)_3$) is responsible for much of the observed attenuation.
Since the beginnings of underwater acoustics, many modelling to determine the absorption coefficients has been proposed. The most important point of the propagation simulation is applying a realistic acoustic wave attenuation method which is adapted to the characteristics of the media. The model mainly used today was proposed by (Francois & Garrison 1982) which is a very complete and accurate method for determining the seawater absorption coefficient. Later, however, a simplified parameterization of the magnitude of the attenuation in seawater (Ainslie & McColm 1998) which maintains a similar accuracy to the parameterizations of Francois and Garrison was published. This is a function of frequency, depth, z, salinity, S, temperature, T and pH. However, shift phase due to absorption was not taken into account. In (Lieberman 1948) a clear presentation of the chemical processes causing the attenuation is presented. A complex attenuation formula based on Mediterranean conditions was published in (Niess & Bertin 2006). This formula presents a complex version of the Ainslie and McColm formulation, which retains the attenuation magnitude and introduces the phase shifts predicted by Lieberman.
A new method of computing the acoustic signal with complex attenuation for a neutrino shower in water and ice was developed by the ACORNE Collaboration (Bevan et al. 2009). This complex attenuation formula was used for the in situ simulations and analysis performed in this thesis. For the Mediterranean Sea the mean conditions are: T=15ºC, S=37 PPT; pH=7.9 and the pressure according to depth. The method allows the most up to date knowledge of the absorption to be incorporated naturally, which is known to be complex in nature. For this reason, the ACORNE method is an accurate tool to predict the acoustic bipolar pulse amplitude at the detector.

In essence the absorption consists of three components, two of these are complex, high pass filters with cut off frequencies ω_B ($\sim 2\pi \times 10^3$ rad s^{-1}) for boric acid and ω_{Mg} ($\sim 2\pi \times 10^5$ rad s^{-1}) for magnesium sulphate. The third is the pure water component, which is real. The ACORNE parameterization uses a_x values that are the respective absorption coefficients in dB/km; boric acid (w_B), magnesium sulphate (w_{Mg}), boric acid and magnesium sulphate absorption coefficients (a_B, a_{Mg}), water coefficient absorption (a_w), and total absorption coefficient ($a_{dB/km}$):
Boric Acid:

$$w_B = 1560\pi\sqrt{\frac{S}{35}}e^{T/26} \tag{1.13}$$

Magnesium sulphate:

$$w_{Mg} = 84000\pi e^{T/17} \tag{1.14}$$

Boric acid absorption *coefficient:*

$$a_B = \frac{1.893\times10^{-4}}{2\pi} e^{\frac{pH-8}{0.56}} \tag{1.15}$$

$$a_{Mg} = \frac{0.52\times10^{-3}}{2\pi}(1+\frac{T}{43})\frac{S}{35}e^{\frac{-z}{6}} \tag{1.16}$$

Water coefficient absorption*:*

$$a_w = \frac{49\times10^{-9}}{4\pi^2} e^{-(T/27+z/17)} \tag{1.17}$$

Total absorption coefficient:

$$a_{dB/km} = \frac{a_B w_B s}{s+w_B} + \frac{a_{Mg} w_{Mg} s}{s+w_{Mg}} + a_w w^2 \tag{1.18}$$

,

where $s = w^2$, being w the angular frequency component of the acoustic wave.

Another important issue in underwater acoustics is the noise. The noise can interfere with the desired received signal and even mask it if the noise level is high enough. The signal to noise ratio SNR compares the power (PW) signal with respect background noise and can be measured by:

$$SNR = \frac{PW_{signal}}{PW_{noise}} = \left(\frac{A_{signal}}{A_{noise}}\right)^2 \tag{1.19}$$

$$SNR_{dB} = 10log\left(\frac{PW_{signal}}{PW_{noise}}\right) = 20log\left(\frac{V_{signal}}{V_{noise}}\right) \tag{1.20}$$

$$SNR_{dB} = PW_{signal\ dB} - PW_{noise\ dB} \tag{1.21}$$

Environmental noise in water varies with location and depth. Different sources can affect to the background noise such as sea agitation, wind, biological noise and shipping. There is a kind of noise called self-noise which is the one generated by the receiving system. Self-noise can come from the sea surface, from reflections in the mechanical structure and from the electronics of the receiving system, interfering as electromagnetic noise.

1.2.3 Ultrasounds

The audio spectrum detectable for the human auditory system covers frequencies from 20 Hz to 20 kHz. The sounds at higher frequencies than 20 kHz and lower than 1 GHz are considered ultrasounds (Kuttruff 2006). Despite the ultrasounds are not perceived by the human ear, they are perceived and used by some species in nature (insects and mammals) and they use it, normally, for communicating and echolocation.

Ultrasounds have particularities that made them and interesting tool for many applications in the industrial field, medicine and underwater researches. The first ultrasonic generator was developed in the twentieth century through a piezoelectric material. Next section describes in more detail the characteristics of a piezoelectric ultrasonic transducer and its application in underwater acoustics. This aspect is important since the emitter transducers designed in the thesis are based on piezoelectric effect emitting in the ultrasound range.

The propagation of ultrasound in air is more limited since its absorption is higher, for this reason in most applications the propagation media of ultrasonic waves are liquid or solids. In spite of the sound absorption is higher in the ultrasound range than at lower frequencies, in water media, low frequency ultrasonic waves are able to reach distances of few km with the enough power emission. Moreover, higher directional sound beams are generated with ultrasounds since the wavelength are shorter than for lower frequencies. All these aspects, make the ultrasound regime an effective way of communicating, positioning and researching in underwater media applications.

1.2.4 Piezoelectric Acoustic Transducer

In the late nineteenth century, it was found that when some crystals are exposed to mechanical stress, an electrical field is generated, this effect is referred to the direct piezoelectric effect. It was discovered that this effect occurs also in reverse, when an electric field is applied in these materials a mechanical distortion is produced, this is known as the inverse piezoelectric effect. Different crystals and ceramic materials present the piezoelectric effect, and over the last decades they have been used as electromechanical transducers. Nowadays, piezoelectric ceramics are commonly used for acoustic transducer design.

The equations that define the piezoelectric materials relate the mechanical, electrical and piezoelectric behaviour of ceramics. The basic equations state the inverse and the direct piezoelectric effect (Kuttruff 2006).

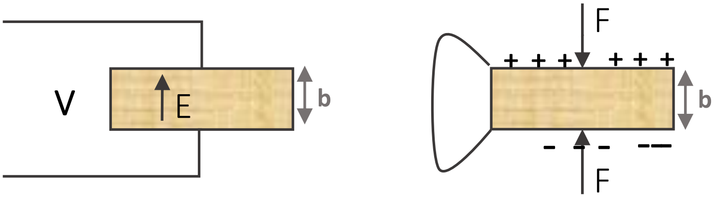

Fig. 1.8. Schematic of the piezoelectric effect; the inverse piezoelectric effect (left image) and the direct piezoelectric effect ceramic (right image).

The first equation states that when electrical voltage *V* is applied to a piezo disk, a electrical field will be established in the disk, see Fig. 1.8. This leads to change of thickness *b* proportional to the field strength *V/d*, where *d* is the piezoelectric module, as a result of an elastic tensile stress *σ* created by the electric field *E*. In reverse, if a relative change of thickness *ξ/d* is forced in the disk material, it become electrically polarised. At short-circuited electrodes, the polarisation generates a charge *Q* on the electrodes producing a deformation *S*, which is, the dielectric displacement *D*. The parameter *e* is the piezoelectric constant.

$$\sigma = e\frac{U}{d} = -eE \tag{1.22}$$

$$D = -e\frac{\xi}{d} = eS \tag{1.23}$$

The piezoelectric constant *e* can be changed for the piezoelectric module *d* (Sherman & Butler 2007) and the equations states as:

$$S = -dE \tag{1.24}$$

$$D = d\sigma \tag{1.25}$$

Taking into account all the factors that are involved in the piezoelectric process, the phenomenological equations of state are defined as:

$$S = S^E T + d^t E \tag{1.26}$$

$$D = dT + \varepsilon^T E \tag{1.27}$$

where *T* is stress, s^E is a matrix of elastic compliance coefficients, d is a matrix of piezoelectric coefficients, d^t its transposed matrix, and ε^T is a matrix of permittivity coefficients.

If an alternate electric field *E* is applied to the piezoelectric material, the material will oscillate with the same frequency. Moreover, it has been experimentally observed that the vibration amplitude is maximum when the electrical field frequency has specific values, they are known as resonance frequencies of the material. The equivalent circuit for the piezoelectric actuator is represented by a parallel combination of the electrostatic capacitance with the electrical elements *L*, *C* and the mechanical loss element *R*. This controls the transducer reactance which is a function of frequency. The resonance frequency f_R is given by:

$$f_R = \frac{c}{2a} \tag{1.28}$$

where *a* is the ceramic thickness and *v* the sound speed in the piezoceramic which is given by:

$$v = 1\sqrt{\rho s_{11}^{E}} \qquad (1.29)$$

where *r* is the volumetric mass density and s_{11}^{E} is the mode 11 coefficient of the elastic compliance matrix.

The acoustic impedance of the ceramic is defined by the speed of sound in the ceramic c and the volumetric mass density ρ:

$$Z_c = \rho\, c \qquad (1.30)$$

The piezoelectric transducer is based in the electroacoustic transduction mechanism which converts energy between electrical and mechanical forms. This effect is reversible (Kinsler 1999). It has two ports. One of them being the input terminal to which the signal to be converted is applied. While the second one is the output terminal which yields the result of the conversion. When energy is applied to the ceramic *(I, V)* it is converted into mechanical movement *(u, F)* which produces the transmission of an acoustic wave through the media. Fig. 1.9 shows an electromechanical transducer representation. A piezoelectric transducer can act as receiver as well, in this case, when a sound wave arrives to the piezoelectric transducer produces a mechanical movement in the ceramic which is converted into electrical energy. The parameter *V* is the voltage across the electrical inputs to the transducer and *I* is the current at the electrical inputs, the force on the radiating surface is referred to *F* and the speed of the radiating surface as *u*.

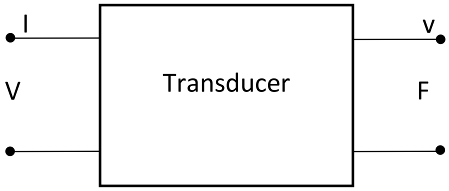

Fig. 1.9. Representation of an electromechanical transducer; voltage (V), current (I), velocity (v) and force (F).

Other type of electroacoustic transducers are also used for underwater acoustics (electrostrictive, magnetostrictive, electrostatic, etc.), however piezoelectric transducers have quite good characteristics for being used in underwater applications, hence this type of transducer is the most commonly used in underwater sound. For these reasons, the piezoelectric transducer was chosen for the design of the acoustic emitters developed and described in this thesis.

When a transducer acts as a source, the force F on the diaphragm and the particle speed u of the adjacent medium are related by:

$$F = -Z_r v \qquad (1.31)$$

where $Z_r = R_r + jX_r$ is the radiation impedance.

The transducer responses are measures of the transducer ability to perform these functions. They are defined as the transducer output per unit of input as a function of frequency, for fixed drive conditions (Sherman & Butler 2007). The frequency response of the transducer normally represent a curve that shows some of the most important characteristics of the transducer behaviour. It is possible to identify the resonance frequency of the transducer which makes maximum the real part of the admittance.

The mechanical quality factor, Q_M, determines the spectrum bandwidth of the piezoceramic resonance curve and it relates the resonance frequency ω_0 with the resonance bandwidth $A\omega$. Next equation states the mechanical quality factor:

$$Q_M = \frac{\omega_0}{2\Delta\omega} \tag{1.32}$$

The transducer radiated power is independent of distance in a lossless medium, but, since the pressure varies inversely with distance, it is necessary to define a reference distance for the source level, conventionally 1m from the acoustic centre of the transducer. The sensitivity of a transmitter can be expressed as the ratio of the acoustic pressure extrapolated back from the far field to 1 m from the source to the amplitude of either the driving voltage V or driving current I:

$$S_V = \frac{P \quad (1m)}{V} \tag{1.33}$$

$$S_I = \frac{P \quad (1m)}{I} \tag{1.34}$$

The input electric impedance of the transducer Z_{ET} (Ω) is the relation between driving voltage and current as $Z_{ET}=V/I$. The admittance is defined as the inverse of the impedance. The sensitivity and current sensitivity is defined by:

$$S_{TX,I} = S_{TX,V}|Z_T| \tag{1.35}$$

The electroacoustic is not completely efficient, since part of the energy is lost in the electric energy to acoustic energy conversion, and vice versa. It can be described through its efficiency (Uchino 2003). The efficiency η is defined as the relation between the acoustic power radiation W and the input electrical power W_{TX}:

$$\eta = \frac{W}{W_{TX}} \tag{1.36}$$

A complete underwater transducer is principally composed of matching (also called heading), piezoelectric material and backing layers, as it is shown in Fig. 1.10. The backing is added to the back of the transducer in order to damp the acoustic back wave and to reduce the pulse duration. The matching layers are used to increase sound transmission since it matches the impedance of the piezoelectric element with the sound transmission media. The matching layer achieves maximum wave transmission when accomplish, for a specific frequency, a thickness of one quarter of the wavelength *(λ/4)* and its acoustic impedance Z_{ML} is the geometric mean of the piezoelectric material impedance Z_T and the media impedance Z_L, therefore the best approximation of Z_{ML} for achieving maximum transmission is $\sqrt{Z_L\, Z_T}$.

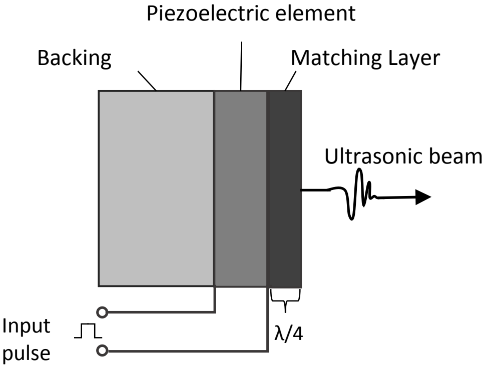

Fig. 1.10. Basic emitter transducer for underwater acoustic applications.

Normally, transducers radiate sound with directionality, the sound pressure level emitted with the transducer changes with the radiation angle, this is known as directionality (Hodges 2010). The transducer directionality depends on frequency and distance until the far field distance is achieve where the transducer directionality become independent of distance, being inversely proportional to distance.

The transducer far field, also known as Rayleigh distance or 'Fraunhofer region' is the distance where the spherical divergence of the acoustic pressure radiated starts and the energy is expanded faster, it is defined as:

$$X \geq \frac{\pi a^2}{\lambda} \tag{1.37}$$

Maximum Response Axis (MRA) is the direction where the maximum acoustic intensity, $I_0\,(r)$ is found. The directionality factor is the ratio of the maximum acoustic intensity to the acoustic intensity averaged over all directions, $Ia\ (r)$, at the same distance, r, in the far field, it is defined as:

$$D_f = \frac{I_0(r)}{I_a(r)} = \frac{I_0(r)}{W/4\pi r^2} \tag{1.38}$$

Where W is the total radiated acoustic power.

The directionality of a piezoelectric transducer depends on the frequency (wavelength) of the signal, dimensions of the piezoelectric element area and on the acoustic phase of the vibrations on the piezoelectric material surface. Normally, the directionality pattern consist if angular regions of lobes (high intensity) and nulls (low intensity), as it is shown in Fig. 1.11.

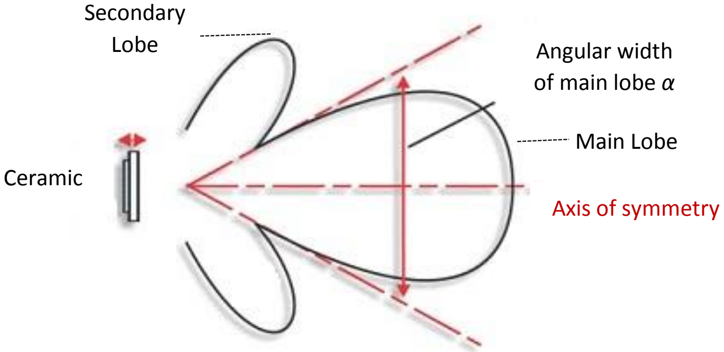

Fig. 1.11. Example of far-field directionality pattern for of plate ceramic, showing the main and secondary lobes.

1.2.5 Electro-Acoustic Transducer Calibration

The calibration of an electroacoustic transducer permits to know its performance and efficiency in a frequency range of interest, and therefore, its response to the electrical (emitter) or mechanical (receiver) impulse. Typically, the response is measured in the direction of the MRA using a hydrophone at a radial distance in the far field where the pressure variation is inversely proportional to *r* and the beam pattern does not change with distance. The measurement system must be free from reflections and the pulse length must be long enough for the system to reach steady-state. Usually the signals used for the measurement are tone burst at different frequencies under a range of interest for calibration, and also signals as sine sweep or maximum length sequence (MLS) may also be used to evaluate the transducer response.

The transmitting response of a transducer gives the pressure in the medium per unit of electrical excitation as a function of frequency and is one of the most important parameters for characterizing a transducer. The response per volt is called the Transmitting Voltage Response *TVR* referenced for underwater applications at 1 m and a pressure reference P_0 of $1\ \mu Pa$ expressed in dB (re 1 μPa/V at 1m). The electric voltage signal applied to the transmitter transducer is recorded V_{EL} and its pressure field is determined from the receiving voltage of the calibrated hydrophone giving the pressure at one meter P_R. Then the *TVR* is determined following:

$$TVR\ = 20log_{10}\frac{P_R/P_0}{V_{EL}}\ \left[dB\ re\frac{1uPa}{V}\ at\ 1\ m\right] \qquad (1.39)$$

The Sound Pressure Level *SPL* generated by the transducer is another common characterization value for acoustic transmitters. It is defined as the ratio of the pressure *P* at 1 meter from the source ($1\mu Pa$ *@ 1m*) expressed in dB and can be determined as a function of frequency and directionality:

$$SPL = 20log_{10}(P/P_0)\ [dB\ re\ 1uPa\ at\ 1m] \tag{1.40}$$

The receiving response of a transducer is the electrical response to the reception of a sound pressure field. It is referenced in V/Pa or V/µPa. It can be calibrated through the direct-comparison (substitution) method by using a broadband projector generating a pressure field, which can be first measured by a calibrated reference hydrophone (RH), giving a measured voltage V_{RH} from which the pressure can be deduced P_{RH}. Then the hydrophone under calibration (H) is placed in the same location and a voltage V_H *is* measured. Also, the receiving voltage response can be measured from both the reference hydrophone and the one under evaluation at the same time, being both at the same distance from emitter, provided that the angular dependence is the same. The *RVR* is:

$$RVR\ = 20log_{10}\frac{V_H}{P_{RH}/P_0}\ \left[dB\ re\frac{V}{1uPa}\right] \tag{1.41}$$

Other common method for the calibration of the acoustic transducer sensitivity is the reciprocity-based technique. This method allows to calibrate hydrophones with non-calibrated ones. However, it usually requires free field configuration and two of the transducers have to work in reciprocity, since they work as emitter and receivers (Ardid et al. 2007). The technique requires three non-calibrated hydrophones (designated by letters *a*, *b*, *c*), the sensitivity of transducer *c* can be obtained in just three steps involving four measurements: *Vb*, *Vc*, *Vc'* and *Ib* (voltages and current in the transducers *b* and *c*). The expression for determining the sensitivity through the reciprocity method *S (V/P)* is:

$$S = \left(J\frac{|V2_c||V3_c|}{|V1_b||I3_b|}\right)^{1/2} \tag{1.42}$$

where the reciprocity parameter J depends on the acoustic propagation conditions, it is $J = 2d/(\rho f)$ for spherical free field. It depends on distance, d, between emitter

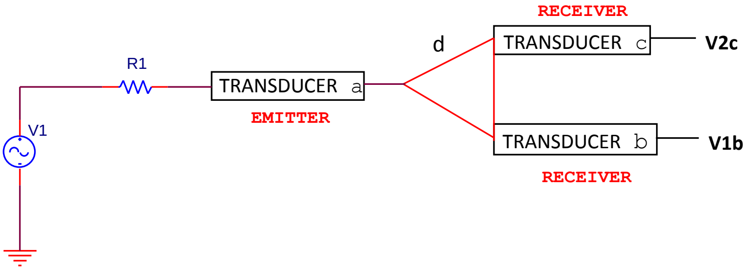

and receiver, media density (1000 kg/m^3 in water) and working frequency, the diagram of measures for reciprocity calibration is shown in Fig. 1.12.

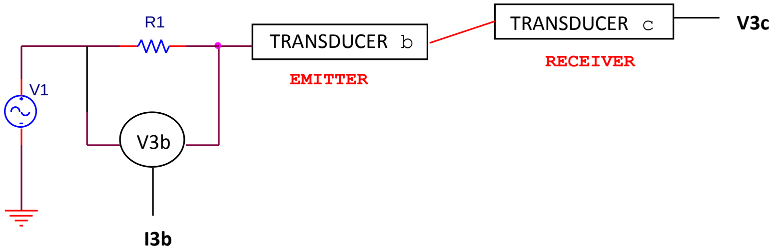

Fig. 1.12. Diagram of reciprocity calibration

Other important calibration measure is the directionality of the transducer which can be measured for both the transmitting and receiving response as function of the angle for the frequencies of interest. The directionality response is measured from the direction of the *MRA*, in this thesis corresponded to the reference of 0°, and the angle range of interest using a hydrophone at a radial distance in the far field.

In addition, impedance, admittance, efficiency and power factor are often measured as function of frequency giving information about different characteristics of the transducers.

1.2.6 Acoustic Transducer Array

Acoustic transducer arrays are generally used to achieve more powerful and directional sound emissions. The array directionality is formed from the directionality pattern of each individual transducer and the adjusting of their relative amplitudes and phases. Following this philosophy, a previous linear array of eight-hydrophones of about 8 meters length was developed by the Northumbria University team for the generation of emulated UHE neutrino-induced pulses (Ooppakaew 2012).

The beam pattern for an array composed of m evenly spaced hydrophones in a line can be calculated as follows. The signal arriving at each hydrophone is given by:

$$S_1 = Scos[\omega(t + \tau)] \qquad (1.43)$$

where τ_j is the time delay of each hydrophone; $\tau_j = j\ (d/c)\, sin\ (\theta)$, being θ the conical angle or polar angle measured from the line.

It has been observed that in a line array composed of some transducers separated in the same distance one from each other, the main beam obtained from the emission or reception is reduced in width when the number of transducers increases. The MRA of the array can be driven by adjusting their phases, applying a time delay in the signal emission. For a linear multi-hydrophone array separated at the same distance (d), the delays (τd) need to be:

$$\tau d(j^{th}\ hydrophone) = j\, d/c\, \sin(\theta) \tag{1.44}$$

1.2.7 Acoustic Parametric Generation

According to linearity theory when two acoustic waves with frequencies f_1 and f_2 interact in space and time the acoustic field presents different contributions of the initial frequencies only. However, when two acoustic waves (f_1, f_2) of high amplitude travel together in a medium which causes nonlinearities in the acoustic wave interaction, new acoustic waves with secondary frequencies appear in the media from the combination of the primary beams. The secondary acoustic waves have frequencies equal to the sum and difference of the primary following $n{\cdot}f_1 \pm m{\cdot}f_2$ (n and m=0, 1, 2, 3…), they are called intermodulation frequencies. This phenomena is called the acoustic parametric effect. It was introduced by Westervelt (1963) pointing that this process of non-linear generation of new frequencies is limited to a certain distance from the transducer, called the array length, given by the distance of interaction or absorption length. This may be considered as a set of virtual acoustic sources contained along the length of interaction; the source seems to be shaded exponentially as distance increases from the transmitter. This process is called the parametric array and its representation is shown in Fig. 1.13. The secondary beam is produced with a directionality pattern similar to the one of the primary beams, which offers the advantage of generating a low-frequency directional beam. The Westervelt analysis showed that the far field of the difference frequency component would have very narrow beams with very low side lobes compared to conventionally radiated beams, characteristics that is worth in some practical applications. For instance, we will use it for the generation of the acoustic neutrino signal with the compact array calibrator, described in Chapter 3.

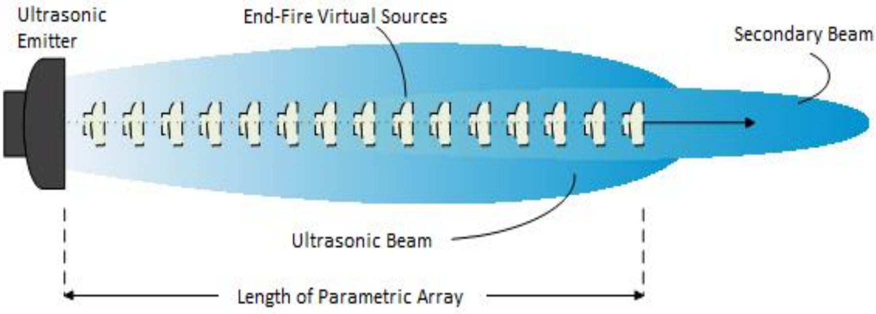

Fig. 1.13. Schematic of a parametric array behaviour

These acoustic sources have become useful as precision depth emitters because they provide highly directional acoustic beams of relatively low frequencies, which would be absorbed much less than the other waves and, hence, propagate farther. The main disadvantage of parametric transduction is its low-power conversion efficiency, which is usually less than 1%; that is, equivalent to at least 20 dB of power loss. However, an advantage for long distances propagation is that the secondary (low) frequency signal has lower attenuation.

The following formulation is an estimated wave equation for the acoustic pressure based on Westervelt, Beyer (Beyer 1975) and Kinsler (Kinsler 1999) it is obtained after simplifying some nonlinear parameters:

$$c^2\left(1+\tau\frac{\partial}{\partial t}\right)\nabla^2 p-\frac{\partial^2 p}{\partial t^2}=-\frac{\beta}{\rho c^2}\frac{\partial^2}{\partial t^2}\left(p^2\right) \tag{1.45}$$

where τ is related to the shear and bulk viscosities of the media *and* $\beta = 1 + B/2A$ where B/A is the nonlinear parameter of the media ($B/A \approx 5$ for sea water). In many cases, the parameters τ and β can be considered as insignificant.

A theoretical treatment was formulated for transient, or broadband, parametric acoustic sources based on the Westervelt formulations and developed by Moffett & Mello (Moffett, M.B.; Mello 1979). This treatment generates spectra and waveforms for specified modulation envelopes. Therefore it could be useful for designing primary transient signals which generate parametric signals with predetermined characteristics. The pressure distribution along the axis for the secondary beam generated through the parametric emission of transient signals can be deduced from:

$$p(x,t)=\left(1+\frac{B}{2A}\right)\frac{P^2 S}{16\pi\rho c^4\alpha x}\frac{\partial^2}{\partial t^2}\left[f\left(t-\frac{x}{c}\right)\right]^2 \tag{1.46}$$

where S is the area of the transducer surface, ρ, c are the density and the sound velocity, α is the absorption coefficient in the medium respectively. P is the pressure amplitude of the primary signal and $f\,(t\ -x\,/c)$ is the envelope of the primary transient signal which modulates the primary frequency.

1.2.8 Undersea Acoustic Positioning

Acoustic positioning systems (APS) were developed in the 1950s and 60s, the tracking of towed sensors and vehicles, locating underwater pipelines and cables, the monitoring of drilling and dredging operations as well as the survey and monitoring of numerous objects, are now common applications. In recent years the significance of acoustic positioning has increased as more activities have taken place in deep water areas. The ability of the APS is measured in terms of accuracy, coverage and reliability.

APS measure ranges and directions to transponders fitted to underwater vehicles and objects, or derive acoustic ranges from stations deployed onto the seabed (International Marine Contractors Association (IMCA) 2009). These latter units are held stationary by a clump weight with buoyed mooring (or some other form of fixed seabed framework). Several types of system such as ultra-short baseline (USBL) and short baseline systems (SBL) provide positioning relative to a host vessel or vehicle, whereas long baseline (LBL) systems allow either a relative or absolute positioning framework to be developed. Many other scenarios exist including beacons being installed on remotely operated vehicles (ROVs), autonomous underwater vehicles (AUVs) and other types of towed vehicles. The systems have been developed specifically to meet the challenges of operating in deep water with sufficient accuracy and system reliability. The main elements of deep water acoustic positioning systems will include:

- Transmission and reception of acoustic pulses to track or position a limited number of objects – both static and mobile;
- Processing and applying corrections to data to provide accurate and consistent performance parameters;
- Incorporation of peripheral data such as speed of sound in water, depth, heading and motion;
- Display of position relative to a certain reference system, e.g. vessel;
- Some form of noise and interference mitigation to enable continued working in harsh environments.

In this thesis, the acoustic application of one of the designed emitters is for positioning a LBL system of the underwater telescope KM3NeT. The APS of KM3NeT provides the required information during the deployment and operation phases of the telescope. APS data are used to retrieve the positions of each line array which composes the telescope. The positioning is based on a Long-Baseline (LBL) reference system consisted of acoustic transceivers distributed in the sea bottom at known positions and acoustic receivers (hydrophones) placed at the storeys of the detection lines.

The LBL is a positioning technique that allows the localization of underwater equipment inside of a limited area of interest. This technique consist of a group of transponders distributed around the area of interest and located on the seafloor at fixed and known positions, forming an array of transducers (Tomczak 2011) and the receivers that are located in the equipment that needs to be positioned. Emitters and receivers of the LBL system are time synchronized and when the emitters, placed at known positions, send the signal detected by the receiver, the Time of Flight (ToF) can be determined. Then, by knowing the sound velocity in the media, the travelling distances from the emitters to the receiver is obtained. Normally, a minimum of three transponders emission at the receiver point are needed to determine the relative position of the receiver, and the position of the receiver is calculated through triangulation method.

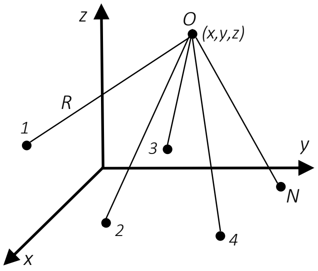

Fig. 1.14. LBL position approximation case.

A typical LBL position determination is shown in Fig 1.14, where there is a receiver O in the unknown position (x, y, z) and some emitters N located at known locations (x_i, y_i, z_i). The signal is send by an emitter at a Time of Emission (ToE) and propagates with a sound speed c arriving at some numbers of receivers at a Time of Arrival (ToA_i). The sound speed could vary point to point and refraction could appear causing slight deviation on the acoustic ray. The equation that determines, for the spherical cases, the distance between the emitters and the receiver is defined by:

$$R_i = c(ToA_i - ToE_i) \qquad i = 1 \ldots N \tag{1.47}$$

where:

$$R_i = \sqrt{(x - x_i)^2 + (y - y_i)^2 + (z - z)^2} \tag{1.48}$$

In the case, there are more than three emitters signal per receiver the accuracy on determining the receiver positions increases and the positioning system became more robust. Typically, the signals used for the LBL acoustic positioning systems are tone burst at different ultrasonic frequencies, normally, the low ultrasonic frequency range is more used since the attenuation in the media is lower than for higher frequencies. The type of signals used for these purposes are sine, sine sweeps and maximum length sequence MLS, which has wide spectrum. Filtering and autocorrelation methods are used for improving the detection of the signals used in the positioning in cases where the noise could mask the direct signal (Picão et al. 2010). The wide-spectrum signals are especially efficient for the cross-correlation method, moreover, with this method signals at different frequencies ranges could be emitted at the same time without interfering.

1.3 Acoustic Positioning System (APS) of KM3NeT

1.3.1 Introduction to the APS

The acoustic positioning system (APS) is needed to provide mandatory information during both the deployment and the operation phases of the KM3NeT telescope. During the deployment phase the APS provides the position of the telescope's mechanical structures, in a geo-referenced coordinate system, with an accuracy of about 1m. Using a built-in auto-calibrating Long Baseline (LBL) and an external Ultra short Baseline (USBL) the APS must be also able to determine the absolute position of the detector to allow safe deployment and to determine the absolute pointing direction of the telescope, which is necessary for the localization of astrophysical sources.

During the telescope operation, in order to effectively reconstruct muon tracks, generated by the interaction of cosmic neutrinos with water nuclei, via the optical Cherenkov technique, the coordinates of the optical sensors must be known with an accuracy of about 10 cm. In the deep sea, DUs are anchored to the sea bed but they are free to move along their vertical expansion under the effect of currents, thus their positions must be determined and monitored. Oceanographic properties of the installation site will be monitored by dedicated structures, called Calibration Units (CUs). DUs and CUs will be connected by means of junction boxes (JBs) with an electro-optical seafloor network. A LBL of acoustic transmitters placed on the seabed in known positions and an array of acoustic receivers rigidly connected to the mechanical structures of the telescope will be used, therefore the optical sensor positions could be continuously calculated via triggered emission of acoustic signals. The distances from acoustic emitters and receivers of the line are of the order of 1 km, so acoustic signals emitted suffer a considerable attenuation.

The KM3NeT APS is composed of three main sub-systems: 1) an array of acoustic receivers rigidly connected to the telescope mechanical structures; 2) a LBL of acoustic transmitters (beacons) and receivers, anchored on the seabed at known positions; 3) a farm of PCs for the acoustic data analysis, on-shore. On shore, the positions of the acoustic receivers are calculated by measuring the ToF of the LBL beacons' signals on the acoustic receivers, calculating the distances from emitters and receivers considering the sound speed and, thus determining, via multi-lateration, the position of the acoustic receivers with respect to the geo-referenced LBL. These three sub-systerms are described in next sections.

The synchronized electronics and the data transmission/acquisition allows for calculating the latencies of the whole data acquisition chain with an accuracy of better than 100 ns. The APS, in combination with compass and tilt, pressure, current and sound velocity data, is expected to measure the positions of the digital optical modules in the deep sea with an accuracy of about 10 cm.

1.3.2 The Long Base-Line APS

The LBL positioning system of KM3Net is composed by an array of acoustic transmitters and receivers hosted on the DUs bases and on the Calibration Units bases (CBs). Each DU base will host a digital hydrophone, each CB will host an acoustic beacon and a digital hydrophone placed at known distance from the beacon. The LBL of the acoustic beacons installed on the CBs is complemented by an array of autonomous acoustic emitters (battery powered and driven by local clock) placed outside the footprint of the telescope, that improve the resolution of triangulation calculation for receivers placed on DU at the edge of the telescope field. Moreover, autonomous beacons must be used, during the installation of the first CBs, to create a temporary LBL field (Viola 2015). Since the submarine network of Phase 1 in Capo Passero does not foresee CBs, the Junction Boxes will be used as calibration bases.

The positions of acoustic beacons, receivers and autonomous beacons must be geo-referenced during the deployment operation using GPS signal, available on board the ship that performs the deployment, with an accuracy of ±1 m. The main LBL system is time-synchronized and phased with the detector master clock. This allows the implementation of LBL auto-calibration and the possibility to accurately measure the ToF, that is the difference between the ToA and the ToE of acoustic signals emitted by each beacon and received by the acoustic receivers on Dus tagged by the same, absolute, detector master clock. The LBL acoustic beacons are reconfigurable by dedicated RS-232 bidirectional link between shore station and CU base electronics: acoustic emission signal parameters (amplitude, waveform, and timing) can be set for “in situ” optimization of the signal detection. Fig. 1.15 shows the principles of the LBL system.

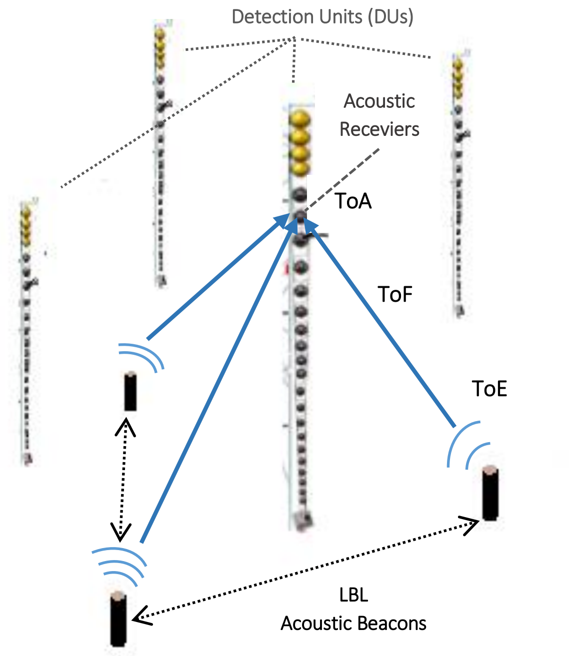

Fig. 1.15. Layout of the Long-Base-Line (LBL) configuration of the Acoustic Positioning System (APS) of KM3NeT.

LBL beacons can be reconfigured via a dedicated RS232 connection with a Central Logic Board (CLB) installed on the CB electronics, in order to allow reconfiguration of acoustic emission signal parameters (amplitude, waveform, timing) for "in situ" optimization of the signal detection. The signal emission trigger is received from the CLB on a CB, synchronized with the detector master clock. The positions of acoustic beacons and receivers on the DU bases must be geo-referenced during the deployment operation using a USBL (Ultra-Short Base Line) system available on board the ship that performs the deployment. In KM3NeT-IT this system relies on a self-consistent set-up made of a transmitting/receiving USBL transponder array installed aboard the ship and on several transponders, installed on submarine vessels (e.g. ROVs) or submersible structures. Following the KM3NeT-IT experience, the USBL positioning procedure has accuracy close to 1 m. Fig. 16X shows an sketch of a typical USBL system.

For KM3NeT-FR the positioning of the LBL elements will be performed thanks to a custom version of the RAMSES positioning system. In this system, the installation of an additional set of few USBL autonomous transponders, moored on tripods at the sides of the installation field is foreseen. This will permit, with minimal costs to set a reference and quickly re-calibrate the USBL system installed on the deployment ship during sea operation and facilitate the ROV navigation inside the telescope volume. The detection of USBL transponder signals by the LBL receivers will also permit cross-calibration of the USBL and LBL.

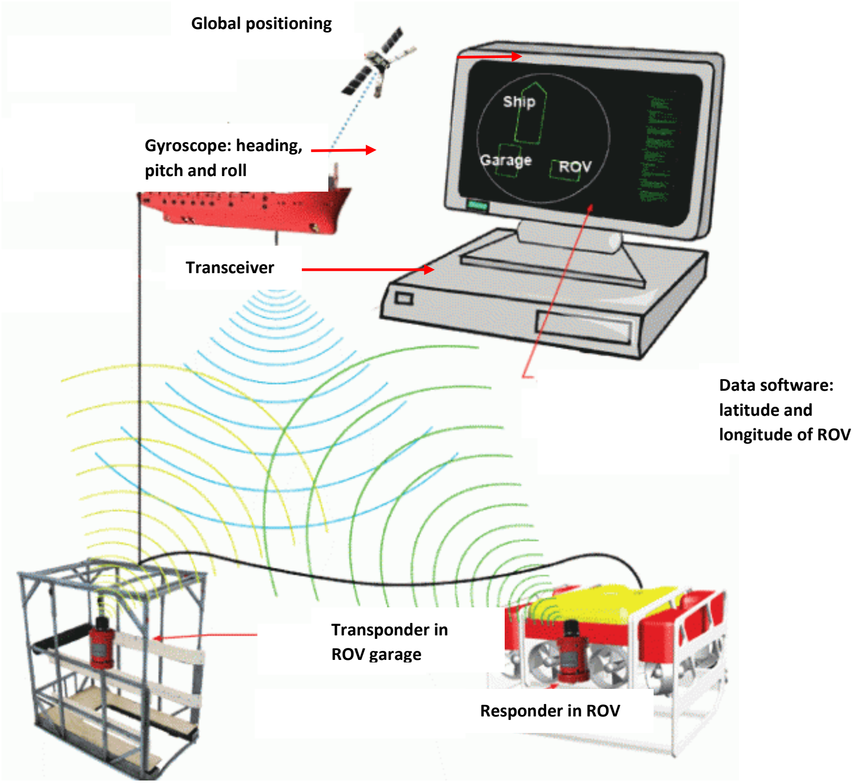

Fig. 1.16: Sketch of a typical USBL system for absolute positioning and ROV navigation.

1.3.3 DOM positioning procedure

The Acoustic Positioning data analysis is performed on-shore by a farm of PCs. These PCs receive, on an intranet, data from the Digital Acoustic Receivers (DARs), parsed from the main data stream. The receiver of the analogue signals are pre-amplified and digitized by a dedicated electronic board placed in the proximity of the receiver. The signal front-end and digitization board is also equipped with a data format converter to make acoustic data available in standard PCM-like format (hereafter AES) format.

The clock signal to each DAR is provided by the CLB, directly recovered from the Detector Master clock. This makes the system fully synchronous with the detector. The master clock frequency derived from the CLB is 25 MHz and the data sampling frequency is about 195.3 kHz. Data from each DAR are sent and treated by the DOM CLB, which time-stamps the received data and can select, via proper command from shore to propagate one or both data streams received from the DAR and to reduce the number of amplitude bits to be sent to shore. Fig. 1.17 shows data acquisition chain of the DAR array. These options allow flexibility of the system, aimed at adjusting the dynamic range of the DAR for low and high amplitude signals and permit also the reduction of the data flow to shore, when target signals (e.g. LBL beacon signals) have been clearly identified in amplitude and frequency. For biology and acoustic neutrino detection high-resolution data from a limited number of selected DARs will be continuously sent to shore.

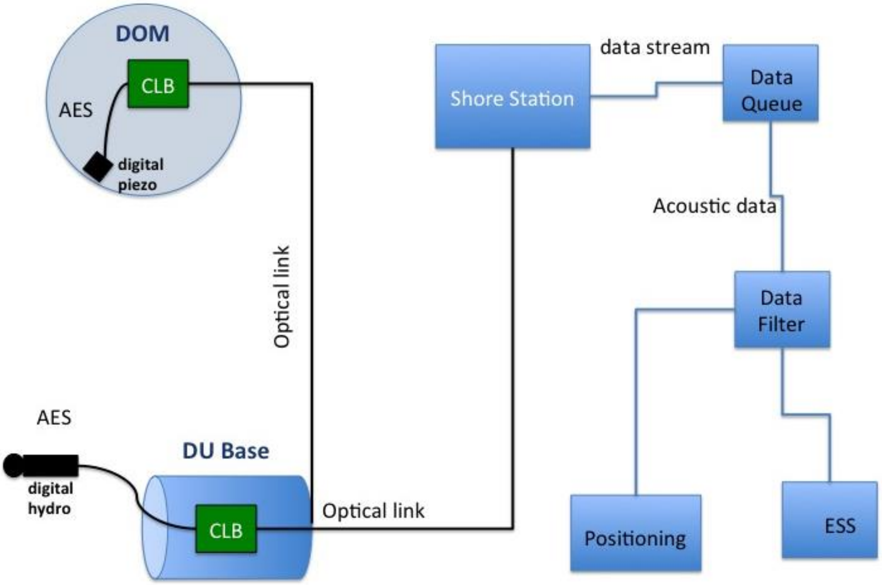

Fig. 1.17. Data acquisition chain of the Digital Acoustic Receiver (DAR) array, both for the hydrophone and the internal piezo-sensor.

The absolute GPS time is stamped in the data stream by the CLB, tagging unambiguously the acoustic signal detection time. The CLB sends continuously the received acoustic data stream to shore, embedded in the main DOM data-stream. Since all DOMs of the detector are synchronous and phased with respect to the GPS time signal transmitted from shore the whole acoustic receivers array is synchronized to the GPS master clock. Each DOM sends to the shore station, via optical fibre, the acoustic data, embedded in the main data stream, containing also data from PMTs and “slow control” probes. In the shore laboratory acoustic data are parsed and analyzed to identify LBL beacon’s signals and to calculate position of the receiver via multi-lateration.

The acoustic data filters analyze the piezo DAR data stream in real time searching for active beacon’s signals and storing a ToA data packet, for each identified beacon signal, with its quality factor, into the database. The DOM positioning algorithm reads, from the database, the ToA packets acquired during a beacon emission cycle by the piezo in the DOM, the beacons ToE, the position of the beacons and eventually calculates the average of the piezo position during the cycle (120 seconds) using a multi-lateration algorithm. In this case the Sound Velocity Profile (SVP) along the water column where the DU is installed must be measured, using data from the Instrumentation Unit. The multi-lateration code will be run using, as initial guess value, the DOM position calculated in the previous cycle. For the very first cycle the nominal position of the DOMs in the DU after unfurling will be used.

The beacon cycle duration is the same as per LBL calibration (120 seconds), that also allows cancellation of spurious signals due to surface reflections based on ToA - ToE difference. Being the depth of the higher DOMs about 700 m above of seabed for standard KM3NeT DUs (Capo Passero and Toulon) and about 300 m above seabed in the case of ORCA DUs (Toulon), the time emission differences between beacons are, indeed, also suitable to disentangle direct signals from spurious reflections also for the DOM DARs. The RMS value of the reconstructed coordinates of the piezo will be also stored in the DataBase.

The DOM Position Code will be based on the multi-lateration class for 3D positioning of the IT++ library, a C++ library of classes and functions for linear algebra, numerical optimization, signal processing, communications, and statistics under the GNU General Public License. The multilateration class implements geometry-based methods for localization based on spherical multilateration (which uses ToA ranging techniques), hyperbolic multilateration (using Time Difference Of Arrival, TDoA) and hybrid multilateration (both ToA and TDoA are used). In addition, it allows computing the theoretical performance of the algorithm based on Cramer Rao Lower Bound (CRLB). This step requires that the filtering algorithms have, as input, a) the characteristics of the signal emitted by each single active beacon (namely the signal waveform in the time domain), and b) the number of active hydrophone channels (1 or 2), c) the sampling frequency (195.3 kHz) and d) the signal quantization bits (24-default-, 16 or 12), this information is stored in the Data Base as run initialization and configuration parameters. The absolute ToA of the acoustic signal in the CLB-time is obtained directly from raw hydrophones' data flow. Hydrophones data (such as piezo data, used in the DOM position reconstruction) are transmitted by each CLB in proper packets (similarly to PMT data) and time stamped with the absolute CLB time (KM3NeT Collaboration 2011) properly set using the capabilities of the White Rabbit gear.

The absolute ToE of each acoustic beacon and the waveform of the signal to be emitted are set during run initialization and configuration, and are stored in the data base. Once again, the absolute time of emission of the signal is time-stamped thanks to the White Rabbit gear running on the CLB. The distance between each beacon (k) and each hydrophone (i) will be then calculated using the simple sound propagation algorithm:

$$D\ (i,k) = [ToA'\ (i,k) - ToE'(k)]\ /\ csound\ (depth{=}seabed + [hydro\_height + beacon\_height]\ /2) \tag{1.49}$$

where the apex indicates that the proper electronics time-delay (latencies) of the hydrophone and of the beacon must be considered in the calculation. These latencies are measured and stored in the data base.

The value of sound (sound velocity in sea water at the site) must be measured in advance using proper devices (profiling CTDs, Conductivity Temperature and Depth probes) or measured using site characteristics monitoring devices installed aboard the Instrumentation line. The Sound Velocity Profile (SVP) at each site is determined by the data of the CTDs and the sound velocimeters installed on the Instrumentation Units (IU). In Capo Passero a larger set of data will be available thanks to 2 sound velocimeters and 3 CTDs installed aboard the towers of the KM3NeT Italy project. The uncertainty on the absolute value of csound causes the largest error in the distance measurement: csound must be known at the level of few 0.1 per mille to achieve ~1 cm accuracy at 100 m and 10 cm at 1 km. However this uncertainty leads to a systematic error over the whole water volume with little impact on relative positioning.

Once all the distances D (i,k) are measured, the software tool runs a global minimization algorithm based on least mean square method to determine the actual position of all LBL elements. The use of different algorithms is also foreseen, and a proper entry in the database indicates which algorithm has been used for the position determination. A minimum of four LBL active beacons are needed to run this procedure.

1.3.4 The Internal Acoustic Receivers (Piezo-Electric Sensors)

The piezo-electric digital acoustic receiver is glued to the inner side of the glass sphere of each KM3NeT digital DOM (Fig. 1.18). The sensor is equipped with a cylindrical piezo-ceramics Pz27 (Ferroperm) with diameter of 18mm and height of 11.5 mm. The piezo ceramics and electronics are contained in a passivized aluminium tube of 20mm height and 20 mm outer diameter. The design sensitivity of the sensors is -160 ± 6 dB re 1V/Pa at 50 kHz with a ± 3 dB variation (long time average) in the 10–70 kHz range. However, these specifications hold when the sensor is glued to the inside of the glass sphere of a KM3NeT optical module and its response to pressure signals depends very strongly on the operation environment of the sensor. The sensitivity was reduced by a factor of 5 in amplitude (~14 dB) w.r.t. to the precursor design of the sensors with analogue readout. For the latter, a sensitivity of about -145 dB re 1V/Pa was measured in situ in the relevant frequency range. The distributions show a very flat behaviour in the range 10 kHz to 80 kHz. Beyond that frequency the anti-alias filter sets in. Below ~5 kHz a strong rise of the noise can be observed before the effect of a high pass filter, which is intended to prevent saturation of the sensor due to strong low frequency noise, becomes visible.

The tube is electrically on ground potential. Within the sphere, pressure is slightly below atmospheric value, cooling is achieved by the ambient water at a temperature of about 13°C. The digital data, clock signal and power supply are routed to a mating socket on the octopus board. The sampling frequency of the ADC is 195.3125 kHz derived for the 25 MHz clock. The ADC was chosen for this purpose because it can be operated in low power mode and contains a full band on-board digital FIR filter.

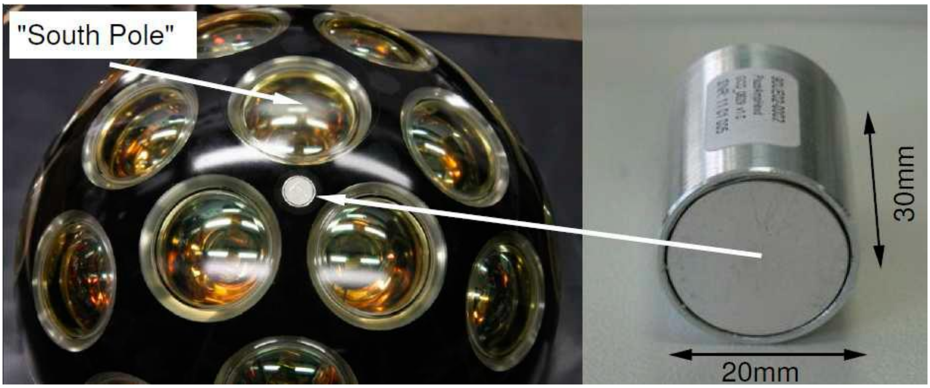

Fig. 1.18. Internal piezo-electric acoustic sensor of DOMs.

The readout of the ADC and the transmission of the data to the CLB is done with the Lattice Semiconductors FPGA ICE40LP1K-QN84. This is a low power device, which can be operated in the lab using a volatile flash memory that is erased when the power supply is switched off. For operation within the DOM, the firmware is written permanently into a non-erasable memory. The firmware submits the ADC data in AES3/EBU format. The firmware for the FPGA has been developed and has been tested to work with a commercial sound card in a PC that is designed to receive standard AES format data.

1.3.5 The External Acoustic Receivers (Digital Hydrophones)

External hydrophones will be hosted on the base of the DUs and on Calibration Bases, where no DOM is foreseen. These hydrophones will be used to calibrate the LBL, that is precisely measuring the relative distances among LBL elements and –when autonomous beacons are used- to measure the ToE of autonomous beacon. The selected hydrophone is the DG0330 manufactured by Colmar, Fig. 10X shows a picture of the external hydrophone. It consists of a spherical piezo-ceramic element, read-out by an analogue board splitting the signal in two lines with different gains (+46 dB and +26 dB respectively). The double gain feature has been implemented to avoid signal saturation when the hydrophone is placed close (about 1 meter) to the beacon -as in the case of Calibration Bases- and use the high gain channel to analyse data received from far (>500 m) beacons and to study fainter acoustic signals (bio-acoustics, environmental noise, acoustic neutrino detection). The two streams are sampled by a stereo 24 bit commercial ADC (CS-4270) and converted into AES protocol using a DIT (Digital Interface Transmitter). The clock frequency provided by the CLB is 25 MHz, and the sampling frequency of the device is 195.3 kHz. The hydrophone picture and its dimension and connection scheme are reported in Figure 1.19.

All the electronics is encapsulated in a hard epoxy resin moulded to the cable and to the ceramic head with an additional polyurethane moulding layer. An external stainless steel jacket is used for clamping the hydrophone. Proper connection to sea-ground is used to avoid risks of floating high voltage potential between the electronics ground and the sea ground. The power supply is 12 VDC and power consumption is less than 100 mA @12 V. The hydrophone is designed to accept power supply in a wider range from +9 VDC to +18 VDC. The time latency of the hydrophone electronics (including 4.5 m cable) has been measured using a dedicated setup and its value is 50.65 ±0.25 µs for the low gain channel and 50.71±0.25 µs for the high gain channel.

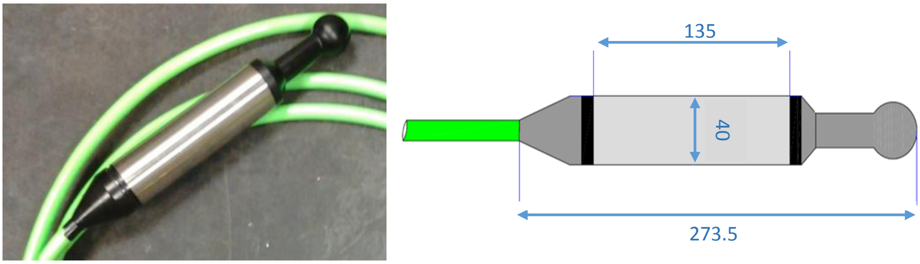

Fig. 1.19: The digital Colmar hydrophone used as external hydrophone in KM3NeT.

The hydrophones are delivered from the company after pressure-crush test at 400 bars (4000 m water equivalent) and shallow water calibration (that is sensitivity curve vs. frequency at 1 bar).

Two hydrophone productions are available, without and with an analogue signal high-pass filtering stage. The filter frequency is 700 Hz, to reject the low frequency ambient sea-noise (which follows a 1/f shape, and flattens at about 5 kHz) thus improve Signal to Noise ratio in the detection of beacon pulses (20-40 kHz). The not-filtered version can also be used for acoustic noise monitoring and marine bioacoustics. For Phase 1 the version of the DG0330 with high-pass filter will be used.

The external hydrophone is connected to the DU base and CB container though a Microwet Seacon MC-5-BH connector manufactured in hard-anodized aluminum. A 4.5 m long deep-sea cable (Falmat XtremeNet FM022208-08) terminated with a Microwet Seacon MC-5-IL (M) connector (hard-anodised aluminum) is part of the device. The hydrophone data are transmitted to the CLB for time-stamping and transmission to shore. The physical connection is obtained through a piggy-back extender of the CLB equipped with a RJ45 connector through which the power, data and clock signals are routed to/from the hydrophone.

1.3.6 The Acoustic Beacon

The acoustic beacons (AB) are the active elements of the KM3NeT Long Base-Line. The Acoustic beacons forming the “built-in” KM3NeT LBL will be installed in the calibration bases (CB) and Junction Boxes (for KM3NeT-IT). The same AB will be used as stand-alone LBL beacons (autonomous beacons) and will be installed on mechanical tripods, hosting the beacon and a battery pack to ensure correct functioning for few years. The AB is a broadband range acoustic emitter (20 kHz- 50 kHz) able to work at rating depths up to 440 bars in underwater environment. It provides the emission of short intense signals (Sound Pressure Levels of 180 dB re 1 µPa @ 1 m at 34 kHz) and has LBL functionality. The acoustic beacons were developed and tested by the Universitat Politècnica de València (UPV), as part of this thesis, and in association with the company Mediterráneo Señales Marítimas (Spain). Therefore, the work and steps performed for the design and development of the acoustic beacons for the KM3NeT Long Base Line positioning system is fully explained in the next chapter.

Acoustic beacons prototypes were installed on the base of the NEMO Phase II detector and in the ANTARES IL for deep sea long-term tests. They were successfully tested: several kinds of acoustic signals (monochromatic pulses and sweeps) were emitted, and detected in real time by the AMADEUS system (at the ANTARES Site) and by the SMO-NEMO Phase II hydrophones and PPM-DU (at the Capo Passero Site). The design of the electronic board for the LBL emitter was quite challenging due to the versatility and reliability required and the limitations imposed of working in deep sea. The board should provide short “high power” signals, starting from limited power available; additionally, the system has to be reconfigurable (signal type, amplitude, duration, and repetition rate) via an RS232 port of the CLB in the CB for “in situ” optimization of the signal detection. For the sake of positioning the time synchronization and calibration with respect to the detector master clock must be very accurate and stable. The Beacon Board is piloted by a dedicated CU base electronics that provides the bidirectional link to shore. Acoustic waveforms to be emitted are stored in a local memory that can be updated from shore via RS-232 link. The signal emission trigger is received from the CU base electronics, synchronized with the detector master clock.

The APS is important for a safe and accurate deployment of the mechanical structures and for precise reconstruction of neutrino induced events. In addition to these functionalities, referred to the detector positioning, the APS could also be an excellent tool to study the feasibility of an acoustic neutrino detector and a possible correlation between acoustic and optical signals. Next section presents the acoustic neutrino detection as other effective way of studying the neutrino interaction. The new detector KM3NeT is an excellent opportunity to continue with this investigation.

1.4 Neutrino Acoustic Detection

Ultra-High Energy (UHE) neutrinos (~10^{20} eV) have been of great interest for the study of ultra-high energy cosmic ray sources and to test fundamental physics due to its properties of being high-energy, stable and weakly interacting elementary particles. Besides Cherenkov light, radio or acoustic wave techniques have been proposed to detect the neutrino-induced energy deposition in water, ice or salt. These techniques, with much longer attenuation lengths, allow for very large target volumes utilizing either large ice fields or dry salt domes for radio or acoustics, and the oceans for acoustic detection.

Measuring acoustic pressure pulses in huge underwater acoustic arrays is a promising approach for the detection of cosmic neutrinos with energies exceeding 100 PeV. Acoustic detection of UHE neutrinos is based on the thermo-acoustic effect (Askaryan 1957), which is explained in more detail in subsection 1.4.1. Basically, when an UHE neutrino interacts with a nucleus in water, its energy is released in a volume of about a centimetre in radius and several meters in length. This phenomenon induces a local heating in a very short period of time leading to a short pressure pulse signal with bipolar shape in time and a very directional pattern (pancake-like), being emitted mainly in the perpendicular plane of the shower axis (Bevan et al. 2009).

Over the last few decades there have been a series of experiments looking into acoustic neutrino detection in both water and ice media, such as AMADEUS (Aguilar 2011), SPATS (Abdou et al. 2012), ACORNE (Thompson & Perkin 2008) and SAUND (Vandenbroucke 2005). A lot of knowledge was gained with all these experiments which have mostly been used for fundamental feasibility studies, referred to environmental conditions and its influence on the acoustic neutrino detection, background noise and acoustic signal propagation and localization. Moreover, acoustic neutrino flux limits were established and improved with the experience of these detectors. The acoustic detectors are composed of many acoustic sensors distributed in a wide instrumented volume; by measuring the acoustic induced neutrino pulse with several sensors it will be possible to infer the neutrino direction. The interest in this technique is related to the large attenuation length (~km) of the sound in water (or ice). Consequently it is possible to instrument a huge volume using a relatively low number of sensors. The detection technique is still under study and could be implemented in a new optical neutrino telescope KM3NeT (Ageron et al. 2008). The acoustic detection would allow the combination of those two neutrino detection techniques for a hybrid underwater neutrino telescope, especially considering that the optical neutrino detection technique needs acoustic sensors to monitor the position of the optical sensors (Viola et al. 2013, Viola et al. 2015).

1.4.1 The UHE Neutrino and the Thermo-Acoustic Effect

The thermo-acoustic effect, following a UHE neutrino interaction was first predicted by G. A. Askarian in 1957 (Askaryan 1957) further developed by Learned in 1979 (Learned 1979) and confirmed experimentally (Sulak 1978). The shower, originated by UHE particle interacting in water, develops almost at the speed of light releasing a macroscopic energy in the medium. The resulting energy deposition in a cylindrical volume of a few centimetres in radius and several metres in length (from 5m to 10 m) lead a local heating of the medium which is instantaneous with respect to the acoustic process. This temperature change induces an expansion or contraction of the medium depending on its volume expansion coefficient. According to the thermo acoustic model, the accelerated motion of the heated volume forms a pressure pulse of bipolar shape in time which propagates in the surrounding medium.

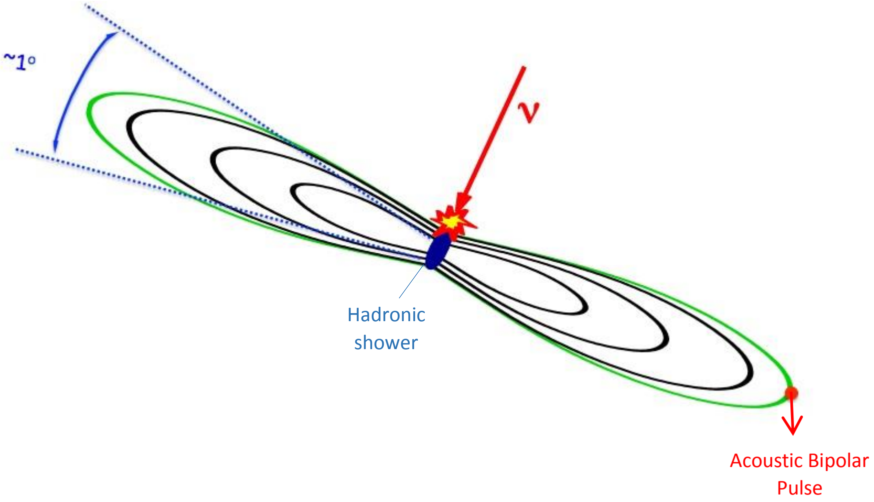

Figure 1.20. Scheme of the neutrino energy deposition in the water and the subsequent generation and propagation of the bipolar pulse.

Coherent superposition of the elementary sound waves, produced over the volume of the energy deposition, leads to propagation within a flat disk-like volume called *pancake* in the direction perpendicular to the axis of the particle cascade (see Fig. 1.20); the total acoustic radiation is confined to a narrow angle which is less than 1º. It is a very directional *pancake* and short bipolar pulse. The bipolar pressure pulse has a peak-to-peak amplitude of the order of 10 mPa (5 mPa) per 1 EeV cascade energy at a vertical distance of 200 m (500 m) from the cascade (Bevan et al. 2009). After propagating several hundreds of metres in sea water. The peak-to-peak signal length is several tens of microseconds, resulting in a spectral energy density peaked at about 10 kHz, whereas more recent studies predicted a higher frequency of 23 kHz. As a reference example, shown in Fig. 1.21, at 1 km distance in direction perpendicular to an ultra-high neutrino energy of energy1 EeV= 10^{18} eV.

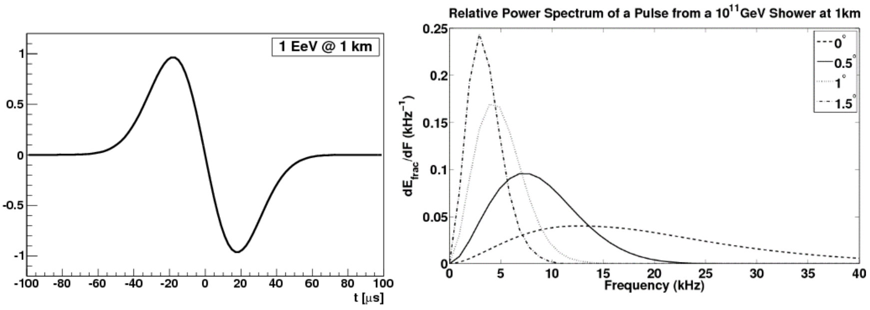

Figure 1.21. Acoustic signal from an energetic neutrino induced particle shower (left) and relative power of a pulse as a function of the frequency (right). The spectrum is plotted for various angles w. r. t. to the plane perpendicular to the particle shower axis.

According to the model, the energy deposition of charged particles traversing liquids leads to a local heating of the medium which can be regarded as instantaneous with respect to the typical time scale of the acoustic signals. Because of the temperature change the medium expands or contracts according to its volume thermal expansion coefficient α. The accelerated motion of the heated medium produces a pressure pulse which propagates through the medium. The wave equation describing the pulse is:

$$\vec{\nabla}^2 p(\vec{r},t) - \frac{1}{c_s^2}\cdot\frac{\partial^2 p(\vec{r},t)}{\partial t^2} = -\frac{\alpha}{C_p}\cdot\frac{\partial^2 \varepsilon(\vec{r},t)}{\partial t^2} \qquad (1.50)$$

Here $p(\vec{r},t)$ denotes the pressure at a given place and time, c_s the speed of sound in the medium, C_p its specific heat capacity, α the thermal expansion coefficient and $\varepsilon(\vec{r},t)$the energy deposition density of the particles.

The spatial and temporal distribution of ε is not accessible to laboratory experiments at the relevant primary neutrino energies $E \approx 10^{18}$ eV and hence is subject to uncertainties. Simulations depend on both the extrapolation of parameterisations for lower energies into this regime and on the transcription of simulations for extended air showers to showers in water. Monte Carlo simulation of neutrino interactions in water for a cascade energy has been developed in previous studies (Bevan et al. 2007) (Simeone 2008), where the energy deposition is modelled using Monte Carlo points with a density proportional to energy.

1.4.2 Acoustic Background

The acoustic neutrino signal detection in sea water is affected by the background noise present in deep sea such as the continuous ambient noise and transient signals with bipolar shape coming from fauna and anthropogenic sources. Moreover, refraction due to a depth-dependent sound-velocity profile can channel surface noise towards the detector or reduce it. The ambient noise is caused by the agitation of sea surface and thermal noise. It governs the frequency range of interest, i.e. the frequency range with the best signal-to-noise ratio, which is in the range 10 to 50 kHz. The RMS of the noise in this frequency range is 7.1, 17, 53 and 130 mPa for sea state 0, 1, 3 and 6, respectively. The rate of occurrence for these conditions is site dependent, Fig. 1.22. shows the power spectral density of underwater noise in shallow water.

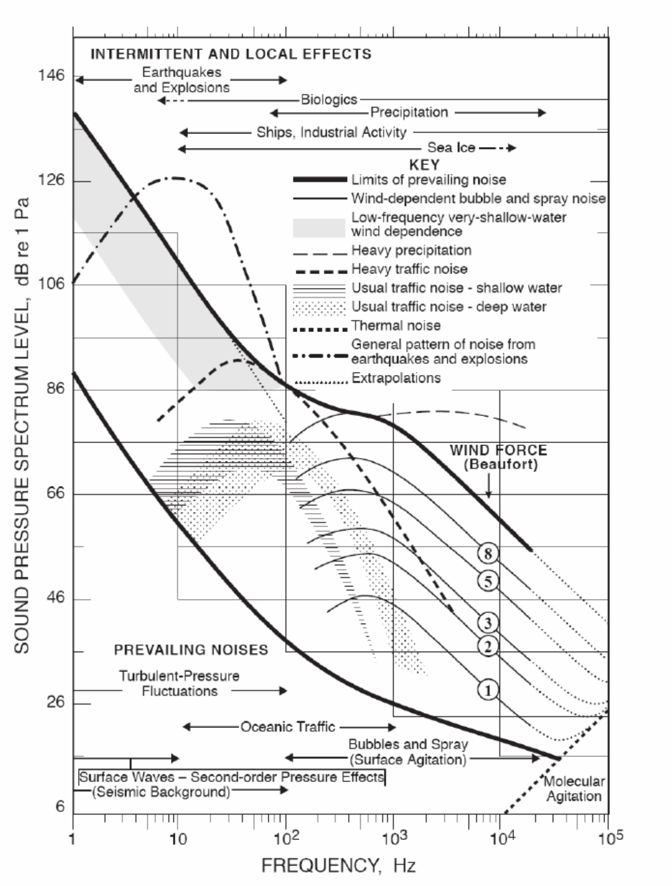

Fig. 1.22. Power spectral density of underwater noise measured by Wenz in shallow water (Wenz 1962).

The sources of the transient background which is mimicking neutrino-induced signals are frequently signals from cavitation of ship propellers and sea mammals. Especially dolphins generate bipolar signals with their echolocation clicks. The transient background is very variable in rate of occurrence and spatial density, its composition is site-dependent. These background signals have to be discriminated from neutrino-induced signals in order to be able to ensure the neutrino signal detection.

The major contributions to this spectrum, as function of frequency, was summarized from the data taking with OvDE experiment in NEMO Collaboration (Riccobene 2005) as follow:

1) Below 10 Hz. The main stationary noise source is the seismic background and the transient signals can be attributed to explosions or earthquakes.

2) Between 10 Hz and 2 kHz. The diffuse noise is due to naval traffic and transients to ship motion. Only a negligible part of the neutrino signal energy lies in this frequency regions while most of the ambient noise power is at low frequency.
3) Between 2 kHz and 40 kHz. This is the most important and most variable region of the spectrum. The main contribution to stationary random signal in this region is due to wind and rain interactions with the sea surface; the variability is strictly linked to the weather conditions. Transient signals arise from ship cavitation, sonar and cetaceans, moreover quasi deterministic stationary signal are due to acoustic pingers. In this frequency range lies most of the neutrino signal energy.
4) Above 40 kHz. Only few data in this region are known in literature and none of them is recorded in deep water; anyway the main contribution to the PSD in this part of the spectrum is believed to arise from thermal noise of water molecules. This contribution, reported in figure 5.7 as extrapolation, has a dependency on frequency proportional to f^2 so dominates at high frequency.

1.4.3 Acoustic Sensors Array

In most test setups, the acoustic sensors are grouped to clusters or acoustic antennae, each with a volume in the range of a cubic metre and four to six sensors (Graf 2013). The data of all sensors is digitised individually but the proximity of sensors is utilised in the processing strategies for the data (Richardt et al. 2014). This concept has several advantages: Random coincidences of noise mimicking a neutrino-induced signal can be suppressed by a factor of one over the square root of sensors in the antennae. For coincidence test and comparison of the signals between different sensors, only small time scales on the order of milliseconds have to be analysed, thus reducing the necessary computational effort. In addition, the direction to the source can be reconstructed on the antenna level and by combining several antennae the source position can be triangulated. The geometry of the sensor array and primarily the spacing of active elements is not governed by the attenuation length of sound (as it is for light in Cherenkov detectors) but by the geometry of the sound emission: the pancake, with dimensions of 10 to 100 m parallel to the cascade axis and several kilometres perpendicular to it (depending on the initial energy of the cascade). This translates into an asymmetric spacing of adjacent acoustic sensors or antennae: the horizontal spacing can be on the order of several hundred metres; the vertical spacing should be denser with sensors/antenna every few ten meters.

These considerations can be used to determine a rough estimate for the energy threshold of the acoustic detection method: assuming a signal-to-noise ratio of 1, where a neutrino-induced signal can be clearly identified online in the background which is on the 10 mPa level. The discussed array geometry leads to a typical distance between cascades and neighbouring sensors inside the array on the order of 200 m. Consequently, cascades with signal amplitudes of 10 mPa at the sensors and with energies above 1 EeV can be detected. If an external trigger is available, e.g. from the optical part in an opto-acoustic detector, the threshold would be significantly lower as additional information (interaction vertex and event time) would be utilised to search for the acoustic signal inside the background.

1.4.4 Acoustic Signal Processing

One of the most challenging issues in the acoustic neutrino detection field is developing an algorithm able to analyse the acoustic data recorded by the underwater array hydrophone that is able to detect the acoustic signal produced by the shower induced by neutrino interaction in water (Graf 2013). The complexity of this task is large; small signals have to be found in the ambient noise at a signal-to-noise ratio near or even below unity, and also neutrino-induced signals have to be distinguished from neutrino-like background signals. For the first task, digital signal processing techniques, usually matched filters or related techniques, are employed (Danaher et al. 2007). The second task can be approached on two levels: First, for the signal classification of data from one sensor or an antenna, machine learning algorithms (primarily boosted decision trees or random decision forests) show promising results. When those algorithms are used for features extracted from antenna data, classification errors in the percent range are achieved (Neff et al 2013). The second level is given by the angular emission characteristic of a neutrino interaction: the pancake. All other sources are expected to show a different geometry: either a point source or an extended source, but not a cylindrical one. With the existing small test setups, taking advantage of this last point is not possible, as the number of acoustic antennae is too low. However, clustering algorithms can help here, looking for aggregations of signals that are causally connected, e.g. emitted on a straight line or from the same point in space over a sequence in time.

1.4.5 Acoustic Neutrino Calibration

From the experience gained with the previous experiments related to acoustic neutrino detection, improvements in the hardware (sensors) and software (algorithms) has been developed, and they will be applied to the new telescope KM3NeT. However, distinguishing the acoustic neutrino signal from the background noise at deep sea keeps being a difficult task. For this reason, new methods for training the acoustic neutrino detection are needed, such acoustic transmitters that send artificial acoustic signatures similar to UHE neutrino interactions in the sea. Since the emission and reception of the signals sent with the acoustic neutrino calibrator to the detector would be synchronized and controlled, it will help to recognize the neutrino-like signal and work on better filtering and detection algorithms.

Previous work was developed in acoustic neutrino-like signal sources; a phased emitter array (Saldaña 2011) (Ooppakaew 2012) and parametric emitter array (Adrián-Martínez et al. 2013b). The first work, an eight-hydrophone linear array of about 8 meters length was developed by the Northumbria University team for the generation of emulated UHE neutrino-induced pulses at the frequency of 23 kHz. A bipolar acoustic generation was built using 8-bit PIC microcontrollers for processing and control. Signal processing techniques were applied to array hydrophone modelling and experimental data. The eight-hydrophone transmitter array was able to generate bipolar acoustic pulses of 23 kHz. The simulation showed that the eight hydrophones arranged over an eight-metre spacing structure can mimic the anticipated pancake behaviour predicted from neutrino-induced showers as well as generating the acoustic bipolar pulse shape of sufficient amplitude for detection at ANTARES. Finally, the system was tested from a vessel at the ANTARES site in September 2011. A range of test signals including 23 kHz bipolar pulses, sine signals and orthogonal signals were injected into seawater to simulate neutrino interactions and investigate signal coding. Signal processing techniques were applied to the data deployed in order to recognise the signals emitted. However, the vessel was far away from the position planned (~1km), hence the signal received was too weak and no signal was detected.

The second work developed for in situ evaluation of the acoustic neutrino technique was a compact array calibrator prototype developed by the Universitat Politècnica de València group (Adrián-Martínez 2015). The goal was designing an autonomous and optimized system able to reproduce the acoustic signal (shape and directionality) produced by neutrino interaction using the parametric acoustic sources technique. The parametric acoustic source technique was tested and validated for the emission of low-frequency bipolar pulses with high directionality allowing to set a compact array design. The calibrator was able to work in two operation modes: low and high frequency. On one hand the low frequency mode allows the system to deal several acoustic-related tasks in an underwater neutrino telescope such as calibration of the receiver sensors, or use it as emitter for acoustic positioning purposes. On the other hand the high-frequency mode is used for acoustic neutrino detection calibration by generating directional bipolar pulses using the parametric technique. The prototype was successfully tested in low-frequency mode. However, the assembly of the transducers was a critical aspect. Due to the low efficiency of the parametric generation, at long distances, the interaction of the parametric beams was crucial in order to reach enough amplitude levels. For better interaction of the three beams, all of them should travel parallel. This aspect forced the selection of the most favourable radiation surface or, in a future prototype, the elements re-assembly in order to have the same radiation behaviour along the entire cylindrical surface array. The power electronics for high frequency mode were not completed in order to be able to use the compact calibrator with all functionalities, and because of this limitation it has not been tested in situ yet.

After all the achievements gained with the compact array calibrator the group of Universitat Politècnica de València (Adrián-Martínez et al. 2013a) decided to design a new compact array based on the parametric emission which is part of the work developed in this thesis (Saldaña et al. 2016).This step was also taken for the fact that the new optical neutrino telescope KM3NeT is under deployment and since it will include an acoustic positioning system, it could be an excellent opportunity to test the acoustic neutrino detection technique. The proposed design for the acoustic calibrator is a compact array system composed of piezo-tube ceramic transducers which emits in the radial direction. The new proposed array calibrator design was performed to obtain a more energetic and directional bipolar pulse. It is a flexible system composed of five piezo-tube ceramics structured in the same axis-line by using a straight aluminium bar that holds the tube transducers from the inside. This ensured to have a good alignment of the array transducers which helped to have the same radiation behaviour of each element. The array system was designed in a way that permit to configure the number of the emitters (three to five elements) and the distance between them without difficulty. This allows to find and use the best solution configuration for the emission of the artificial acoustic neutrino signal. Moreover, the piezo-ceramics selected for the new calibrator were properly selected in function of the resonance frequency, power emission, dimensions and costs. All the details about the development, characteristics and state of the new UHE neutrino array calibrator will be explain in Chapter 4 of this thesis.

The final goal of the acoustic calibrator is its deployment in the vicinity of the detector. Depending on the deployment setting, the distance between the emitter calibrator and the detector could vary from 0.5 to 3.5 km. The furthest distances would occur when the calibrator would operate from the sea surface, and the closest from the seabed. Consequently, the acoustic calibrator will need to send a powerful signal in order to reach the detector with enough pressure to be detected. The generated neutrino signal suffers attenuation when propagates through the underwater environment due to spherical divergence and the media absorption. In order to predict the pressure level of the neutrino acoustic signal (transmitted with the array calibrator) at the detector, simulations of the acoustic wave propagation are needed.

The method used for the neutrino signal propagation prediction is detailed in section 1.2.2. As an example of its application in the propagation of a neutrino bipolar pulse signal, a bipolar pulse of 1 Pa and 23 kHz was used for applying the propagation simulation based on the ACORNE attenuation method. Fig. 1.23 shows the results of the bipolar pulse propagation until 2500m of distance (Saldaña 2011). The bipolar pulse amplitude at 23 kHz and 2500m of depth is attenuated 0.5785 Pa per 1 Pa (attenuation of 0.4215 or -7.5 dB), moreover the signal has a phase shift which slightly distorts the pulse.

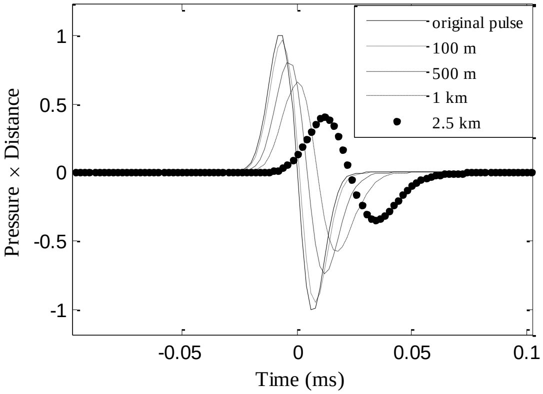

Fig. 1.23. Simulation of the UHE neutrino attenuation with the distance in the Mediterranean Sea using ACORNE method for the acoustic bipolar pulse at 23 kHz.

This method of predicting the amplitude and shape of the acoustic bipolar signal, after travelling through the underwater media, until the detector site will be applied to the experimental bipolar pulse signals recorded from the emission of the acoustic neutrino calibrator. The acoustic bipolar pulses recorded from the calibrator emission will be measured experimentally in the laboratory tank and swimming pool and they will be extrapolated until the detector site after applying the ACORNE attenuation method. This will allow to know ‘a priori’ the levels reached at the detector with the neutrino calibrator array.

2 Acoustic Beacon Development for the positioning system of KM3NeT

In this chapter the Acoustic Beacon (AB) developed as part of the Acoustic Positioning System (APS) of KM3NeT is described. In a first stage, the previous work done for developing the first emitter prototype is introduced. This prototype was installed in other neutrino telescopes, such as ANTARES and NEMO, in order to be tested *in situ*. The analyses and results obtained from the tests are shown. With this aim, signal processing techniques such as advanced cross-correlation methods and filtering with broad-band ultrasound signals were also applied for optimizing the acoustic emission and position detection. In a second stage, the design phases of the final acoustic beacon system are explained and the work done for a precise laboratory test is detailed. In a third stage, the integration of the first AB units on the detector positioning is described, and the results obtained from the in situ test are presented. Finally, the simulation studies the optimal positions selection for integrating more acoustic beacons in the LBL positioning system of the detector is shown.

2.1 Validation of the Emitter Prototype

The work on developing a first prototype (Larosa et al. 2012a) of the acoustic beacon begun before this thesis (Larosa 2012b). The aim of this work was to set and develop the AB, based on the previous work, in order to accomplish the main requirements for the APS of KM3NeT detector and validate it as emitter. The AB prototype was composed of an acoustic transducer and an electronic board named Sound Emission Board (SEB) (Llorens et al. 2012). The first part of this section makes a brief introduction of the prototype system, showing its acoustic and electronic characteristics, the emission operation and the acoustic transmitting levels.

The AB prototype was integrated in the ANTARES and NEMO detector sites to be tested *in situ*. In this thesis, the work performed in the processing and analysis of the data recorded during the tests is presented. This study allowed checking its functionality and reach under similar conditions to those of KM3NeT telescope, and therefore, validate the AB prototype as promising acoustic emitter for the KM3NeT detector. In the second part of this section, the characteristics of the *in situ* test performed is described, the signal processing techniques are explained and the results in terms of Time of Arrival (ToA) detection and acoustic reach are shown.

2.1.1 Ultrasonic transducer FFR SX30

The selected transducer was a commercial Free Flooded Ring (FFR SX30) manufactured by Sensor Technology Ltd. , which is an efficient transducer that provides reasonable power level over wide range of frequencies and deep ocean capability. The transducer have ring geometrical form, where the hydrostatic pressure is the same on the inside and the outside. This characteristic form reduces the change of the properties of piezoelectric ceramic under high hydrostatic pressure. According to the manufacturer they can work in the 20 kHz - 50 kHz frequency range; without depth limitation for operation (tested up to 440 bars) with a transmitting voltage response of 133 dB re. 1μPa/V at 1m for frequency of 30 kHz. These transducers are simple radiators and have omnidirectional directionality pattern in the perpendicular plane to the axis of the ring, while in the planes containing the axis there is a minimum (reduction of about 5 dB) of sensitivity response at 60º. The FFR SX30 transducer has dimensions of 4.4 cm for the outer diameter, 2 cm for the inner diameter and 2.5 cm height. The transducer was moulded in a long cylindrical shape in order to adapt it to the mechanical holding and have a better protection. The sensitivity of the moulded transducer has very low variation with respect to the bare transducer; presenting a reduction of 1 - 2 dB for some frequencies. The maximum input power is 300 W with 2% duty cycle.

2.1.2 Sound Emission Board (SEB)

The SEB was designed for low-power consumption and it is adapted to the neutrino infrastructure using power supplies of 12 V and 5 V with a consumption of 1 mA and 100 mA, respectively. It is able to emit arbitrary intense short signals based in the Pulse-Width Modulation technique. The communication of the board with the PC is established with the standard protocol RS-232 through an adapter RS-485 put in the board. The transmitting power achieved with the transducer and SEB is 173 dB (re. 1μPa@1m) for 35 kHz frequency (the middle panel of Fig. 2.1).

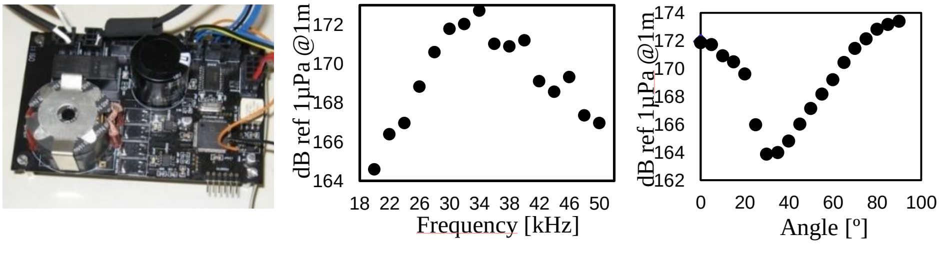

Fig 2.1. Left: a picture of the Sound Emission Board (left), Transmitting Power (TP) versus frequency (middle). Right: TP versus angle for the frequency of 30 kHz.

2.1.3 Detection Strategy and Signal Processing Techniques

The distance from emitters and receivers can be of the order of 1-2 km, therefore acoustic emitted signals suffer a considerable attenuation and arrive to the acoustic receivers of the detection units with a low signal to noise ratio. The noise masks the signal making its detection and the accurate knowledge of its arrival time a difficult goal (M Ardid 2009). Therefore, signal processing techniques had to be used to improve detection capabilities (Adrián-Martínez et al. 2015).

The time of arrival (ToA) is determined by the difference between the emission time and the initial time of the receiving signal. The receiving time is obtained by two different methods: the threshold method in time domain (mainly used for the sine signals) and the cross-correlation method (mainly used for the broadband signals), such as sine sweep and maximum length sequence (MLS) signals (Bou-Cabo et al. 2013). The threshold method determines the initial time of the received signal by taking a rise time value of the received signal envelope after applying a band-pass filter centred in the frequency of the emitted signal. The cross-correlation method determines the arrival time of the received signal by taking the interval of time corresponding to the maximum peak of the cross-correlated signal with the expected emitted or received signal. This technique is more favourable for broadband signals (sweeps and MLS) because they have a narrower correlation peak and consequently the mean peak is easier to discern from the other peaks with good precision. Fig. 2.2 shows a tone (first row), a sweep (second row) and a MLS (third row) received signals for a distance of 112.5 m between emission and reception (E-R) in some measurement tests made in Gandia’s harbour. On the left, the receiving signals in time domain after applying a high order band pass filter are shown (the original recorded signal in time is noisy so the receiving signal is masked). On the right, it can be seen the cross-correlation of each signal (without prefiltering) where direct signal reflections are easier and more effective to discern that working in the time or frequency domain, especially for the broad bandwidth signals (narrower auto-correlation peak).

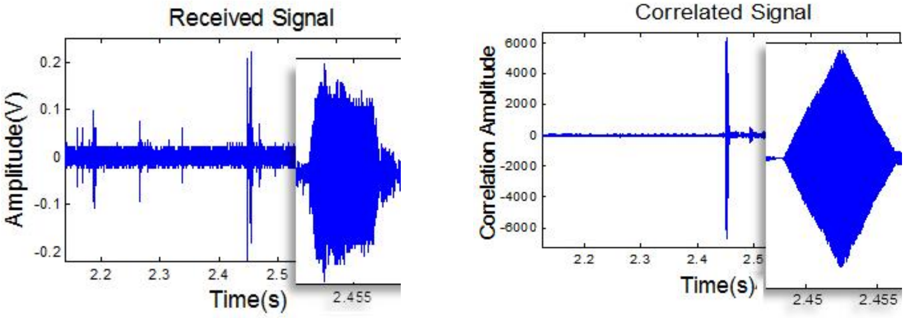

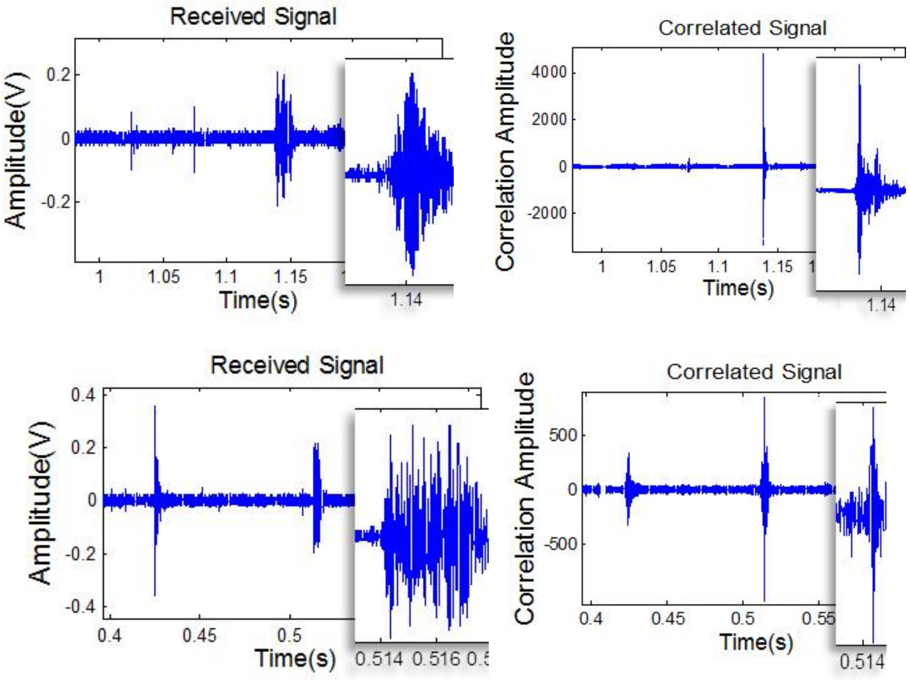

Fig 2.2. Example of recorded signals at 112.5 m E-R distance in the harbour of Gandia.

The right graphic of Fig. 2.3 shows an example of cross-correlation method for received sine sweep signal from 28 kHz to 44 kHz and the left graphic of Fig. 2.3 shows an example of threshold method for received sine signal of 40 kHz signal. The cross-correlation method has advantages in terms of accuracy in the time of detection and improves the efficiency of the detection time and the signal to noise ratio (S/N). Besides, it has a better discernment for echoes.

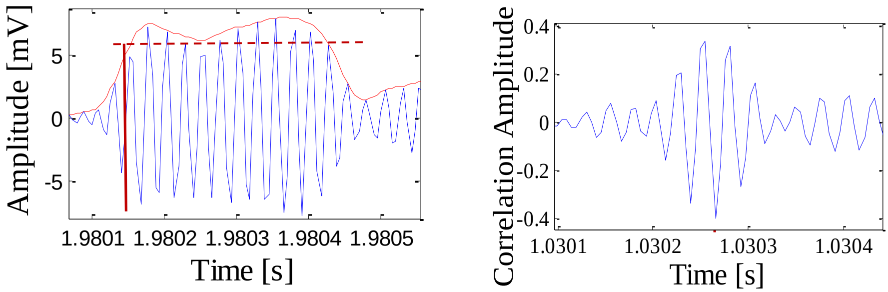

Fig 2.3. Examples of: received sine signal of 40 kHz with envelope (left graphic), cross-correlation of received sine sweep signal from 28 kHz to 44 kHz (right graphic).

2.1.4 In Situ Tests in ANTARES and NEMO

The AB prototype was finally integrated in the active anchor of the Instrumentation Line (IL), of the ANTARES detector (Marselle, France) in 2011. And in the base of the NEMO Phase II tower (Capo Passero, Italy) in 2012. In both detectors the acoustic transceiver was integrated in an anchor of a detector line and the SEB was installed, separately, in a cylinder container named Laser Container holding also other electronic parts and the Laser Beacon system (LB) used for timing calibration purposes. A cylindrical container of titanium provides the mechanics structure where the different devices of the laser beacon are integrated (Ageron 2011).

Different *in situ* tests were performed with the AB prototypes installed in the neutrino telescope infrastructures (Saldaña et al. 2015). The signals emitted during the tests were selected at different frequencies, as well as, using different types of signals in order to make a deeper study of its functionality. The selected signals were three sine signals of 20 kHz, 30 kHz and 40 kHz, two sine sweep signals from 20 kHz to 48 kHz and from 28 kHz to 44 kHz, and a MLS signal. The received signals were analysed through specific methods and strategies in order to extract the Time of Arrival (ToA) variation stability, and the pressure level reach.

In order to analyse and study the received signals from the in situ test of the emitter prototype, the next analyses and studies of the receiving acoustic data were performed:

- Recorded Signal Spectrogram.
- Signal in time and frequency domains.
- Correlation of the recorded signal with the emitted signal.
- Amplitude, arrival times and gap between consecutive receptions.
- Pressure amplitude per floor.
- Power emission of the system from data.
- Arrival times of each signal received per hydrophone (ToA).

2.1.4.1 ANTARES In Situ Test

Data recorded in ANTARES test was taken by the hydrophone HTI-27 placed in the 22nd storey of the line L12 at 395 m from bottom (pointing to the top) and in a distance of 240 m from the IL. The emitter is placed at the IL, 3 m over the base of the line, therefore, the distance between emitter and receiver is of 460 m, the configuration schematic of the emitters and receivers is shown in Fig. 2.4. Under this configuration, receiver sensitivity was -133 dB re V/µPa for the frequency range from 20 kHz to 50 kHz. Concerning to the emitter it was orientated in an angle of 31.6º respect to the receiver, hence the transmitting power was about 163 dB re 1 µPa @ 1m. The emitted signals, they were sent in sequences of 20 pulses. Recorded signals analysed had durations of around 50.3 seconds. The emission sample frequency was 400 kS/s and recorded signal were sampled at 250 kS/s. The synchronization between emission and reception was determined with the time stamped of the acoustic events triggered in the test.

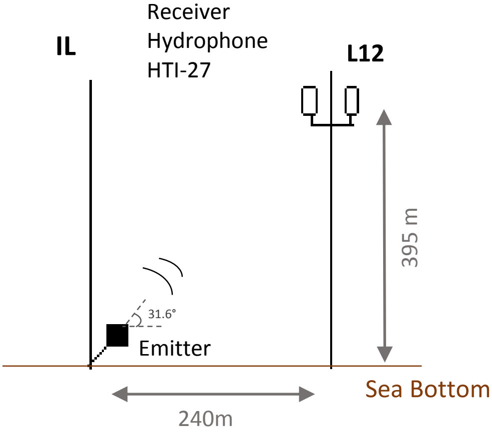

Fig 2.4. Schematic of the ANTARES acoustic test configuration.

As an example of the received signals during the test, Fig 2.5 shows a sine sweep signal sequence recorded in the test performed and its cross-correlation. It shows that working with the cross-correlation, the amplitude of the signal increases 100 times more, with a consequent improvement in the acoustic detection. Fig. 2.6 shows a single received signal of the Sine Sweep emission in time and frequency domains. The signals are clearly detected and have good signal to noise ratio, so they can be analysed using different methods in time or frequency domains. A decrease in amplitude between 28 kHz and 30 kHz was observed in this *in situ* tests.

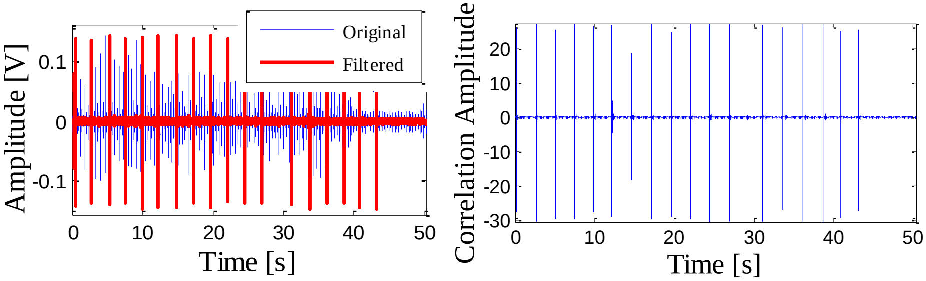

Fig 2.5. Sine sweep signal from 20 kHz to 48 kHz: recorded signal (left) and correlation (right).

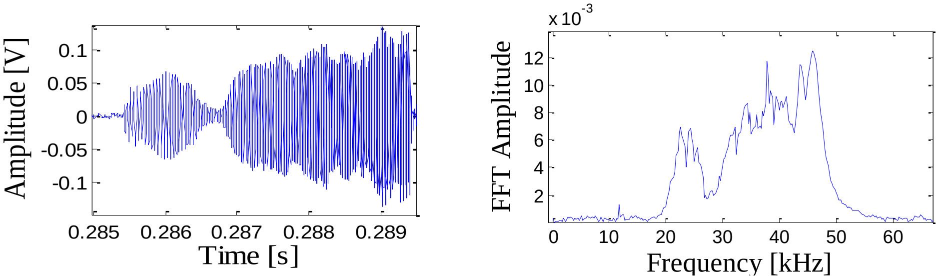

Fig 2.6. Sine sweep signal from 20 kHz to 48 kHz: a single received signal in time (left) and frequency (right).

- *Signal Propagation Study*

A signal propagation simulation was performed in order to estimate the detection reach of the emitted signals with the AB prototype over farther distances (on the km range). For this aim, the procedure followed for the signal extrapolation in distance was using an algorithm that works in the frequency domain and propagates each spectral component considering the geometric spread of the pressure beams as 1/r and its absorption coefficient (Bevan et al. 2009) (Francois & Garrison 1982). The propagation code starts taking the received signals from the experimental measurements (by the receiver HTI-27) in time domain and converting them into the frequency domain. Then, knowing the receiver sensitivity, the pressure amplitude of each spectral component is obtained and also the pressure amplitude at 1 m from the source. In this point, the propagation losses were calculated for each spectral component considering the medium absorption coefficient (for the conditions of the ANTARES telescope) in addition to attenuation generated by spherical divergence. Fig. 2.7 shows a diagram of the signal propagation procedure.

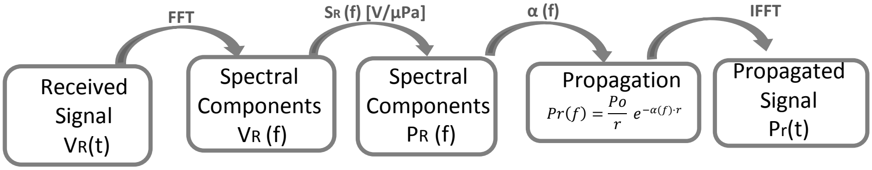

Fig 2.7. Diagram of signal propagation simulation procedure.

	N^{er} of pulses	**Amplitude in time [Vpp]**	**Pressure [Pa]**	**Signal to noise ratio [dB]**
Sine 20 kHz	9	0.293±0,005	0.925±0.016	12.033
Sine 40 kHz	8	0.258±0,004	0.647±0.010	10.737
Sine Sweep 28kHz-44kHz	9	0.286±0,007	0.760±0.019	12.144
Sine Sweep 20kHz-48kHz	9	0.294±0,006	0.828±0.017	12.144

Table 2.1. Detection characteristics of the received signals with the emitter prototype in the *in situ* ANTARES test. Emitter and receiver are distanced of 460 m and the angle of the emitter is 31.6º.

The simulation of the received signals propagation was performed until a distance up to 2.16 km in order to know the pressure levels reached, the amplitude signal received by the hydrophones and its correlation amplitude. The pressure amplitude of the acoustic waves emitted by the FFR+SEB prototype as a function of the distance is shown in the left plot of Fig. 2.8. It was determined for 20 kHz and 40 kHz tone bursts, and from the sine sweeps (20 kHz to 48 kHz range, the pressure amplitude was taken for the frequencies of 30 kHz, 35 kHz and 40 kHz). The acoustic pressure values at 1 km from source are between 33 mPa and 46 mPa, depending on frequency. At 1.5 km the pressure values are between 22 mPa and 25 mPa. These signals could be detected by the ANTARES receivers since they can detect signal pressure amplitudes of 20 mPa under calm sea conditions. The waves sent by the emitter at 2160 m of distance from source do not reach the minimum detection levels, which are between 10 mPa and 13 mPa, depending on frequency. The signal to noise ratio (S/N) of the acoustic received signal propagated is shown in the right plot of Fig. 2.8. There is a favourable signal to noise relation (>0) for the acoustic signal up to about 1 km.

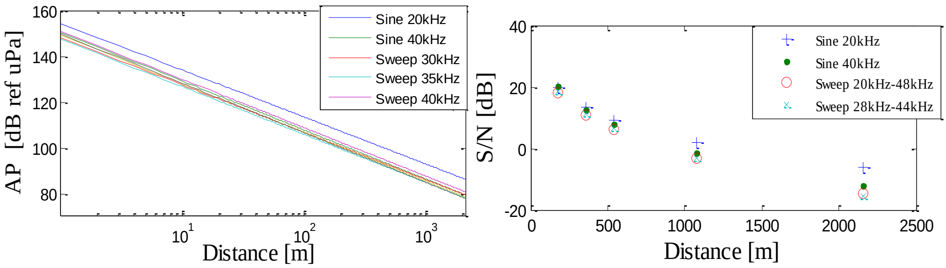

Fig 2.8. Pressure amplitude as a function the distance (left). On the right, the signal to noise ratio (dB) per signal for sea water conditions of ANTARES site.

Finally, in order to determine the reach of the system in terms of time detection accuracy for the environmental background noise conditions, the propagated signals were introduced in 100 random (but known positions) of the real noise registered in the ANTARES site. We studied the ability of detecting them as a function of the distance (from 180 m to 2.16 km) using the cross-correlation method. The diagram of Fig. 2.9 shows the procedure of determining the correlation of the propagated signal in the environmental noise of the detector.

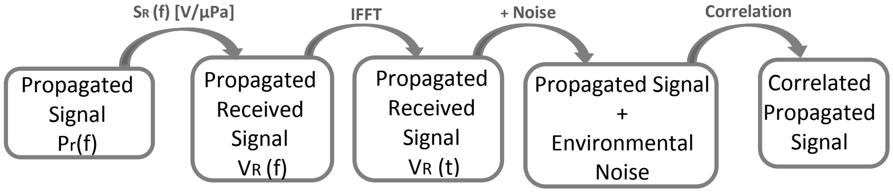

Fig 2.9. Diagram of propagated signal correlation.

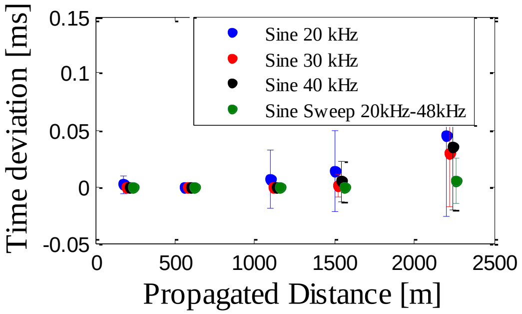

Fig 2.10. Values of deviation time (mean and sigma), with respect the true time, for the detected propagated signal with noise. It is determined by the correlation detection method.

The values of deviation time (mean and sigma) for the detected signal with respect the true time are shown in Fig. 2.10. The obtained results show that the sweep signal can be detected at a distance of 2.16 km with good accuracy. Notice, that even if the signal to noise ratio is not favourable, it is possible to detect the signals emitted up to a 2.16 km with reasonable accuracy by using the detection signal technique describe above (correlation method).

2.1.4.2 NEMO In Situ Test

In the case of the test performed in NEMO tower test the data recorded was taken by hydrophones from all floors of the tower in which the emitter is located on the base. The distance from emitter to the first floor is about 100 m and between floors is around 40 m and the tower has a total of 8 floors with two hydrophones per floor. The hydrophones from floor 5 were not working. All recorded signals analysed had durations of about 300 seconds and they were sampled at 192 kS/s. Concerning to the emissions, every kind of signal was emitted in sequences of 8 pulses. The emission sample frequency is 400 kS/s. For the analysis the recorded signal was split in sections of 5 seconds.

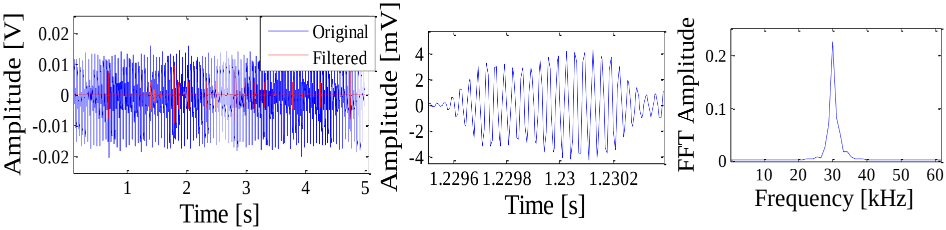

Fig 2.11 Recorded pulses from a 30 kHz sine signal emitted: recorded signal (left), a single received signal in time (middle) and frequency domain (right).

The left plot of Fig. 2.11 shows 5 s of a 30 kHz sine signal sequence recorded with one of the hydrophones, in this case hydrophone 1 placed in the second floor (right side of Fig. 2.4). Twenty pulse detections of 600 µs duration are identified. A band pass filter of 25 kHz to 35 kHz band width was applied to the signals. The middle plot of Fig. 2.11 shows a zoom in one single received pulse and the right plot shows the spectral components of the pulse. The Fig. 2.12 shows a zoom of 1 second of the recorded signal filtered. The spectrogram (see Fig. 2.13) permits the detection of the 30 kHz tone pulses received from the acoustic emitter since they have a good signal to noise; Looking at the spectrogram of one receiving signal very close echoes are visible.

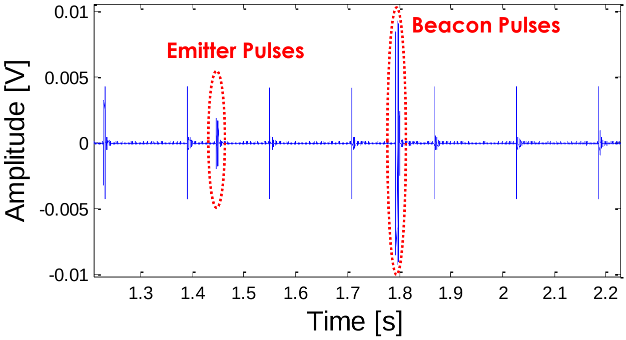

Fig 2.12 Recorded pulses filtered from the sine signal of 30 kHz emission.

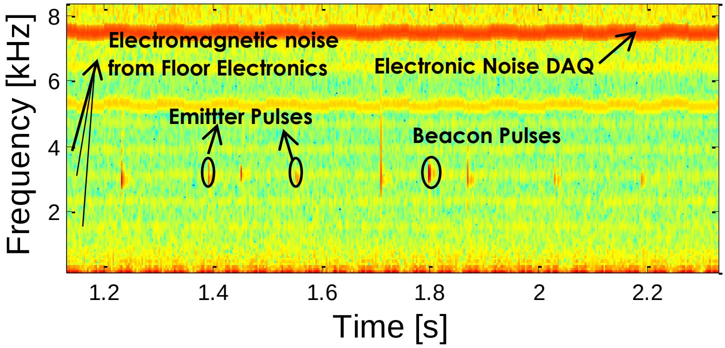

Fig 2.13. Spectrogram from recorded pulses from a 30 kHz sine signal emitted. Some signals and noise are identified.

- *Time of Arrival (ToA)*

The Time of Arrival was determined by the difference between the emission time and the initial time of the receiving signal. The emission time of the pulse emitted is determined with the local emission time (kept with the trigger in emission), plus 125 µs delay between the trigger command and the start of the frame, plus the delay of the SEB+FFR emitting response. The initial time of the receiving signal is determined with the initial receiving pulse time considering the delay of the DAQ system. The receiving time is obtained by two different methods; the threshold method of the signal received in time domain and the cross-correlation method of the received signal with the emitted signal. All the arrival times obtained in the test are relative; therefore it is only possible to know the ToA variations for the hydrophone from the same emitted sequence.

In general, the ToA obtained with the sine signals using the threshold method showed low variation in determining the detection time of signal. The correlation method used with the sine sweep signal gives the best results in terms of low variation in detecting the signal time and stability. Its signal to noise ratio increase emitting signals of longer duration (in this case the maximum duration is 800 µs).The ToA obtained gives information about the position movement of the hydrophones along the line. It seems to be well determined since the distances obtained, supposing that the sound speed is 1500 m/s, match with the real distances from the emitter to the hydrophones. As an example of the ToA obtained at the NEMO test, Fig. 2.14 shows the ToA obtained from the sine sweep signal from 20 kHz to 48 kHz applying the cross-correlation method. Assuming that the sound speed is 1500 m/s, the ToA values match with the estimated distances from the emitter to the hydrophones along the line. Table 2.2 shows the stability of the ToA values obtained from all hydrophones per signal, the variation of the ToA results is between 29 µs and 65 µs with the threshold method and 27µs and 103 µs with the correlation method. The results of the tests performed *in situ* show that the time of arrival obtained matches with the expected distances from the emitter to the hydrophones, as well as, a good stability is obtained.

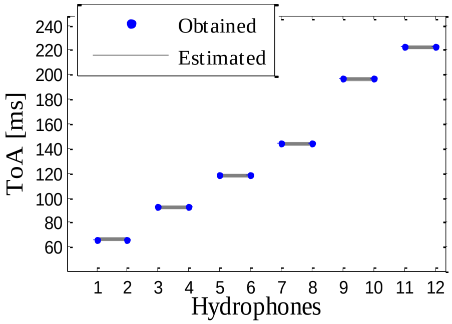

Fig 2.14. Time of arrival (ms) obtained with a sine sweep signal from 20 kHz to 48 kHz.

	Threshold method	**Correlation method**
Signal	**Standard Variation [ms]**	**Standard Variation [ms]**
Sine 20 kHz	0.065	0.103
Sine 30 kHz	0.031	0.046
Sine 40 kHz	0.029	0.029
Sweep 20-48 [kHz]	-	0.027

Table 2.2. Stability of ToA values from all hydrophones per signal.

The signal to noise ratios obtained by using the filter and threshold in time and cross-correlation methods to determine the amplitude are shown in Fig 2.15 for a distance between the emitter and receiver of 180 m.

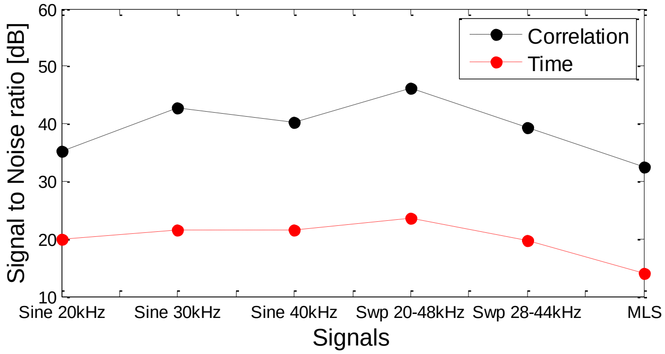

Fig 2.15. S/N ratio both in cross-correlation and time domain method.

Fig. 2.15 shows that using the cross-correlation method is possible to obtain accurately the signal amplitude and getting an increase of between 15 and 20 dB in the S/N ratio, with a consequent improvement in the acoustic detection, especially for broadband signals.

To conclude this part, the results obtained in both test performed with the acoustic transmitter prototype developed, show that it satisfied the requirements for the acoustic positioning system of KM3NeT and worked as expected in terms of operation and power emission. The time of arrival obtained matched with the expected distances from the emitter to the hydrophones, as well as, a good stability was obtained. In particular, the case of the sine sweep signal using correlation method showed 27µs of stability. Simulations of propagation of acoustic waves emitted in the same conditions of the test showed that they could be detected up to 2.16 km with good accuracy, which can be considered as a favourable reach for a large telescope such as KM3NeT.

With this, we can conclude that the signal processing techniques applied optimizes the signal detection and provide more accuracy in determining the signal arrival time.

For the final version of the acoustic emitter, so-called Acoustic Beacon, some modifications in the design were performed since the requirements and conditions imposed were slightly different. One of the conditions imposed was that the emitter should be all composed in one piece system; electronics and transducer. This was achieved by using a robust vessel where the electronics are housed and connected to the transducer located in the external part of the vessel. Another point for improving in the final version was the power emission which should be increased 10 dB more in order to achieve a level of 180 dB (re 1 µPa/Volt @ 1 m). Moreover, other conditions were required in terms of dimensions, connectors, power consumption and signal controlling. The final version of the Acoustic Beacon is presented in next section.

2.2 Design of the Acoustic Beacon

The acoustic beacon was developed by our group (UPV-IGIC) in cooperation with the company Mediterráneo Señales Marítimas SLL. This work was done for the KM3NeT project, in particular, to be part of its acoustic positioning system (APS). A total of 18 units were required for this aim, they were satisfactorily developed and provided to the project. Currently, there are two units already integrated in the telescope and being under test, so far, they show a good state and functionality.

2.2.1 General description of the Acoustic Beacons

The final version of the Acoustic Beacon (AB) is composed by a piezo-ceramic transducer and an electronic board integrated in a single piece system by a cylindrical hard-anodized aluminium vessel. The next sections explain the design phases of the system, starting with the transducer selection and moulding, the electronic board design and mechanics. Then the test performed for the acoustic calibration of the AB is described and the results in terms of acoustic power emission and directionality are showed. High-pressure tests are described as well. Afterwards, the selection of positions for the integration of the ABs in the positioning system of KM3NeT Phase I telescope is explained. The first ABs were installed and a test *in situ* was performed. The signals recorded by the receivers of first DU lines from the emission of the beacons were analysed, this study is shown in the following sections.

2.2.2 Acoustic Beacon Piezo-Ceramic Transducer

The AB uses the same acoustic transducer as the one implemented in the prototype, the commercial FFR SX30 acoustic transducer. This decision was taken after checking its optimal functionality in the environment of such telescopes, providing the expected acoustic power and good functionality along the time. As described before, it is able to work in the frequency range from 20 kHz to 50 kHz with transmitting voltage responses of 130 dB re 1 µPa/Volt @ 1 m at 30 kHz. The maximum input power is 300 W with 2% duty cycle. These transducers have an omnidirectional directionality pattern on the radial plane and a toroidal (60°) directionality pattern on the axial plane (Ardid et al. 2012) (Larosa & Ardid 2013).

The transducer was moulded to ensure the transducer holding and protection, and, a connector was added at the backwards of the moulding. In this way, it could be connected to the electronic board, which is placed inside the vessel. The connector selected was a BH2M hard-anodized aluminium connector as shown in Fig. 2.16. The moulded transducer was calibrated in laboratory test in order to check the transmitting Voltage Response (TVR) in the frequency range from 20 kHz to 50 kHz with steps of 2 kHz. The values keep quite similar to the ones obtained with the bare transducer, although a slightly modification on the TVR curve was appreciated due to the moulding (Fig. 2.17).

The calibration was performed in the Ultrasonics Laboratory of Escola Politècnica Superior de Gandia (EPSG). The calibration method used was the direct comparison by using a reference (calibrated) receiver. The experimental setup follows the classical scheme of confronted emitter and receiver transducers into a water tank of 1.10 x 0.85 x 0.80 m^3 volume. The transducer was fed using a function generator PCI-5412 (National Instruments©) and a linear RF amplifier 1040L (55 dB, ENI©). To measure the acoustic waveforms a spherical omni-directional hydrophone ITC-1042 (International Transducer Corporation©) connected to the digitizer card PCI-5102 (National Instruments©) was used as receiver system. The hydrophone ITC-1042 presents an almost flat frequency response below 100 kHz with a sensitivity of about -204 dB ±3dB as receiver.

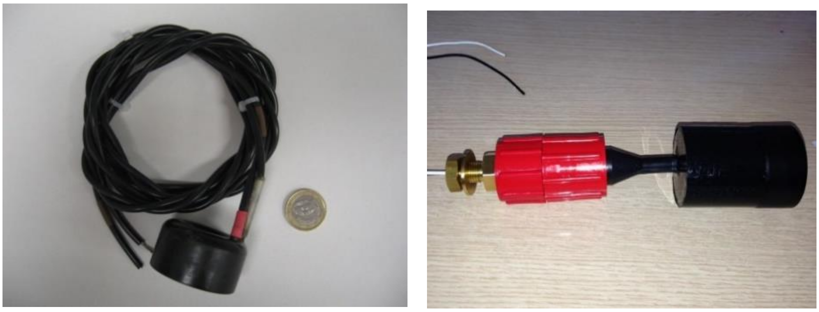

Fig 2.16. Bare (left) and moulded (right) FFR SX30 Transducer.

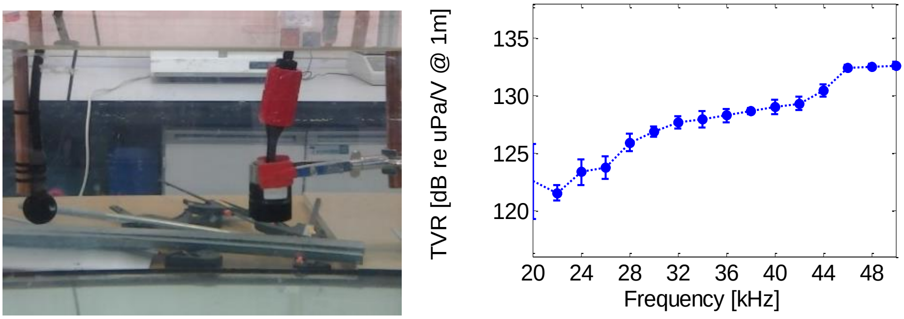

Fig 2.17. Calibration test (left) and Trasmitting Voltage Response of the moulded FFR SX30 transducer (right).

2.2.3 Electronic specifications of the Acoubeacon

The electronic Beacon Board was carefully designed to accomplish all the positioning requirements, as well as, to optimize and amplify the signal power emission (Llorens et al. 2012). The board provides the bidirectional link to shore; this enables the power feed and emission signal reconfiguration for *in situ* signal detection optimization. Acoustic waveforms to be emitted are stored in a local memory that can be updated from shore via RS-232 link. The signal emission trigger is received from shore, synchronized with the detector master clock. The time synchronization and calibration is accurate and stable with respect to the detector master clock. The technical specifications of the AB electronics required by KM3NeT are described in Table 2.3.

Supply Voltage	12 V
Current consumption	≤250 mA
Communications	Serial Port RS-232. Baud rate 9600 bits/s, 8bits No parity 1 stop bit
Trigger Signal	Differential 1Vpp galvanic isolated Accuracy >±1µs
Emission Latency	<10 µs
Synchronization accuracy	<1 µs
Dimensions	Three boards (240x70mm all)
Lifespan	>=20 years

Table 2.3. Electronic specifications of the AB for the LBL APS of KM3NeT.

Fig 2.18. Upper and lower views of the AB electronic boards.

The electronic beacon board consists of three boards (Fig. 2.18): In the block diagram of Fig. 2.19 the yellow part is related with the DsPIC Board, the orange part related to the Supply Board and the red one to the Bridge Board.

The DsPIC Board contains the main DsPIC processor that generates the PWM signal for the class D amplifier, a RS-232 isolated driver to receive the configuration commands protecting the supply of the telescope from emission noise, a galvanic isolated differential trigger reception to synchronize the emission of the beacon, a flash memory to store configuration and signals, and a temperature and humidity sensor to check the internal vessel status. The DsPIC board can also be connected to an external RS485/MODBUS pressure and temperature sensor that can check the external vessel conditions.

The Supply Board receives the 12 V external supply and uses it by means of a common mode filter and a current limiter that protects the telescope supply from noise and inrush current. After this protection the board has two DC-DC converters; one to feed the DsPIC board with 5 V and the other to provide 60 V for the emission. The 60 V are used to charge/discharge the main capacitor in the Bridge Board using a constant current source and a constant current sink. The main capacitor is charged slowly up to the desired emission voltage which is read from the main DsPIC using an ADC input.

Finally, the Bridge board consists of a high power Mosfet H Bridge which amplifies the PWM signal that comes from the DsPIC using the energy stored in the main capacitor. The H Bridge is coupled to the transducer through a transformer that reduces the impedance.

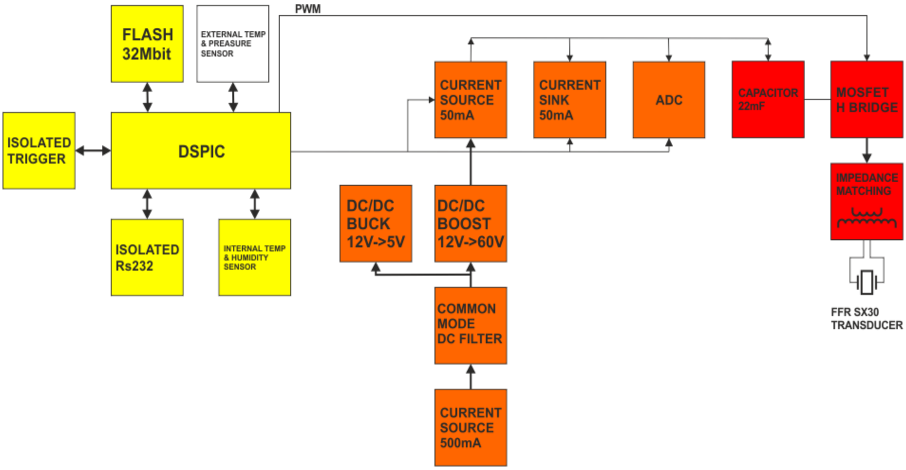

Fig 2.19. Block diagram of the electronic board

A specific firmware was developed in order to adapt the AB to the communication system of the KM3NeT-It telescope. The communications with the electronic board are done via the bus RS-232 by means of pins 4 (TX Beacon), 3 (RX Beacon) and 1 (GND). The beacon unit has a series of commands for the settings of the configuration and a trigger input for synchronizing the emission of the acoustic signal. This trigger goes through pins 5 (Trigger+) and 2 (Trigger-). This trigger input has galvanic isolation and an electrical impedance of 100 Ω. It is triggered with the rise flank of a pulse of 400 mVpp of minimum amplitude and 12 V of maximum amplitude. The beacon has a bootloader that allows the loading of a new firmware through the RS-232 port. Emission signal configuration is done by writing commands through HyperTerminal; it controls the signal and set the capacitor voltage charge for the power emission. This configuration is loaded in the memory for emission when external trigger activates it.

2.2.4 Mechanical specifications of the Acoustic Beacon

The pressure vessel is a sealed system that contains the internal electronics in a secure environment; it isolates the electronics from external pressure and water and keeps them in proper humidity conditions. It is able to safely support pressure levels up to 400 bars. The AB mechanical assembly consists of a cylindrical pressure vessel with a transducer screwed on the front endcap and hold firmly with a clamp (Fig. 2.22). The total length of the system is 575 mm; 400 mm length for the vessel (including the connector) and 175 mm length for the complete transducer.

The acoustic transducer FFR SX30 is located in the front (top) of the vessel conveniently moulded to cable signal using a polyurethane mould. The moulded transducer joint is fixed to the vessel by means of a plastic (Arnite) clamp that guarantee the correct stability and strength of the issuer, without affecting the acoustic properties of the transducer, especially the directionality.

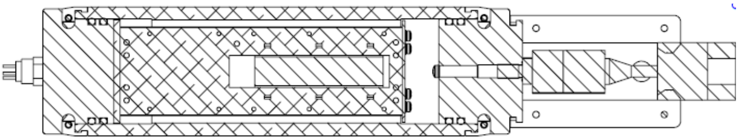

Fig 2.20. Internal part of the Acoustic Beacon

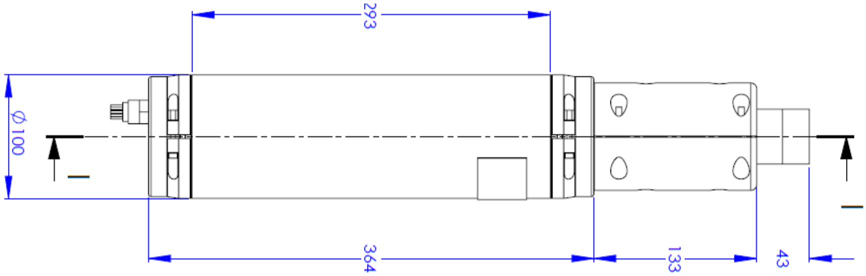

Fig 2.21. External part of the Acoustic Beacon and dimensions

Fig 2.22. Complete Acoustic Beacon

The pressure vessel is composed of a closed aluminium hull and two removable endcaps with collar hulls and a light inner chassis where the electronic board is located. The endcaps have double O-ring seals to ensure sealing and closing by collar hulls. There are entries on both end caps of the vessel; one in the rear endcap for the passage of the power supply to the electronic board, using a Seacon Microwet MC-BH-6M hard-anodized aluminium connector, and one on the front endcap for the acoustic transducer connection to the board through a BH2M hard-anodized aluminium connector. The vessel material is hard-anodized aluminium L6082-T6 (60 microns anonized) and the screws are made of stainless steel AISI316 (A4). Plastic isolation was used to avoid direct connection between steel and aluminium.

2.2.4.1 Pressure Tests

One important requirement for the AB was that it had to be able of supporting the pressure conditions in KM3NeT detector site and keep working with good functionality along time (over 20 years). For this reason, measurements in high-pressure machine were performed to all ABs developed in order to study their support under pressure values of 400 bar, and their behaviour after making the test. The AB were successfully tested at 400 bars for 10 minutes; this test was repeated 3 times for each beacon. The pressure tests were performed in a High Pressure machine (model Hiperbaric 420) at the company Hiperbaric (Burgos). Fig. 2.23 (right) shows the freshwater hyperbaric tank used to simulate the pressure in large water depth and Table 2.4 shows its main characteristics.

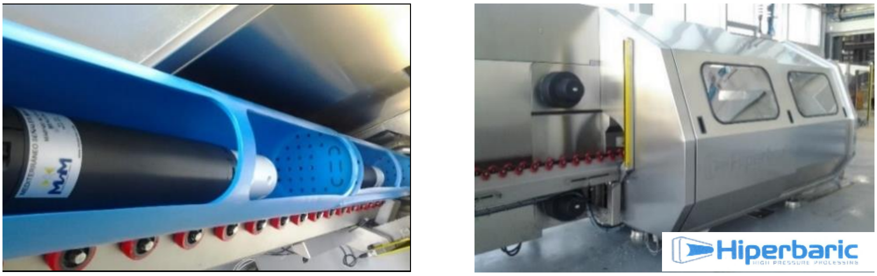

Fig 2.23. Assembly of the pressure test performed at the Hiperbaric installations.

High Pressure Test Characteristics	
Minimum Pressure	370 bar
Maximum Pressure	403 bar
Temperature (°C)	15°C ± 2°C
Time duration	30 min
Fluid	Fresh water

Table 2.4. Pressure test characteristics

2.2.5 Acoustic Test Calibration

The calibration was carried out in the same laboratory and water tank used for the moulded transducer calibration described in Section 3.2.2. The calibration technique applied was the direct comparison using the reference calibrated receiver ITC-1042. The generation part is driven by an arbitrary 14 bits waveform NI-PCI5412 card. The receiver was connected to the digitizer card NI-PCI5102 in order to acquire the received signals, as well as, the emitted signals on the terminals of the emitter transducer of the Acoustic beacon (AB). The AB was fed up with an external power supply of 12 V and connected to PC using a 100x reduction connector with the firmware installed. The signals were configured through a Hyperterminal. The emissions were controlled and activated through an external trigger configured with the generator card PCI-5401 guided to the input trigger of the beacon and synchronized with the acquisition system NI-PCI5102 connected to the receiver ITC-1042. The receiver was mounted in a positioning system control LF-5-DC (MICOS GmbH©), It is able to move in the three dimension X, Y and Z with a precision better than 0.1 mm. The signal length was chosen according to the dimensions of the tank to avoid the interference of the reflected signals from the walls and water surface with the direct signal. The distance between emitter (AB) and receiver (calibrated hydrophone) was of 20 cm. The signals used for the calibration were tone burst of 5 wavelength cycles at different frequencies from 20 kHz to 60 kHz, every 2 kHz, for different capacitor charges (5 V, 20 V, 40 V and 60 V) in both radial (see Fig. 2.25) and axial directions (see Fig. 2.24). The directionality was determined in radial direction for a capacitor charge of 60 V (maximum SPL) for the tone burst of 20 kHz, 30 kHz and 40 kHz for an angular range from -50º to 50º. The frequency sample acquisition used was 20 MS/s. In addition, other type of signal were emitted like sine sweep and MLS signals in order to check its behaviour and the cross-correlation method. The right graphic of Fig. 2.24 shows the sound pressure level (dB re 1µPa@1m) of the acoustic beacon obtained with different capacitor charge (5 V, 20 V, 40 V and 60 V) in the axial direction and Fig. 2.25 at radial. Fig. 2.26 shows the AB directionality at axial direction.

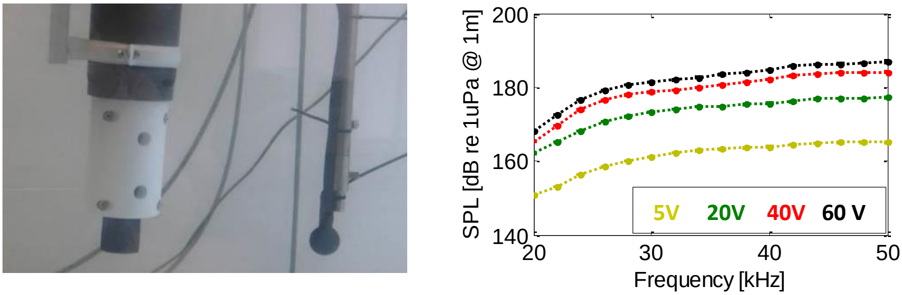

Fig 2.24. (Left) Experimental set-up for determination of axial directionality. (Right) Sound Pressure Level (SPL) versus frequency graph of the AB at axial direction for different capacitor charge.

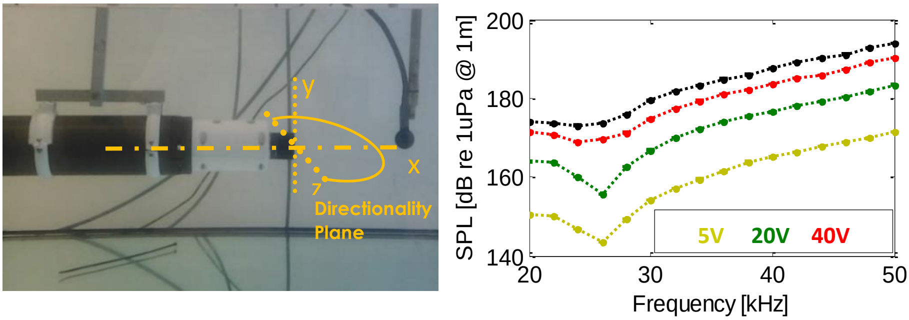

Fig 2.25. Left) Experimental set-up for determination of radial directionality. (Right) Sound Pressure Level (SPL) of the AB radial direction for different capacitor voltage charge.

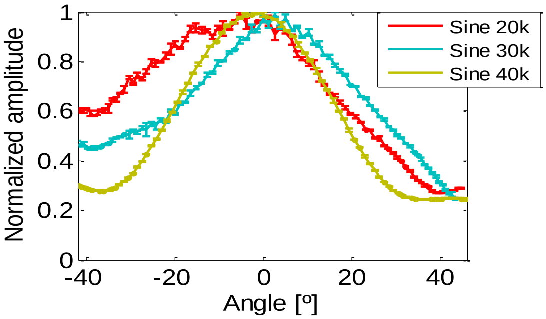

Fig 2.26. Directionality of the AB at axial direction (horizontal)

The SPL curves show that for the maximum capacitor charge (60 V) levels obtained ranging from 174 dB to194 dB for the 20 kHz to 50 kHz frequency range. The directionality at axial direction show a minimum emission value at an angle of around ± 35° from the 0° reference at the centre of the ring transducer. The results obtained show the AB emits a Sound Pressure Level (SPL) of 180 dB (re 1 µPa @ 1 m) at 34 kHz with a variation of ± 6 dB in the frequency range from 20 kHz to 60 kHz. The radial beam pattern is omnidirectional with ± 2 dB for each work frequency and the axial beam pattern is toroidal with ± 10 dB of variation at 60º.

The acoustic emission parameters are configured by commands through a RS-232 serial interface allowing signal reconfiguration from shore. There is a graphical interface for facilitating the user interaction. The signals parameters can be configured as following:

- Signal emitted length: from 0 to 50 ms.
- Maximum emission amplitude: 180 dB @ 34 kHz re 1 µPa a 1 m.
- Type of acoustic signals:
    - Monochromatic signals configurable from 1 kHz to 80 kHz.
    - Sine Sweep signals configurable from 1 kHz to 80 kHz.
    - Maximum Length Sequence (MLS) signals with lengths from 5.12 ms to 40.96 ms (from 10 th to 13 th order and sampled at 200 kS/s).
- Modality of emission: external trigger response (LVDS with galvanic isolation). It disposes two operation emission modes; single and automatic (continue) emission.
- Variable temporal interval of emission between a signal and the successive one for the automatic emission mode from 0.5 s to 300 s.

Positioning acoustic pulses will be emitted in the range of frequencies from 20 kHz to 50 kHz. In this range acoustic signals emitted in water with a SPL of 180 dB re 1 µPa at 1 m can effectively propagate until a distance of 2 km with about 110 dB re 1 µPa (depending on frequency) and it can be easily recognised by the acoustic receivers of the telescope.

2.3 Acoustic Beacon Integration in the Positioning System

As mentioned before, a total of 18 Acoustic Beacons units were satisfactorily developed and provided to the KM3NeT project in 2015. By the end of 2015, the first week of December, two units of the Acoustic Beacons were integrated at the KM3NET-It (Phase I) site (Fig 2.27) through the first sea campaign, one was installed in the Junction Box 1 (JB1) and other in the Junction Box 2 (JB2), Fig 2.29 show a picture of the sea campaign, where the AB holding in the JB is visualized. As well as, the first detection unit (identified as DU-9) was installed on the sea floor of the APS. They were *in situ* tested in January of 2016 and the recorded data was analysed in order to extract some conclusions of the APS functionality.

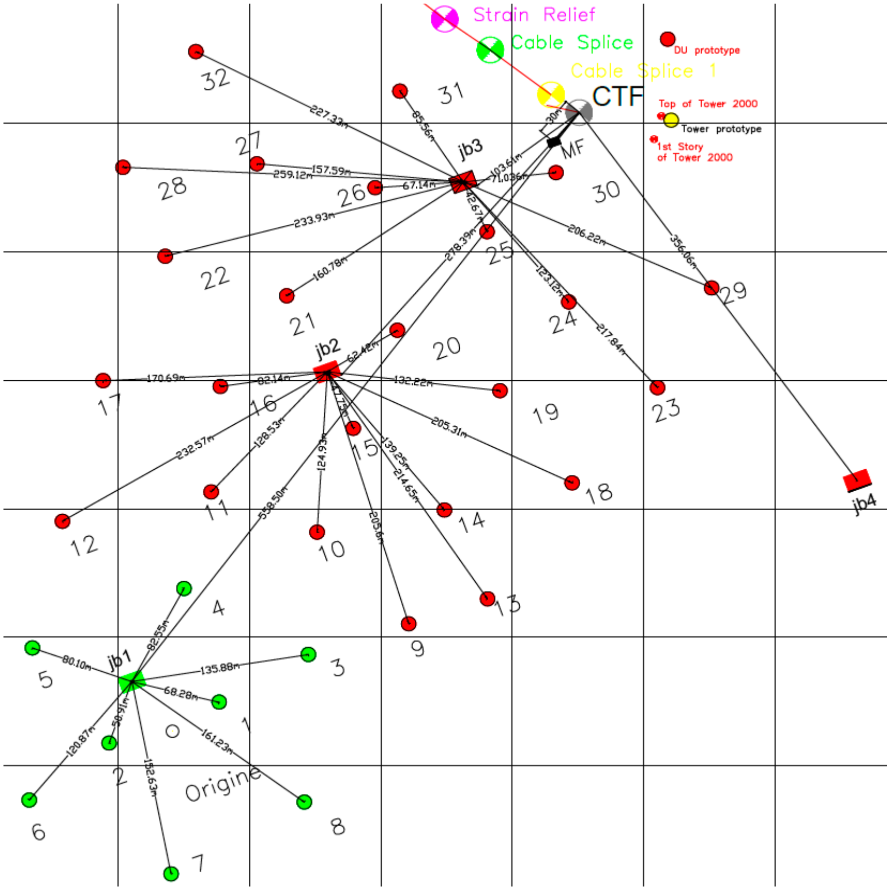

Fig 2.27. Layout of KM3NeT-It Phase I. Positions of DUs from n^{er} 1 to n^{er} 32 and JBs from n^{er} 1 to n^{er} 4 (KM3NeT Project Website) .

The LBL positioning system of KM3NeT-It is composed by an array of acoustic transmitters and receivers hosted on the CBs. Each DU base will host a digital hydrophone and each CB will host an acoustic beacon and a digital hydrophone placed at a known distance from the beacon. The LBL of the acoustic beacons installed on the CBs is complemented by autonomous acoustic emitters (battery powered and driven by local clock) placed in the JBs from number 1 to 4. This will improve the resolution of triangulation calculation for receivers placed on DU at the edge of the telescope field. Moreover, autonomous beacons must be used, during the installation of the first DUs (Phase 1), to create a temporary LBL field. Fig 2.28 shows a map of the KM3NeT-It (Phase I), the points coloured in green correspond to a CB, where JB1 is also included as CB, all of them with an AB installed on its base. The points coloured in red represents to the DUs. JB2, JB3 and JB4 are included; used as CBs as well with an AB installed on them.

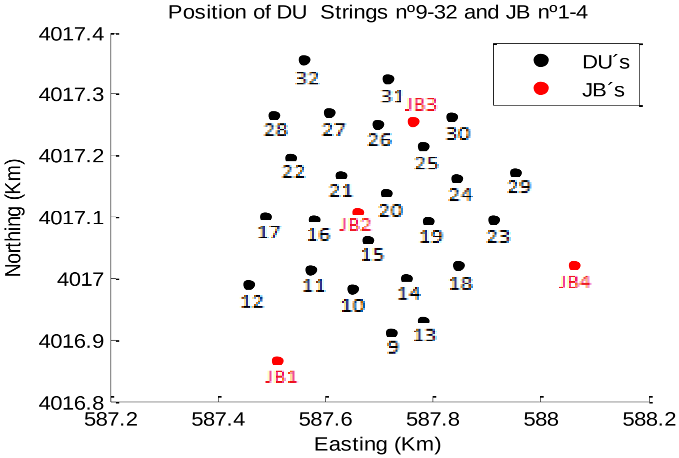

Fig 2.28. Sketch of the KM3NeT-Italy site (Phase I).

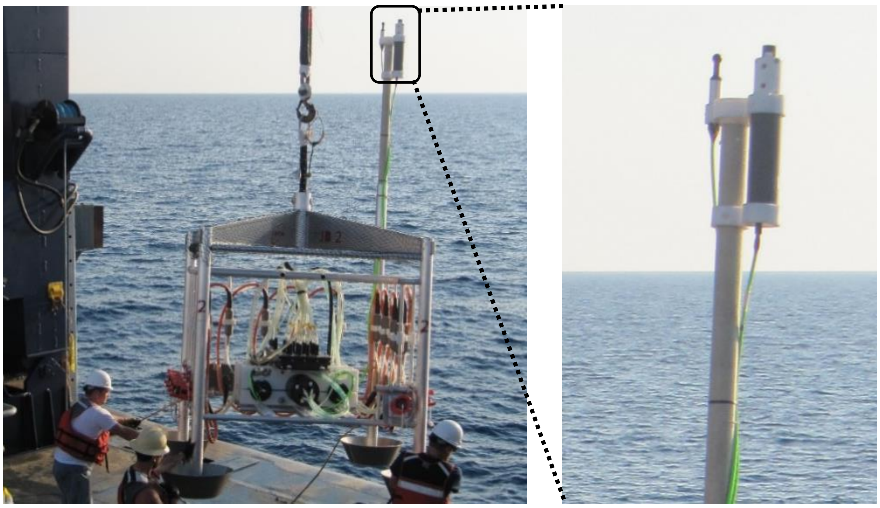

Fig 2.29. Picture of the KM3NeT-IT sea campaign, performed on the 3th December 2015. Junction Box (left) and support of the Acoustic Beacon and hydrophone in the JB (right).

2.3.1 First APS *in Situ* Tests

The first test performed with the APS of KM3NeT-It was carried out on the 7th January 2016. The signals were emitted by the AB placed on the JB1 and recorded by the receivers (piezos) of DOMs from DU9. The distance from the emitter to the DU-9 base was around 215 m. Fig. 3.30 shows the acoustic test configuration in a schematic way. The depth of each DU floor (DOM) can be determined by the equation: $seabed + 72 + 36 \cdot (n-1)\ m$, where n is the number of DOM and *seabed* is about -3500 m. The signals emitted during the test were sequences of eight pulses of a sine sweep from 38 kHz to 39 kHz with a voltage capacitor charge of 30 V. The signal duration length was 5 ms and the pulse repetition rate was configured to be 3 s. The emission sample frequency of the data acquisition system (DAQ) was 195.3125 kS/s. At the time of the test there was not time synchronization between emissions and receptions.

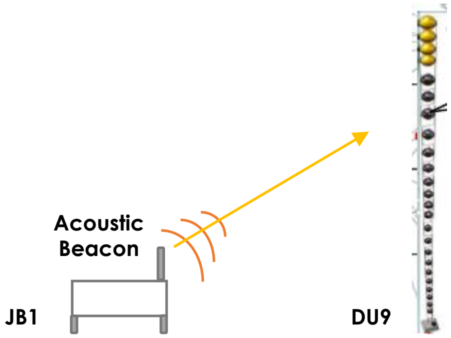

Fig 2.30. Schematics of the first KM3NeT-It (Phase I) acoustic test configuration.

In order to analyse and study the received signals of the test, signal-processing techniques were used. The next processes and studies were done for the receiving acoustic data:

- Recorded Signal Spectrogram.
- Signal in time and frequency domains.
- Correlation of the recorded signal with the emitted signal.
- Determining the received signal amplitudes in time domain.
- Obtaining the received signal arrival times of each piezo-DOM by correlation and threshold method.
- Obtaining the arrival time differences of same received signal for consecutive floors (piezos).
- Determining the gap time between consecutive received signals.

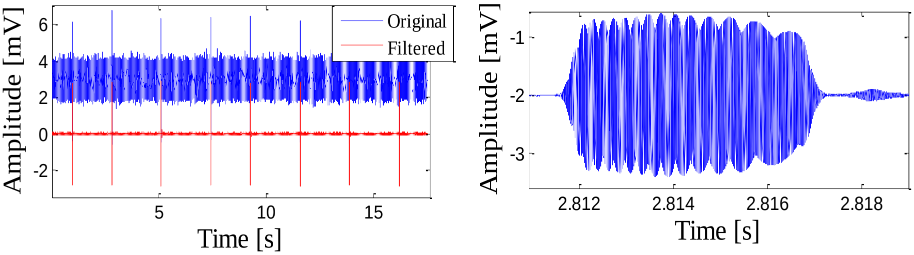

Fig 2.31 Received signal from the AB (JB1) emission of a sine sweep signal from 38 kHz to 39 kHz to piezo from DOM-7: eight pulse recorded sequence (left) and zoom in a single received signal (right).

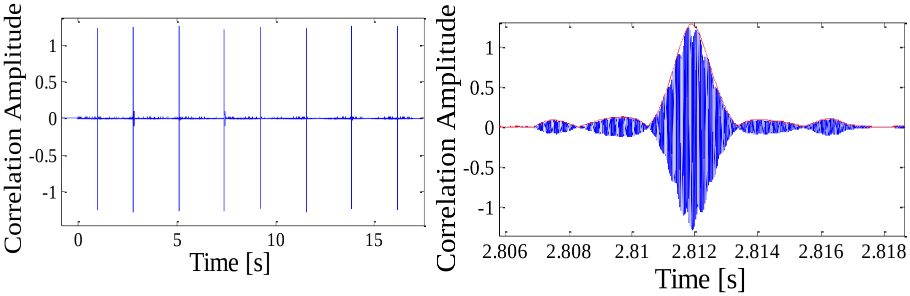

Fig 2.32 Correlation of the received signal from the AB (JB1) emission of a sine sweep signal from 38 kHz to 39 kHz until piezo from DOM-7: correlation of the eight pulses recorded sequence (left) and zoom in of single received signal correlation (right).

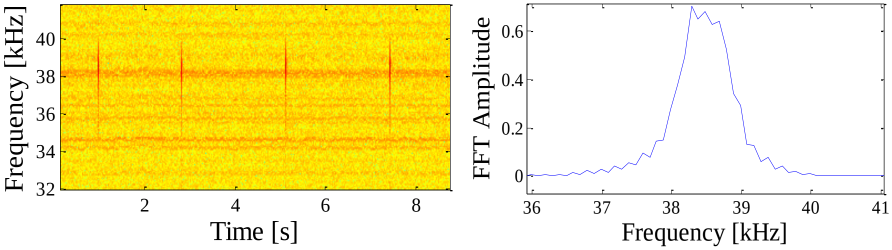

Fig 2.33 Frequency domain study of the received signal from the AB (JB1) emission of a sine sweep signal from 38 kHz to 39 kHz to piezo from DOM-7: spectrogram of the first four pulses from the recorded sequence (left) and Fourier transform (fft) of a single received signal (right).

The recorded sequence signals from piezo of DOM7 are shown in graphics of Fig. 2.31 to 2.33. The figures show the most relevant information about the data in terms of time and frequency domain (filtering, correlation, fft and spectrogram) for the signal sequence and a single signal. The filter applied on the analysis was a Band-Pass Filter (FIR) with a frequency range from 37 kHz to 40 kHz. In Fig. 2.31 the recorded signals, eight pulse recorded sequence (left) and zoom in on a single received signal (right), are shown. The correlation waveform presented some beats and consequently a clear maximum value was not found. Because of the methodology used for determining the maximum correlation value was by means of obtaining the envelope of the correlation signal. Right graphic of Fig. 2.32 shows a single received signal envelope. In Fig. 2.33 the spectrogram of the first four pulses from the recorded sequence (left) and Fourier transform (fft) of a single received signal (right) are shown. The conclusions deduced from this study are exposed in the following points:

- The AB was working as expected in terms of functionality and power emission of the acoustic waves.
- The piezos recorded all the acoustic waves emitted by the AB, being recognized in time and frequency domain studies. Though a significant amplitude variation in the recorded signals by the different receivers was appreciated.
- The recording time length was around 18 s, excepting for DOMs 16, 17 and 18, which had less time recorded than the other ones (recording time length ~9 s), therefore, they recorded fewer receiving signals. This was due to data frames losses on the DAQ during this test.
- The signal amplitudes in time were obtained from the filtered signal, and the correlation amplitude signal from the maximum value of its envelope. Looking at the amplitude signals obtained in each DOM receiver, there is considerable variation in the amplitude value of the received signals. The lowest amplitude values are obtained with the receivers of DOM 2 and 3, followed by the 6, 18 and 8. The receivers with higher level of signal amplitude are those corresponding to DOMs 4, 9 and 12.
- Concerning the study of the arrival time, two different methods were used for obtaining it; by correlation and threshold. The arrival time determined through the correlation method was obtained by taking the time corresponded to the maximum value of its envelope. Whereas, the one determined through the threshold method was obtained by taking a rise time value of the received signal envelope.
- Floor distances obtained from the experimental data were in agreement with the expected ones for the first pulse results (excepting from the 2nd and 3d DOM). For the rest of the pulses, a variety of distance values were obtained that did not correspond with the expected ones. This was, obviously, due to the data frame losses. Therefore, this corroborates that data losses at the beginning were small.
- The results obtained of the signal arrival time with the two methods used (Correlation and Threshold) were similar.
- The time gap between consecutive pulses was determined with the analysis and the value obtained was mainly around 2.3 s, excepting for the gap between 8th and 7th pulse which was around 1.7 s. Again, this may be due to the data frame losses, taking into account that it was configured to be 3 s.

Once the DAQ system data losses will be solved and the time synchronization activated, the next steps to perform on the APS tests will be doing a deeper study on the emitter and receiver’s functionality and sensitivity. This will be achieved by emitting acoustic signals at different frequencies and emission power. In addition, sine sweep signals of wider frequency range could be also interesting to emit, since there will have larger signal to noise ratio. Moreover, it will help to identify possible very near echoes which could not be distinguish with the 1 kHz width range frequency of the sine sweep signal used.

2.4 APS simulation for the installation of extra Acoustic Beacons in KM3NeT-It (ARCA-Phase I) and KM3NeT-Fr (ORCA-Phase I)

In addition to the APS configuration described in the section 3.3, the installation of four extra AB was required from the KM3NeT team in a second step, in order to reinforce the LBL positioning system of KM3NeT-It Phase I. On the other hand, an AB unit placement in the positioning system of ORCA-Phase I (KM3NeT-Fr), was also required, since its inclusion was essential for achieving the LBL triangulation. In order to study what were the best placements to install the beacons in each context, simulations of the pressure levels from the emitters (already planned to be installed) to receivers were performed. These simulations helped to know the areas with less pressure levels. Then, in a second phase, by simulating the AB emission from different configurations with the new beacons, there were determined the most favourable locations in terms of supporting the most critical areas and achieving a good pressure wave spreading in the APS area. The study and simulations performed in each case are described in detail in next sections.

2.4.1 Study for the installation of four extra AB in the APS of KM3NeT-It (ARCA-Phase I)

The study for selecting the most optimal DU base positions to install four more beacons in the APS of KM3NeT-It Phase I was performed. The steps carried out for this selection were, firstly, simulating the acoustic pressure field produced by the emitters that were already set for the LBL system (JB numbers 1 to 4). With this, the areas with low acoustic levels were detected, named critical areas. Then, considering the critical areas, different position configurations for the emitters were studied. By simulating the acoustic pressure spread of each position configuration, the one achieving the best acoustic energy spread into the interesting area (critical area) was chosen as the optimal one. In this section, the steps performed for the DU bases selection to integrate the four extra AB is described in more detail.

The simulation of the pressure signal emitted by the AB integrated at the JBs numbers 1 to 4 and propagated until the DU bases was performed as first step. This allowed to check which DUs received the lowest pressure levels. For this, the received signal from the AB emission at laboratory tank was used by selecting the received signal of the emission of a tone burst of 38 kHz with a voltage capacitor charge of 40 V, and emitted at an opening angle of 0º respect to the receiver, as shown in Fig 2.25. The pressure spectral components of this signal at the DU bases were determined by applying the attenuation of the media absoption and the spherical divergence. The acoustic pressure (Pa) reached at the DU strings bases from the AB emission of each JB is shown in Fig. 2.34.

After this, the APS areas with lowest acoustic pressure levels (so-called critical areas) were recognized, and subsequently, the best DU positions for integrating the new AB were selected. For this selection, different point configurations were simulated in order to find the optimal positions according to the best spread of the acoustic waves around the critical areas. Moreover, the location selection was determined taking into account to favour an optimal triangulation, in order to be able to obtain the receiver positions correctly. Fig. 2.35 show the critical areas and the DUs selected for the integration of the new AB, identified as AB numbers 5 to 8, to the APS.

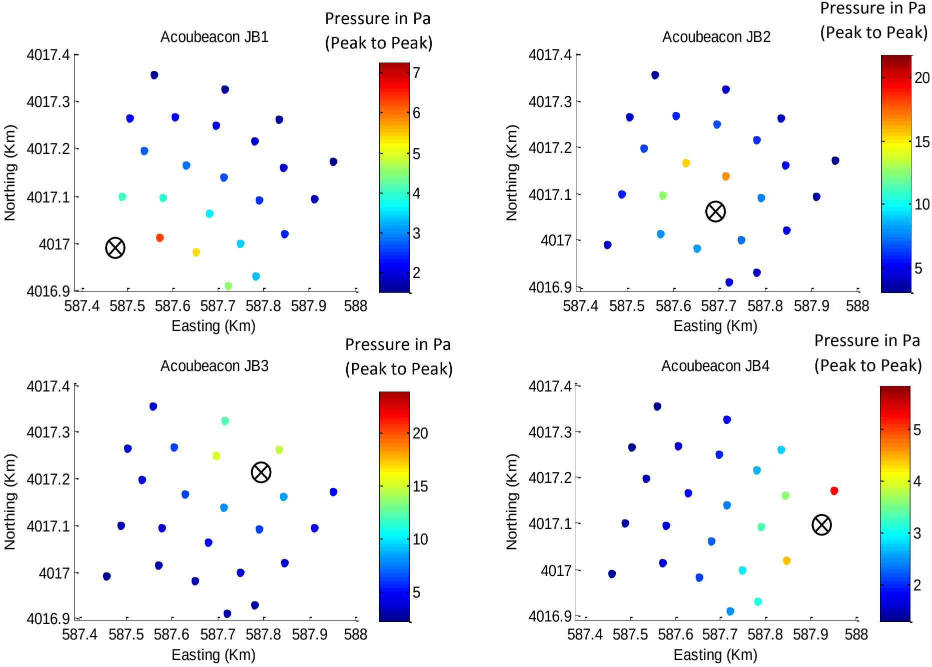

Fig 2.34. Signal pressure received (Pa) in the DU strings Bases from the emissions of the AB placed in JBs numbers 1 to 4.

The proposal of the AB positions (from numbers 5 to 8) was chosen for covering the critical areas and having an optimal triangulation system. The new positions selected correspond to the DU bases of strings 18 (AB5), 17 (AB6), 29 (AB7), 32 (AB8). The next step was, determining the acoustic pressure wave levels at the DU strings bases from the emission of the new AB (numbers 5 to 8). Fig. 2.36 show the acoustic pressure levels reached on the DU bases.

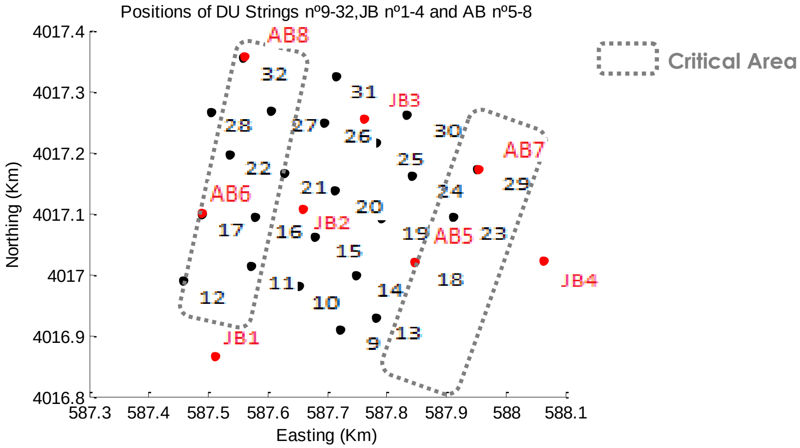

Fig 2.35. Most Critical Areas of APS from emissions of JBs from numbers 1 to 4 and new AB units (from numbers 5 to 8) placed in selected DUs.

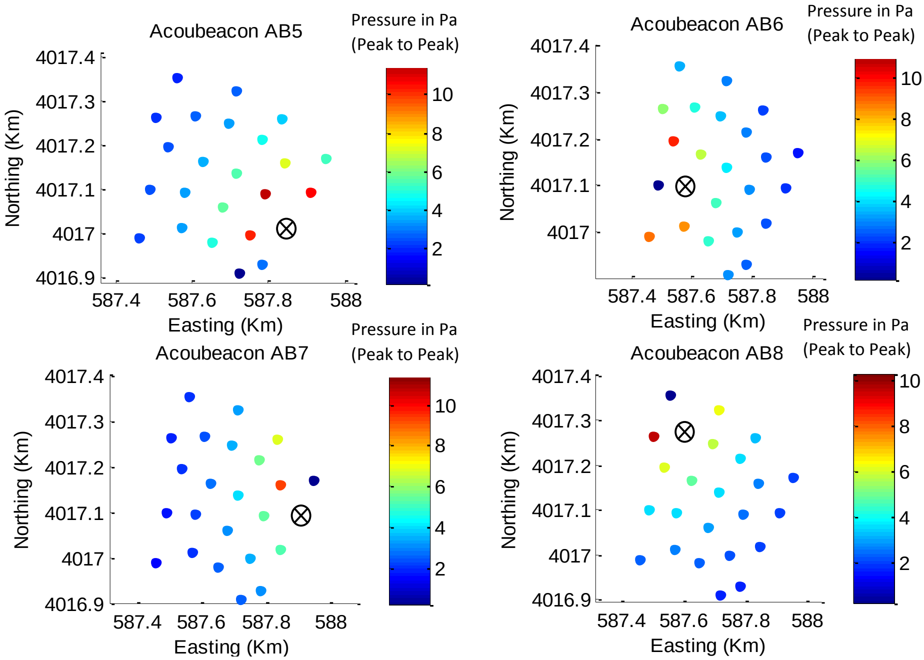

Fig 2.36. Signal pressure received (Pa) in the DU bases from the emissions of the new AB placed numbers 5 to 8.

Minimum Values of Pressure Signal (Pa_{pp})								
DU	**JB1**	**JB2**	**JB3**	**JB4**	**AB5**	**AB6**	**AB7**	**AB8**
9	0,92	0,97	0,55	0,53	3,49	0,65	0,55	0,38
10	1,08	1,53	0,66	0,45	1,95	0,99	0,53	0,49
11	1,22	1,50	0,63	0,36	1,17	1,59	0,45	0,56
12	1,41	0,85	0,46	0,28	0,76	1,64	0,33	0,49
13	0,70	0,93	0,59	0,66	2,57	0,57	0,66	0,37
14	0,72	1,39	0,77	0,61	2,07	0,71	0,73	0,46
15	0,76	2,66	0,95	0,49	1,34	1,03	0,66	0,61
16	0,82	2,08	0,81	0,36	0,91	1,98	0,49	0,75
17	0,84	1,16	0,62	0,29	0,69	3,26	0,38	0,74
18	0,51	0,97	0,80	0,91	1,29	0,52	1,07	0,41
19	0,53	1,46	1,20	0,69	1,10	0,65	1,10	0,54
20	0,56	2,39	1,53	0,51	0,93	0,88	0,82	0,74
21	0,60	2,32	1,23	0,40	0,78	1,28	0,59	0,98
22	0,58	1,29	0,85	0,31	0,60	1,74	0,44	1,22
23	0,39	0,79	0,91	1,16	0,80	0,44	1,97	0,42
24	0,41	1,04	1,55	0,75	0,76	0,53	1,69	0,56
25	0,41	1,21	2,76	0,56	0,67	0,62	1,12	0,75
26	0,43	1,33	2,31	0,42	0,60	0,78	0,73	1,15
27	0,45	1,16	1,25	0,34	0,52	0,98	0,53	1,83
28	0,46	0,90	0,76	0,28	0,46	1,20	0,40	1,73
29	0,32	0,65	0,96	1,06	0,57	0,39	3,26	0,42
30	0,35	0,85	2,24	0,58	0,53	0,50	1,32	0,68
31	0,35	0,88	2,03	0,39	0,46	0,61	0,69	1,25
32	0,36	0,73	0,87	0,28	0,39	0,75	0,42	3,26

Table 2.5. Minimum received values of pressure signal (peak to peak) per DU, taking into account values from all DOMs of each DU, expressed in Pa (peak to peak), from the emissions of the beacons placed in JB numbers 1 to 4 and from the new AB numbers 5 to 8.

From this study, the predicted levels of pressure signal obtained at the DU base varies from minimum values of 0.28 Pa (peak to peak) until maximum values from 10 to 25 Pa (peak to peak). A part of the pressure level calculation at the DU bases, the acoustic pressure level at each DOM surfaces of the DU strings was predicted by following the same procedure.

For this simulation, there was a directionality factor correction applied to the signal taking into account the angle corresponding to the AB-DOM orientation. It was observed that for lines some DOMs which the angle coincides with the minimum of emission (~ 30 °- 40 °), the pressure levels decreased about 12 dB. Table 2.5 show the minimum received values of pressure amplitude (peak to peak) per DU, taking into account values from all DOMs of each DU, expressed in Pa (peak to peak) from the emissions of the beacons placed in JB from numbers 1 to 4 and from the new AB numbers 5 to 8. The minimum levels of signal pressure at DOMs of each DU string are around 0.3-0.5 Pa (peak to peak) and the maximum level around 14-16 Pa (peak to peak). From the simulation of the pressure signal on the Piezo-DOMs surface, we can see that signals with values of about 0.5 Pa (peak to peak) are perfectly detected by the receivers. At least 4 signals from the different emitter are received with minimum values higher than 0.6 Pa (peak to peak) for each DU (the minimum is determined from received signal of all DOMs from the DU). Therefore, even the lowest pressure levels obtained are good for the detection by the receivers, as well as, for being distinguished from noise.

In conclusion, the simulation of the signal emitted by the new ABs shows they help to spread more equitably the sound pressure in the field of DU receivers, reaching the sensors which had low signal pressure values. By integrating the new AB, the APS will be a robust system able to reach all receivers from DUs with a good level of signal and with some redundancy, and therefore, detectable by sensors in DOMs.

2.4.2 Study for the installation of an extra AB in the APS of KM3NeT-Fr (ORCA-Phase 1)

The study for the placement of a new AB unit in the positioning system of KM3NeT-Fr, specifically in ORCA-Phase I (see Fig 1.4) was also required. The inclusion of this beacon was indispensable to achieve the LBL triangulation, since previously there were only two beacons integrated in the positioning system, one at the Calibration Base (CB) and an autonomous beacon in a tripod. Therefore, with the new beacon, there will be a total of three emitters covering the area ORCA-Phase I and allowing triangulation. The requirement for its installation was placing it in one of the DU bases of ORCA-Phase I, and selecting the most optimal position was the main aim of this study.

The positions (x, y) of the DUs for ORCA-Phase I (from numbers 1 - 8) are shown in Fig. 2.38, as well as, the positions of the Calibration Base (CB), the tripod with the AB and the Instrumentation Unit (IU). The ORCA strings have DOMs placed at an inter-distance of 9 m and the distance of the lowermost DOM from the bottom is 40 m.

The first stage of the study was taking a real signal recorded from the AB emission which was a tone burst of 38 kHz with a voltage capacitor charge of 40 V. Then, the signal was propagated until the DU base positions by converting it into pressure spectral components. Applying the attenuation of the media absoption and the spherical divergence in the signal. Fig. 2.37 shows the sound pressure level of the signals propagated from the emission of the AB located on the CB and the Tripod to the DU bases.

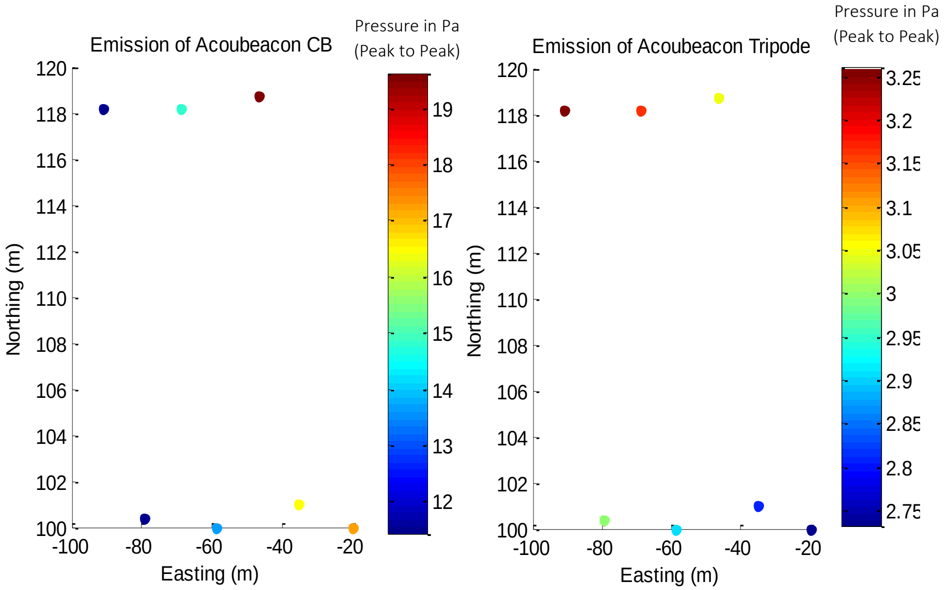

Fig 2.37. Signal pressure received (Pa) in the DU strings Bases from the emissions of the AB placed in the CB (left) and the Tripod (right).

From this first simulation, the acoustic pressure levels at the DU base positions were determined and the critical areas were recognized. At this point, the emission of the new beacon was simulated for different DU base placements in order to find the most favourable according to the best spread of the acoustic waves around the critical areas and an optimal triangulation. From this study the position number 4 was found as the best solution, Fig 2.39 show the acoustic pressure levels reached on the DU bases from the emission of the AB in the string base of position number 4. The pressure value (peak to peak) obtained at DU in position 4 base (where the emitter is placed) is 733 Pa.

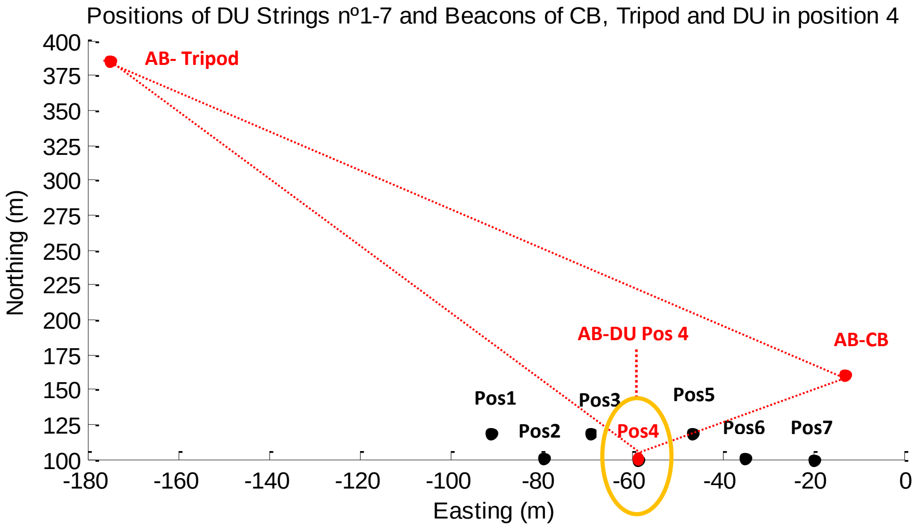

Fig 2.38. Layout of the ORCA-Phase I system; positions of DUs, CB and Tripod and AB.

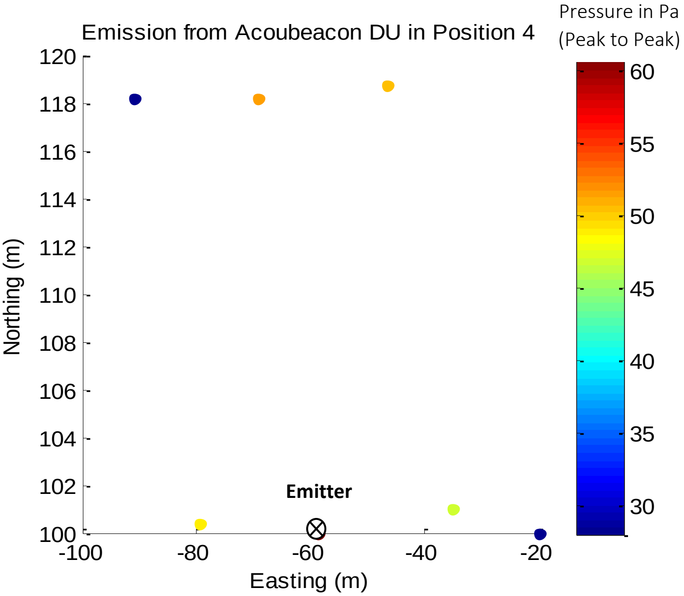

Fig 2.39. Signal pressure received (Pa) in the DU string Bases from the emissions of the AB placed in the DU base of the position 4.

In a second step, the study of the pressure obtained at the DOMs of each DU was performed. The minimum and maximum levels obtained from all DOMs of each DU string were determined (predicted under the simulation performed). It was taken into account the angle of emission, distance and media absorption, from the three AB emissions. Table 2.6 show the minimum values received at all DOMs of each DU string from the emission of the three APS triangulation beacons. Pressure values coloured in orange are the ones who correspond to DU-base where an Acoustic Beacon (AB) is integrated, this is the reason of having a much large pressure value. The predicted pressure values at the DOMs surface are above 0.5 Pa, therefore the signals should be able to be perfectly detected by the receivers according to the specifications of the piezo-receivers and the first tests with ARCA Phase I.

	AB-CB		AB-Tripod		AB-DU base position 4	
DU Position	**Pressure$_{pp}$ (Pa)**	**SPL (dB re 1µPa)**	**Pressure$_{pp}$ (Pa)**	**SPL (dB re 1µPa)**	**Pressure$_{pp}$ (Pa)**	**SPL (dB re 1µPa)**
1	2,52	119,0	1,65	115,3	6,14	126,7
2	2,50	118,9	1,65	115,3	14,01	133,9
3	3,24	121,2	1,65	115,3	15,71	134,9
4	2,98	120,4	1,64	115,3	701,08	167,9
5	4,27	123,6	1,65	115,3	15,12	134,6
6	3,61	122,1	1,64	115,3	12,86	133,2
7	3,75	122,4	1,63	115,2	6,10	126,7

Table 2.6. Minimum received values of pressure level (peak to peak) and SPL per DU, taking into account values from all DOMs of each DU, expressed in Pa and dB. Values received from the emission of the AB located in CB, autonomous tripod and DU base in position number 4.

The predicted pressure levels at the DOMs surface of each DU base varies from minimum values of 1.65 Pa (peak to peak) to 15 Pa (peak to peak) and the maximum values from 3.25 to 44 Pa (peak to peak). A pressure level of 1.65 Pa (peak to peak) which is a SPL of 115. 3 dB re 1µPa at the Piezo-DOMs surface, could be perfectly detected by the receivers according to the specifications of the piezo receivers and to the results of the first tests with ARCA Phase I. Consequently, the pressure levels reached at all DOMs from the emission of the three beacons will be good enough for being easily distinguished from noise.

With this we can conclude that the configuration selected for the LBL triangulation accomplish satisfactorily the requirements for the positioning system of ORCA-KM3NeT Phase 1. Naturally, since there will be only three emitters, the system will not have any redundancy, and this could be problematic.

3 Design of a Transducer Array for the Calibration of Acoustic Neutrinos Detector

This Chapter presents the development of a parametric array transducer able to mimic the acoustic signal generated by Ultra-High Energy (UHE) neutrinos on its interaction in water. Over the last few decades, there were a number of experiments looking into acoustic neutrino detection in both water and ice media (Bevan et al. 2009). The detection technique is still under study and could be implemented in a new optical neutrino telescope KM3NeT (Viola et al. 2015). The acoustic detection would allow the combination of those two neutrino detection techniques for a hybrid underwater neutrino telescope, especially considering that the optical neutrino detection technique needs acoustic sensors to monitor the position of the optical sensors (Viola et al. 2013). In order to study the viability of the acoustic detection, an emitter able to imitate the bipolar pulse signal generated by the neutrino in water will be extremely useful. For this purpose, an acoustic array calibrator was designed. The emissions from the emitter calibrator, which will be time controlled, will allow the sensors to be trained for neutrino detection. Furthermore, it will improve the classification and identification of the acoustic neutrino signals, telling them apart from noise or other transient background signals (M. Ardid 2009), (Ardid et al. 2012).

The following sections describe the philosophy design of the array. Firstly, all the processes involved on a single transducer design and the characterization tests are presented. The parametric emission techniques are described, as well as, the results obtained from their emission with the transducer are shown. Finally, the complete array design and characterization is presented. The work developed with the individual transducer design was previously published in a scientific paper in 2016 (Saldaña et al. 2016).

3.1. Introduction to the Array Calibrator based on the Parametric Technique

The objective of the acoustic array calibrator is the emission of a bipolar pulse signal with similar characteristics to the signal produced by a 10^{20} eV neutrino interacting in water at a distance of 1 km, which would be detected with an amplitude of about 10 mPa in the low-ultrasonic frequency range (maximum amplitude between 5 kHz and 20 kHz) with an opening angle of about 1°. The proposed design for the acoustic calibrator is a compact array system composed of piezo-ceramic tube transducers emitting in the radial direction. The emission is amplified and controlled by specific electronics adapted to them. The emission of the low-frequency (tens of kHz) acoustic bipolar pulse is generated by using the parametric emission technique at a high frequency (hundreds of kHz).

The use of the parametric acoustic source technique to generate neutrino-like signals allows the generation of low-frequency signals with narrow directionality, which is essential in order to obtain bipolar signals with the required “pancake” directionality. This technique was already validated in previous studies using cylindrical transducers (Ardid et al. 2012). The acoustic parametric effect occurs when two intense monochromatic beams with two close frequencies travel together through the medium. According to the linear theory, and as a consequence of the principle of superposition, the resulting sound field is composed only of the initial frequencies. However, due to the non-linearity of the medium, the interaction of the two frequency beams of finite amplitude generates a set of secondary frequency beams, such as the sum and difference of the primary frequency signals. This process of non-linear generation of new frequencies is limited to a certain distance from the transducer, called the array length, given by the distance of interaction or absorption length. This may be considered as a set of virtual acoustic sources (array) contained along the length of interaction; the source seems to be shaded exponentially as the distance increases from the transmitter. The secondary beam is produced with a directionality pattern similar to the one of the primary beams, which offers the advantage of generating a low-frequency directional beam.

The parametric technique for the emission of the low-frequency signal allows us to design a compact array consisting of fewer units with respect to classical solutions. Moreover, this technique will reduce costs and facilitate the deployment and operation of the calibrator. The proposed array calibrator under development is constituted of three to five elements of the piezo tube ceramic structured in the same axis-line, with a distance separation (d) between 10 cm and 20 cm, in order to obtain an opening angle of about 1° with phased emission of the array components. The transducer array will emit in radial direction and produce a bipolar pulse due to the interaction of parametric signals generated by each array element. Fig. 3.1 shows a schematic diagram of the configuration and emission.

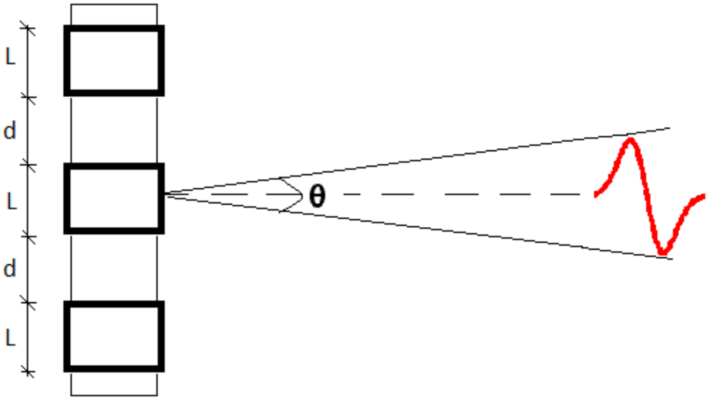

Fig 3.1. Schematic diagram of the transducer array configuration with 3 elements.

In order to increase the functionality of the calibrator and facilitate the calibration under different circumstances, the proposed calibrator is designed to work in different operation modes. The three operation modes are: (1) at linear low frequency range by emitting long non-directional signals (easy to generate and easy to detect); (2) at high frequency range by emitting long parametric directional signals (signal processing techniques could be used to enhance detection of these signals); and (3) at high frequency range by emitting the transient and directional parametric bipolar signal (the most challenging case). These operation modes will enable the array transmitter to achieve different goals, such as training and tuning the acoustic detector, cross-checking the detector hydrophones, and other marine applications. The proposed calibrator design and development was divided into three phases. In the first stage, the study and selection of transducers was done. Once the transducers were selected, their characterization was performed and measures with the single bare transducer emitting parametric neutrino-like signals were realized (Saldaña et al. 2016). In the second phase, the study and selection of backing and matching layer materials were carried out for optimizing the ceramic emission, and for holding and isolating the ceramics as well. As a result, a final prototype transducer (backed and moulded) convenient for this application was selected. Fig. 3.2 shows a diagram of the transducer design with the backing and matching layer configuration. After the transducer design was finished, the design of the complete array system composed of five units was developed. The design steps and the calibration of the complete line-array in the linear and non-linear (parametric) range generation are described in section 3.5.

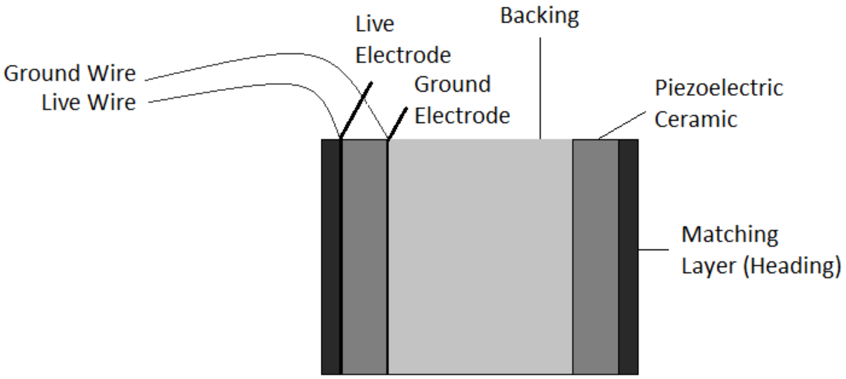

Fig 3.2. Drawing of the transducer unit: ceramic, backing and matching layer.

3.2 Piezoelectric Transducer Selection and Calibration

From the available piezoceramics in the market, two commercial piezo-ceramic tube transducers were selected as emitter candidates of the array calibrator. The selection was made in terms of resonance frequencies, power emission, dimensions, and costs. Both transducers permit high-frequency signal emissions with high power, exhibiting reasonable power levels at low frequency as well. The first candidate was the piezo-ceramic UCE-534541, hereinafter referred to as the large tube. Its dimensions are:

outer diameter, 5.3 cm; inner diameter, 4.5 cm; and height, 4.1 cm. The large tube primary resonance frequency is around 490 kHz with a real impedance of 9 Ω, with a secondary resonance frequency at low frequency, around 35 kHz. The second candidate is the piezo-ceramic UCE-343020, hereinafter referred to as the small tube. Its dimensions are: outer diameter, 3.4 cm; inner diameter, 3 cm; and height, 2 cm. The small tube primary resonance frequency is located around 890 kHz with a real impedance of 6 Ω, with a secondary frequency resonance around 75 kHz. Fig. 3.3 shows a picture of both ceramics, Fig. 3.4 shows the admittance of the large tube and Fig. 3.5 the electrical admittance of the small tube, in these graphics the resonance frequencies are appreciated. The admittance and impedance of the ceramics was determined with the high frequency HF LCR Meter 6500P analyzer from Wayne Kerr Electronics, which is able to measure impedance at high frequency precisely with a fast speed measurement. The capacitance, inductance and impedance basic accuracy is ± 0.05%.

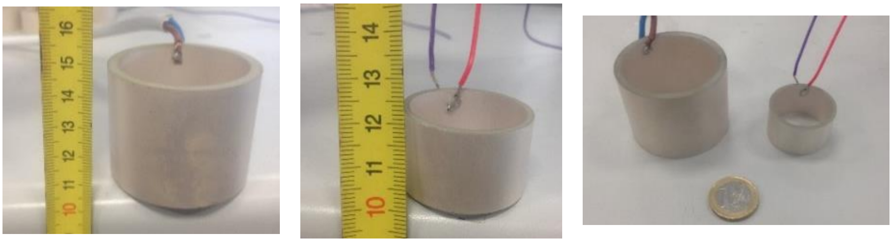

Fig. 3.3. Piezo-ceramic large tube (left panel), piezo-ceramic small tube (middle panel) and both piezo-ceramics (right panel).

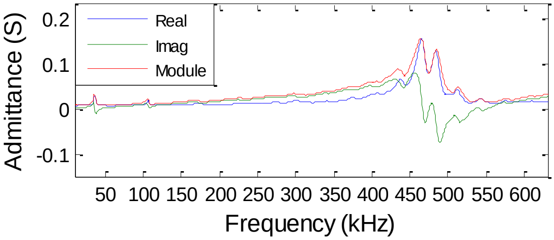

Fig. 3.4. Admittance of the UCE-534541 piezo-ceramic

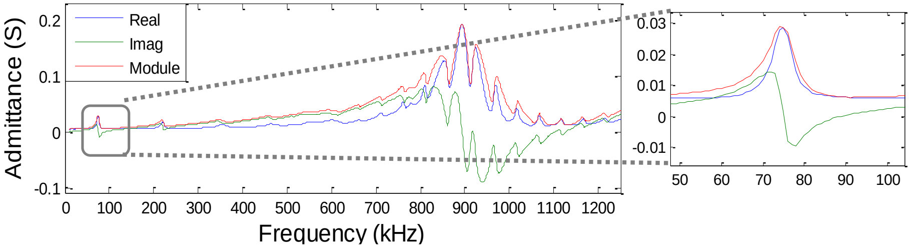

Fig. 3.5. Admittance of the UCE-343020 piezo-ceramic

3.2.1. Transmitting Voltage Response and Directionality

The piezo-ceramics were characterized both at high and low resonance frequencies in a water tank of 87.5 × 113 × 56.5 cm^3 with fresh water at the ultrasonic laboratory of Escola Politècnica Superior de Gandia (EPSG) at UPV. The calibration was performed in terms of Transmitting Voltage Response (TVR), which is the ratio of the pressure signal emitted to the applied voltage, using tone bursts at different frequencies. Moreover, the emission directionality with respect to the equatorial plane of the cylinder was also evaluated. With respect to the emission part, the signal was driven by an arbitrary 14 bits waveform PCI5412 generator (National Instruments©) connected to the ceramic through a linear RF amplifier 1040L (55 dB, ENI©). The receiver hydrophones used for these measurements were omnidirectional, particularly, model RESON-TC4038 for the high frequency range and the model RESON-TC4034 for the low frequency range. The hydrophone (which position is controlled by means of a positioning system) was connected to the digitizer card PCI-5102 were signals were acquired. The generation and acquisition cards were synchronized with the positioning system, their control and management was performed through LabView. The experimental set-up of the calibration is presented in Fig. 3.6. The results (left panel of Fig. 3.7) show the sensitivities obtained at high frequency with resonance frequency (F_R) of 490 kHz for the large tube and 890 kHz for the small tube. The TVR of the large tube is 159 dB (re µPa/V at 1 m) at F_R = 490 kHz with a directionality of Full Width Half Maximum (FWHM) of 10° (left panel of Fig 8X). On the other hand, the TVR of the small tube is 162 dB (re µPa/V at 1 m) at F_R = 890 kHz with a FWHM directionality of 14° (left panel of Fig 3.8). At low frequencies (right panel of Fig 3.8), the TVR varies between 132 and 140 dB (re µPa/V at 1 m). The right graphic of Fig. 3.8 shows the directionality of the large ceramic which is around ±40º at 20 kHz and ±20º at 40 kHz.

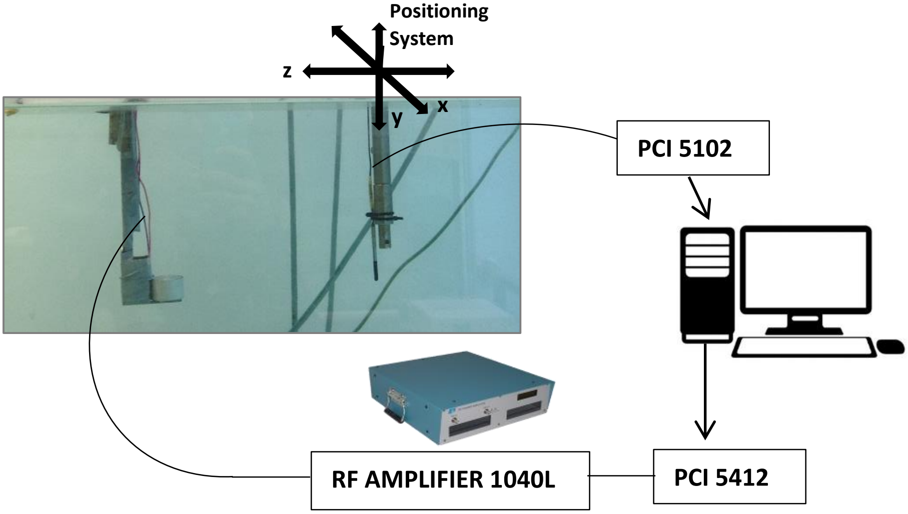

Fig. 3.6. Calibration experimental Set-up with hydrophone RESON-TC4038.

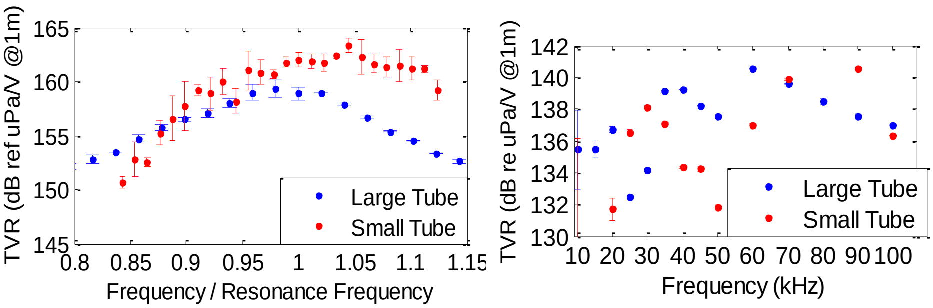

Fig. 3.7. Characterization of the ceramics (left) TVR of large tube at F_R = 490 kHz (blue dots) and for small tube at F_R = 890 kHz (red dots); (right) TVR from 10 to 100 kHz.

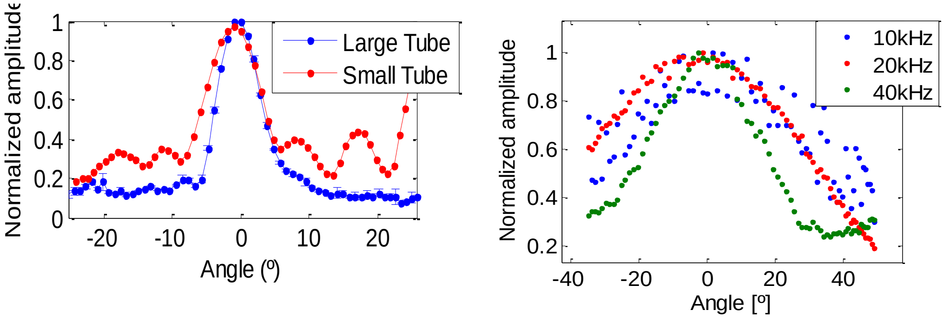

Fig. 3.8. Directionality at 490 kHz for the large tube, in blue, and at 890 kHz for small tube, in red (left). Directionality at 10 kHz, 20 kHz and 40 kHz for large tube ceramic (right)

3.3 Design of the First Single Transducer

This section describes the design and development of the single transducer design as element for the final array calibrator. The complete transducer was constituted by the bare ceramic implemented with a backing and heading material. The reasons of adding these parts to the bare ceramic were for matching the ceramic impedance to the media, optimizing the emission power, facilitating the array construction, protecting and holding it. On the one hand, the backing part helps to guide part of the emission energy from the back to forward and establish the support of the ceramics for the array. On the other hand, the matching layer helps to achieve a better ceramic impedance matching to media and plays an important role as ceramic isolation and protection. Both ceramics (small and large) were tested with different backing materials and headings in order to test which was the most optimal design in terms of acoustic power emission and directionality, for both in the linear and non-linear (parametric) range. The parametric study was done with the aim of parametric generation of two different signals at low frequency-parametric, a sine sweep signal and a bipolar shape pulse signal in time. The steps performed and the results obtained from these studies are presented in the following subsections.

3.3.1. Backing

Some backing materials are able to absorb the energy produced from the back of the active element (ceramic) and reflect part of it forward, providing more acoustic power in emission (Kossof 1966). In addition, the backing element of the transducer will constitute the support of the complete future array calibrator, i.e., playing an important role in the mechanical design of the array (Fig 3.1). Since all elements of the array are identical and emit synchronously (coherent emission) it is expected that the coupling effect of the backing will be negligible. Different materials and thicknesses were studied in order to find the best option in terms of TVR and acoustic impedance. The materials studied as backings were epoxy and aluminium. The large tube ceramic was tested with four different backings; a cylinder of aluminium with a tube hole of 1.5 cm (so-called small hole), a cylinder of aluminium with a tube hole of 2.5 cm (so-called big hole), full of aluminium and full of epoxy. The small tube ceramic was tested with three different backings; a cylinder of aluminium with a tube hole of 1.5 cm, a full of aluminium and full of epoxy. Fig. 3.9 shows the ceramics implemented with the backing elements studied.

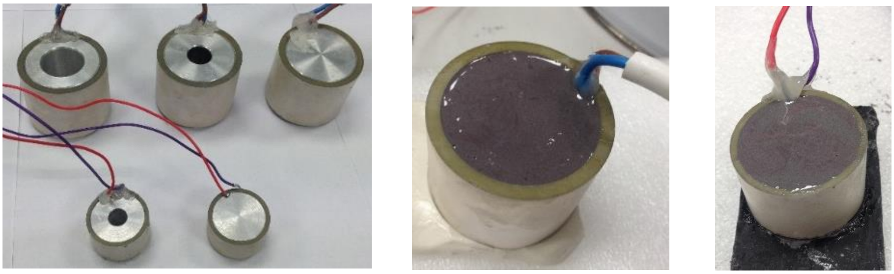

Fig. 3.9. Piezo-ceramics with aluminium backings of different thicknesses (left), large tube ceramic filled with epoxy backing (middle) and small tube ceramic filled with epoxy backing (right).

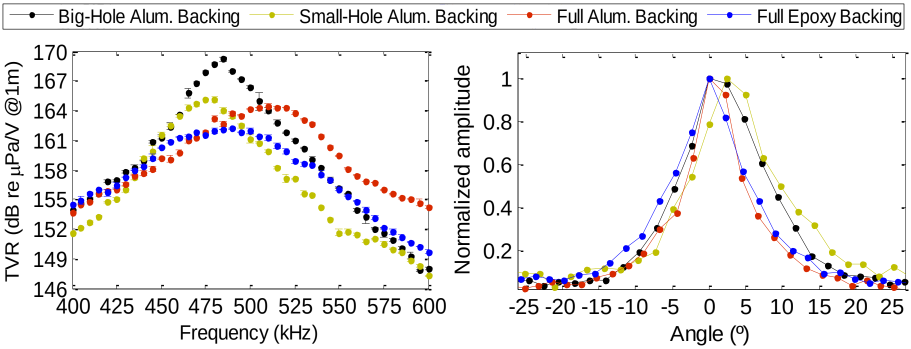

Fig. 3.10. Large tube ceramic characterization with different backings; TVR (left) and directionality (right).

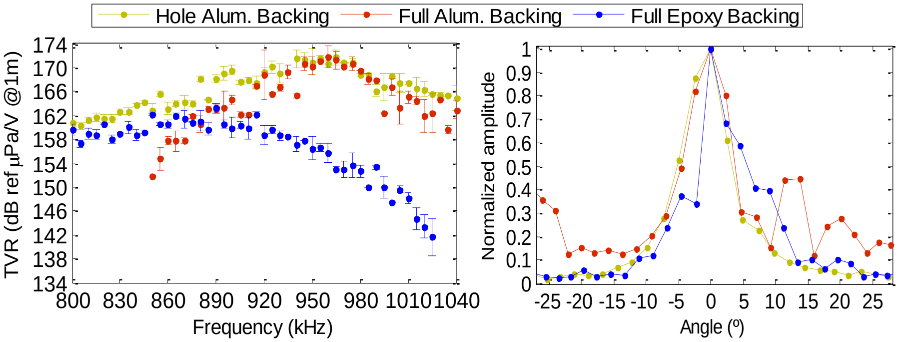

Fig. 3.11. Small tube ceramic characterization with different backings; TVR (left) and directionality (right).

Fig. 3.10 and 3.11 show the results obtained with the characterization of all backed ceramics under study, in terms of TVR and directionality. According to the results, the set of aluminium backing with or without hole (completely filling the tube ceramic) yielded the best results. For the big-hole aluminium backed large-ceramic the frequency response is sharper and the maximum increment respect to the bare ceramic is 10-12 dB. In the case of the full aluminium backed large tube a 3-5 dB increment on the TVR in the resonance range frequency with a flat response, a resonance frequency shifting to 510 kHz, and an increment up to 30 Ω (real) in the impedance was observed. For the small-hole aluminium backed large-ceramic a 4-6 dB increment on the TVR with a flat frequency response. Regarding the small tube backed with aluminium, with and without hole, an increase of 5-7 dB on the TVR, a shift on the resonance frequency to 950 kHz, and an impedance increment to 50 Ω (real) was appreciated. Moreover, there was not any appreciable change in the directionality patterns of both tubes.

3.3.2. Matching layer

The next step to complete the transducers design, was adding the matching layer to the backed ceramics. Ensuring protection, isolation and holding, and matching the impedance of the piezo-ceramic to the impedance media (Li et al. 2012) were the reasons for moulding the bare ceramic. Two interesting materials for moulding underwater transducers were acoustically studied in order to determine the effect on the wave emitted. The matching materials under study were the resin RoyaPox 511 and the Polyurethane EL241F. Both materials exhibit interesting acoustic properties for matching the ceramic impedance to the media due to their specific acoustic impedance (Z), density (ρ) and sound speed (c_L). There is maximum transmission at the layer thickness of $(2n-1)$ λ/4. Since for the first mode, λ/4, the obtained thickness values were too thin for an optimum covering, the matching layer thicknesses were set to accomplish the second mode with thickness 3λ/4 of the wavelength emitted at the ceramic resonance frequency. Such a selection offers the advantage of sufficient thickness to facilitate the covering and obtaining maximum length transmission. The matching layer mould used was a cylinder with the thickness space necessary to cover the ceramic, controlled by a precise metric rule with an estimated uncertainty of ±0.1 mm. The acoustic properties of the materials and the thickness used are summarized in Table 1.1. In order to test both materials with the same ceramic, two large tubes with aluminium backing were moulded with each material. The ceramic covered with RoyaPox 511 is shown on the left panel of Fig. 3.10 and with polyurethane EL241F on the middle panel of Fig. 3.10. The best results in terms of TVR and directionality were obtained with the polyurethane. Afterwards, a small tube ceramic with aluminium backing was moulded with polyurethane, as shown in right panel of Fig. 3.10.

ACOUSTIC PROPERTIES	**Large Tube M.L. RoyaPox 511**	**Large Tube M.L. EL214F**	**Small Tube M.L. EL214F**
c_L (m/s)	2602	1600	1600
Z (MRayls)	2.82	1.857	1.857
ρ (kg/m^3)	1050	1160.7	1160.7
Frequency (kHz)	480	510	960
λ/4 Thickness (mm)	1.3	0.78	0.42
3λ/4 Thickness (mm)	4.0	2.4	1.3

Table 3.1. Acoustic Properties of the Matching Layer (M.L.) materials RoyaPox 511 and EL214F, and thickness (mm) obtained for accomplishing λ/4 or 3λ/4 of the emitted wavelength at the ceramic resonance frequency.

Fig. 3.12. Piezo-ceramic large tube with aluminium backing and RoyaPox 511 moulding (left); Piezo-ceramic large tube with aluminium backing and polyurethane EL241F moulding (middle); Piezo-ceramic small tube with aluminium backing and polyurethane EL241F moulding (right).

The ceramic moulded with the RoyaPox 511 resin showed the same TVR level on the resonance frequency than before moulding (left graphic of Fig. 3.13, in black). The resonance frequency shifted to 450 kHz, but the impedance and directionality were very similar to that obtained with the bare ceramic. For the case of the large tube moulded with the EL241F polyurethane, there was a TVR gain of 5 dB approximately in the resonance frequency compared to before moulding. The resonance frequency shifted to 495 kHz with a sensitivity of 169 dB (re µPa/V at 1 m). The TVR curve for this case is shown in left graphic of Fig. 3.13, in blue. The impedance at the resonance frequency was 12 Ω (real), that is, it was reduced as compared to itself only backed, but being still higher than bare. With respect to the directionality, the pattern did not show any significant variation. The right graphic of Fig. 3.13 shows the TVR of the small tube moulded with the polyurethane. The graph is practically the same as before moulding for the 890 kHz–1 MHz range. However, there was also a peak resonance at higher frequencies, for 1165 kHz with 169 dB (re µPa/V at 1 m) with real impedance of 20 Ω. Directionality pattern did not vary with respect to the bare one. On the other hand, the TVR of the large-tube ceramic backed with aluminium and moulded with polyurethane EL241F was measured at the low-frequency range, from 15 kHz to 100 kHz showing similar levels of sensitivity to the ones obtained with the same bared ceramic (right graphic of Fig. 3.7, in blue).

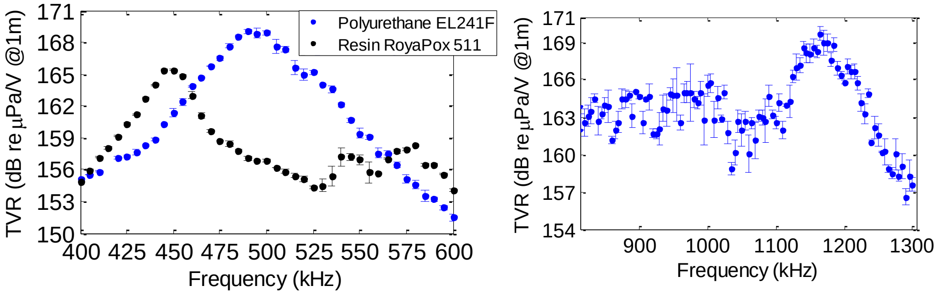

Fig. 3.13. TVR of UCE-534541 aluminum backed and molded with polyurethane EL241F, in blue, and RoyaPox 511 resin, in black, (left graphic) TVR of UCE-343020 aluminum backed and moulded with polyurethane EL241F (right graphic).

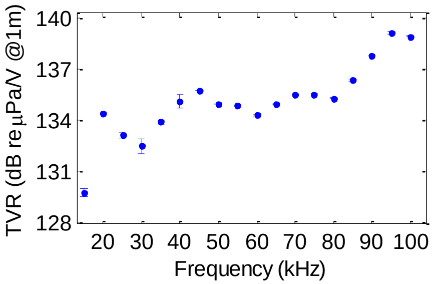

Fig. 3.14. TVR of UCE-534541 aluminum backed and molded with polyurethane EL241F, measured at low-frequency from 15 kHz to 100 kHz.

To sum up the results obtained in this section, the design with the backing filled with aluminium and the moulding with polyurethane EL241F produced an increase on the TVR at resonance of 9 dB for the big-tube ceramic and of 7 dB for the small-tube ceramic. For both ceramics, the design did not change the directionality pattern of the ceramics.

At this point, the next step was studying the moulding and backing effect on the parametric emission for both ceramics, in order to choose the most optimal option as final transducer for the complete array. This is presented in the next subsection.

3.4 Studies on Parametric Emission

After calibrating the transducers in the linear range, the next step was testing the transducers in the non-linear range in order to check that parametric signals could be generated in the media at low-frequency from the emission of modulated signals at high frequency. The best results obtained with the parametric emission of the bipolar pulse signal in terms of efficiency and the directionality, determined which transducer was the optimal for being used in the array calibrator.

Firstly, the parametric acoustic source technique was evaluated by means of the low frequency-parametric generation of a sine sweep signal using the cross-correlation with the expected signal. Following this methodology, it is feasible to recognize the parametric signal, since the correlation produces a clear narrow peak on the signal arrival time, which allows it to be distinguished from near echoes, as well as an increase in the signal to noise ratio (Adrián-Martínez et al. 2015). Afterwards, the low frequency-parametric generation of a bipolar shape pulse signal in time was studied. The generation of the carrier signal for the bipolar pulse generation is explained in (Ardid et al. 2012). These carrier signals of high frequency, e.g., at the frequency resonance of the ceramic, either 495 kHz or 1165 kHz permit the parametric generation. The results are shown for the measures performed with both backed and moulded ceramics; the large and small tube ceramic, hereinafter so-called the large transducer and the small transducer.

In order to confirm the non-linear effect of the parametric signal received three studies in the different aforementioned stages were conducted. The first study aimed at comparing the amplitude of primary and secondary beams by starting from low amplitude emission and increasing it to demonstrate the non-linear effect. The second measurement analysed the secondary non-linear beam generation in the medium by changing the distance between emitter and receiver. The last study compared the directionality patterns of both beams.

The experiment was done in the same water tank as described in Section 3.1. The piezo-ceramic was connected to a linear 55 dB (gain) RF amplifier ENI 1040L to feed the emitter and generate a more powerful acoustic wave in order to achieve the non-linear parametric effect. The receiver was the RESON-TC4034. This transducer is an omnidirectional, broad-band hydrophone with enough sensitivity to detect the primary beam (high frequency) being more sensitive to low frequency, i.e., for the bipolar pulse detection. Additionally, it was connected to a charge amplifier CCA 1000 (Teledyne RESON) which amplifies the received signal, especially for low frequency signals.

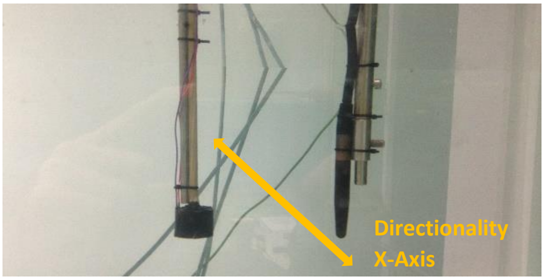

Fig. 3.15. Test alignment of moulded and backed small-tube ceramic and the hydrophone RESON-TC4034 used to measure the parametric signals.

3.4.1. Parametric Sine Sweep Signal

The emission signal for the generation of the sine sweep signal with the small transducer was designed by modulating a sine sweep signal from 20 kHz to 50 kHz using a carrier frequency of 1160 kHz. The left panel of Fig. 3.16 shows the emission signal, where the modulation shape can be observed. The received signal was a mix of the primary beam at 1160 kHz and the secondary beam at low frequency produced by parametric effect. In order to distinguish the secondary beam, a band pass (5–80 kHz) filter was applied. The right panel of Fig. 3.16 shows the received signal, primary (original) and secondary (filtered) beams. The secondary beam (filtered received signal) is multiplied by a factor of 15 in order to be visible together with the original received signal. The analyses of the different parametric studies with this signal were obtained by taking the amplitude value of the correlation of the received signal with the primary beam signal (high frequency) and with the expected secondary beam signal (low frequency). The left panel of Fig. 3.17 shows the correlation of the original received signal with the expected secondary beam signal. There is a clear correlation peak at the arrival time of the received signal.

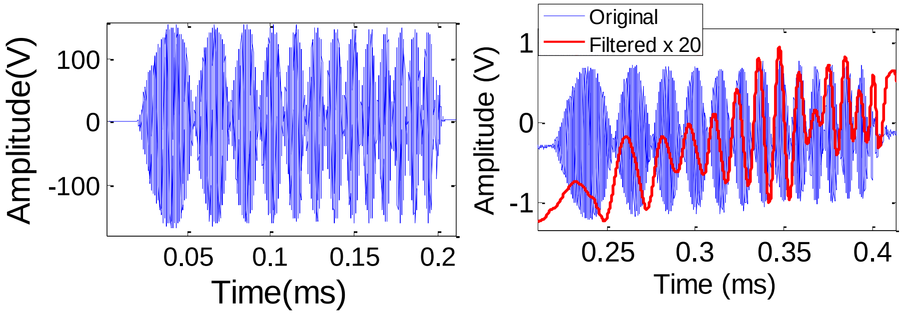

Fig. 3.16. Emitted signal, with the small transducer, for sine sweep (20 kHz – 50 kHz) generation (left panel), received signal (blue line) and the band-pass filtered signal in red line (right panel).

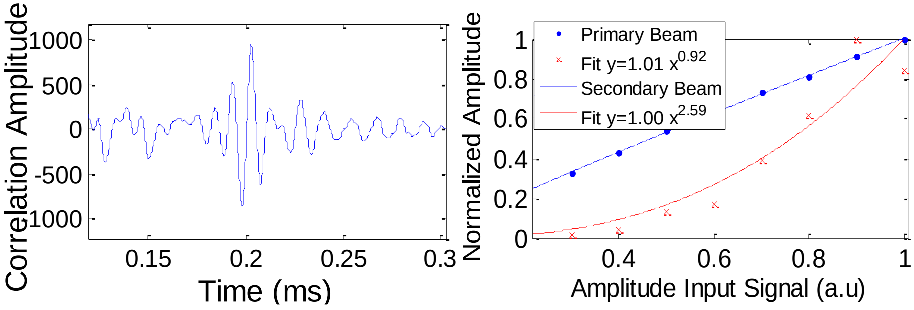

Fig. 3.17. Cross-Correlation of the original received signal with the expected secondary beam (left panel) and correlation amplitude of the received signal with primary beam (blue points) and secondary beam (red points) as a function of the signal emitted amplitude (right panel). The emissions were performed with the small transducer.

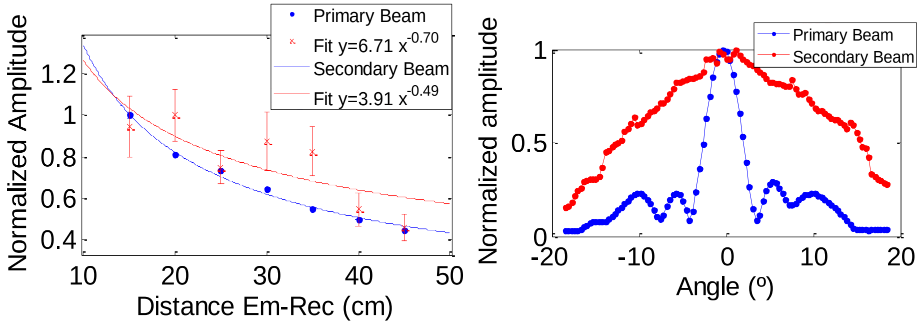

Fig. 3.18. Correlation amplitude of the received signal with both beams as a function of the distance between emitter and receiver (left panel) and directionality pattern of both beams (right panel). The emissions were performed with the small transducer.

The right panel of Fig. 3.17 shows the correlation amplitude behaviour of the received signal, without filtering (original) and with the band-pass filtering (secondary beam) as a function of the input signal amplitude. The data fitting to parameterizations showed that the exponent for the secondary beam is much larger than that of the primary beam, which is evidence of the non-linear effect. The exponent value of the primary beam is 0.92 ± 0.02 and for the secondary beam is 2.59 ± 0.60. The exponent of the primary beam is close to one as expected in terms of linearity. On the other hand, for the secondary beam, the expectation for the exponent was two, but it is larger because of the cross-correlation method used. In fact if we were directly representing the amplitude of the signal of the secondary beam filtered, the exponent would have been 1.69 ± 0.09. However, when using the correlation method for the secondary beam, following the parametric theory, the received signal is correlated with the second time derivative of the envelope squared of the emitted signal. The fact that we use the square in this process should be why the exponent is almost twice the expected value.

The evolution of both beams with the distance is shown in left panel of Fig. 3.18, it shows the different behaviour between them. The ratio of amplitudes between the primary and secondary beam increases as a function of the distance, which is evidence of the secondary beam being generated in the medium through non-linearity effect. Parameterizations were fitted to the data obtaining a smaller exponent for the secondary beam, as expected. For the primary beam the exponent value is −0.70 ± 0.04 while for the secondary beam is −0.49 ± 0.22. The right panel of Fig. 3.18 shows the directionality patterns of both beams. The directionality obtained with the secondary beam is an open angle (FWHM) of 28º. This study does not show an evidence of the parametric effect since the primary beam has a FWHM of 7º.

The parametric study for the sine sweep signal generation with the large transducer was performed by emitting a modulated sine sweep signal from 20 kHz to 50 kHz using a carrier frequency of 495 kHz. The left panel of Fig. 3.19 shows the emission signal, where the modulation shape can be observed. The received signal was a mix of the primary beam at 495 kHz and the secondary beam at low frequency produced by parametric effect. In order to distinguish the secondary beam, a band pass (5–80 kHz) filter was applied. The right panel of Fig. 3.19 shows the received signal, primary (original) and secondary (filtered) beams. . The secondary beam (received signal filtered) is multiplied by a factor of 20 in order to be visible together with the original received signal. The analyses of the different parametric studies with this signal were obtained by taking the amplitude value of the correlation of the received signal with the primary beam signal (high frequency) and with the expected secondary beam signal (low frequency). The left panel of Fig. 3.20 shows the correlation of the original received signal with the expected secondary beam signal. There is a clear correlation peak at the arrival time of the received signal.

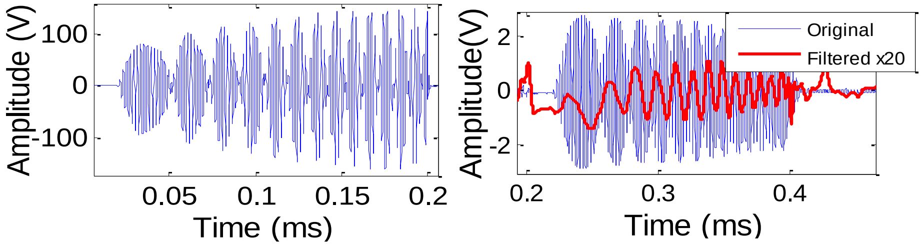

Fig. 3.19. Emitted signal, with the large transducer, for sine sweep (20 kHz – 50 kHz) generation (left panel), received signal (blue line) and the band-pass filtered signal in red line (right panel).

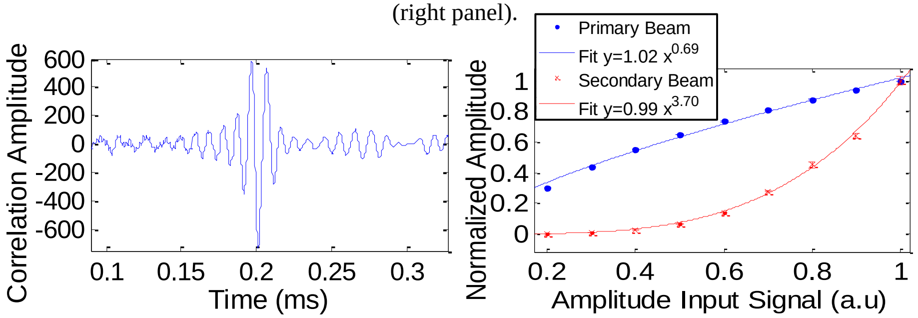

Fig. 3.20. Cross-correlation of the original received signal with the expected secondary beam (left panel) and correlation amplitude of the received signal with primary beam (blue points) and secondary beam (red points) as a function of the signal emitted amplitude (right panel). The emissions were performed with the large transducer.

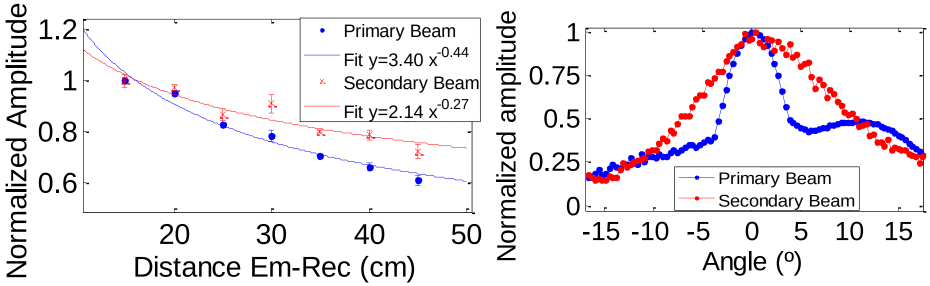

Fig. 3.21. Cross-correlation amplitude of the received signal with both beams as a function of the distance between emitter and receiver (left panel) and directionality pattern of both beams (right panel). The emissions were performed with the large transducer.

The right panel of Fig. 3.20 shows the correlation amplitude behaviour of the received signal, without filtering (original) and with the band-pass filtering (secondary beam) as a function of the input signal amplitude. The data fitting to parameterizations showed that the exponent for the secondary beam is much larger than that of the primary beam, which is evidence of the non-linear effect. The exponent value of the primary beam is 0.69 ± 0.03 and for the secondary beam is 3.70 ± 0.12. We expected an exponent close to one for the primary beam, but it is slightly lower due to saturation effects of the amplifier. On the other hand, for the secondary beam, the expectation for the exponent was two, but it is larger because of the cross-correlation method used. In fact if we were directly representing the amplitude of the signal of the secondary beam filtered, the exponent would have been 1.68 ± 0.15. However, when using the correlation method for the secondary beam, following the parametric theory, the received signal is correlated with the second time derivative of the envelope squared of the emitted signal. The fact that we use the square in this process should be why the exponent is almost twice the expected value.

The evolution of both beams with the distance is shown in left panel of Fig. 3.21, clearly displaying the different behaviour between them. The ratio of amplitudes between the primary and secondary beam increases as a function of the distance, which is evidence of the secondary beam being generated in the medium. Parameterizations were fitted to the data obtaining a smaller exponent for the secondary beam, as expected. For the primary beam the exponent value is -0.44 ± 0.04 while for the secondary beam is -0.27 ± 0.06.

The directionality patterns shown in right panel of Fig. 3.21 show the evidence of the parametric effect for the secondary beam since the pattern for this beam is quite similar to that of the primary beam, and much more directional than the ceramic directly fed at low frequency. The directionality obtained with the primary beam is a FWHM of 8º and for the secondary beam is an FWHM of 16.6º. For instance, the open angle (FWHM) for direct feeding in the frequency range, 20–50 kHz, was between 40º-80° approximately, depending on frequency.

3.4.2. Parametric Bipolar Pulse Signal

The emission signal for achieving the parametric generation of the bipolar-shape pulse with the small transducer was designed by using the carrier signal at 1160 kHz. According to theory, the signal is set so the shape of the secondary signal matches the second time derivative of the envelope squared of the primary signal in amplitude (Moffett, M.B.; Mello 1979). The left panel of Fig. 3.22 shows the emitted signal-shape modulated. The received signal was a mix of the primary beam at 1160 kHz and the secondary beam at low frequency produced by parametric effect. In order to distinguish the secondary beam, a band pass ([5 - 80] kHz) filter was applied. The right panel of Fig. 3.22 shows the received signal, primary (original) and secondary (filtered) beams. The secondary beam (bipolar pulse) is multiplied by a factor of 10 in order to be visible together with the original received signal (non-filtered). As expected, the secondary beam has a bipolar pulse-shape. The analysis of the different parametric studies with this signal were obtained by taking the amplitude value of the signal received at high frequency (primary beam) and of the bipolar pulse signal (secondary beam).

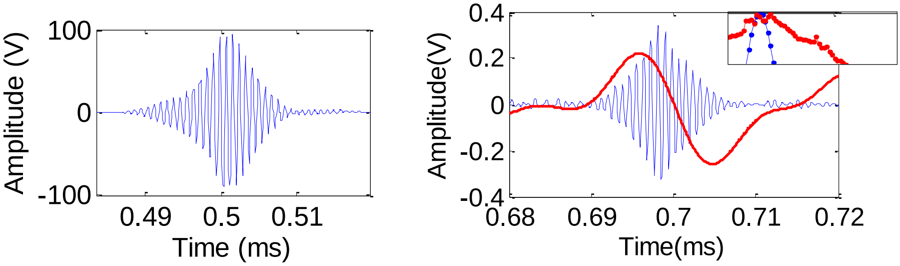

Fig. 3.22. Emitted signal, with the small transducer, for bipolar pulse generation (left panel); received signal in blue colour and bipolar signal obtained after applying a band-pass filter in red (right panel)

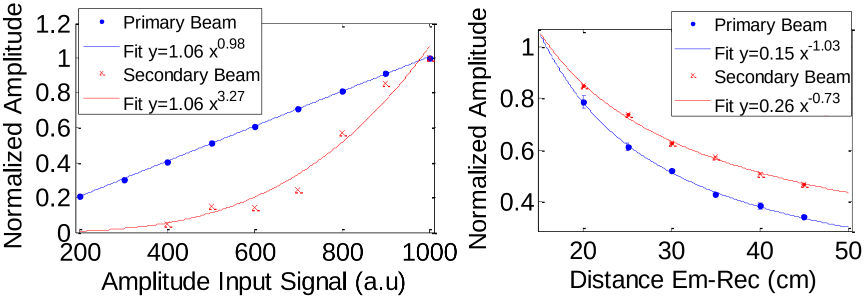

Fig. 3.23. Amplitude of the received (blue) and filtered signal (red) as function of input signal amplitude (left panel) and amplitude of the received signal for both beams as function of distance between emitter and receiver (right panel). The emissions were performed with the small transducer.

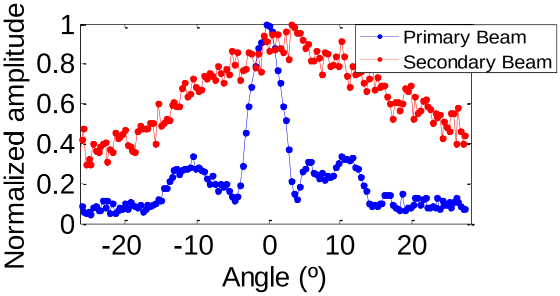

Fig. 3.24. Directionality pattern of both beams. The emissions were performed with the small transducer.

The right panel of Fig. 3.23 shows the amplitude behaviour of the received signal, without filtering (original) and with the band-pass filtering (the parametric bipolar signal) as function of input signal amplitude. The fitting data to parameterizations showed that the exponent for the secondary beam is twice the exponent of the primary beam, representing the non-linear effect. The exponent value of the primary beam is

0.98±0.01 and for the secondary beam is 3.27±0.39. In the right panel of Fig. 3.23 the evolution of both beams with the distance can be observed. The ratio of amplitudes between the primary and secondary beam increases as a function of the distance, which is evidence of the secondary beam being generated in the medium. For the primary beam the exponent value is -0.73 ± 0.03 while for the secondary beam is -1.03 ± 0.03. Fig. 3.24 shows the directionality patterns of both beams. The directionality obtained with the secondary beam is an open angle (FWHM) of 32°, which does not show an evidence of the parametric effect since it is close to the values obtained in the non-linearity low frequency range (right panel of Fig. 3.8).

The parametric study for the bipolar-shape pulse signal generation with the large transducer was performed by using the carrier signal at 495 kHz showed on the left panel of Fig. 3.25. The received signal was a mix of the primary beam at 495 kHz and the secondary beam at low frequency produced by parametric effect. In order to distinguish the secondary beam, a band pass ([5 - 80] kHz) filter was applied. The right panel of Fig 3.25 shows the received signal, primary (original) and secondary (filtered) beams. The secondary beam (bipolar pulse) is multiplied by a factor of 30 in order to be visible together with the original received signal (non-filtered). As expected, the secondary beam has a bipolar pulse-shape. A peak after the bipolar pulse is appreciated. That is due to the signal response of the transducer, to what can affect to the shape of the signal tail and the generation of an oscillation after the last signal pulse. The analysis of the different parametric studies with this signal were obtained by taking the amplitude value of the signal received at high frequency (primary beam) and of the bipolar pulse signal (secondary beam).

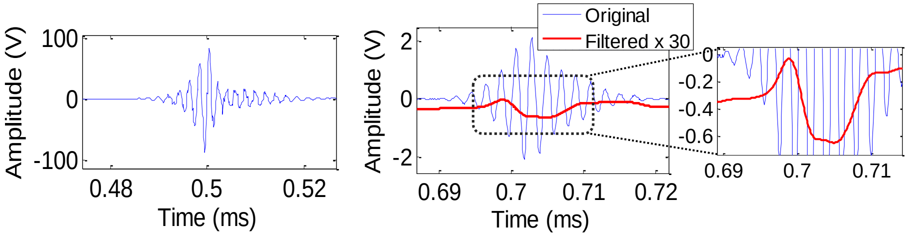

Fig. 3.25. Emitted signal, with the large transducer, for bipolar pulse generation (left panel); received signal in blue colour and bipolar signal obtained after applying a band-pass filter in red (right panel)

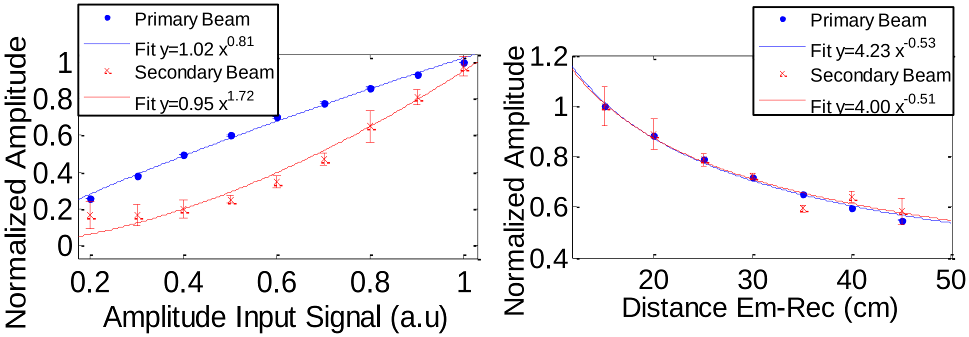

Fig. 3.26. Amplitude of the received (blue) and filtered signal (red) as function of input signal amplitude (left panel) and amplitude of the received signal for both beams as function of distance between emitter and receiver (right panel). The emissions were performed with the large transducer.

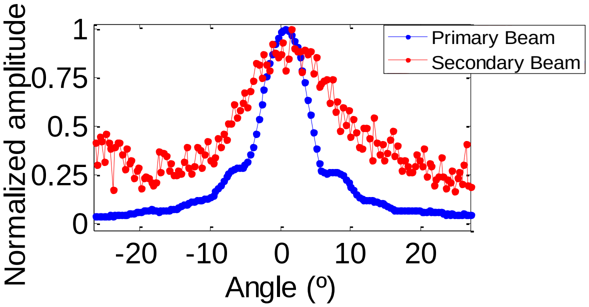

Fig. 3.27. Directionality pattern of both beams. The emissions were performed with the large transducer.

The left panel of Fig. 3.26 shows the amplitude behaviour of the received signal, without filtering (original) and with the band-pass filtering (the parametric bipolar signal) as function of input signal amplitude. The fitting data to parameterizations showed that the exponent for the secondary beam is twice the exponent of the primary beam, representing the non-linear effect. The exponent value of the primary beam is 0.81±0.03 and for the secondary beam is 1.72±0.26. The exponent for the primary beam is slightly below one due to saturation effects of the amplifier. In the right panel of Fig. 3.26 the evolution of both beams with the distance can be observed. No conclusive results could be obtained from this due to the fluctuations observed in the measurements and on the detection of the bipolar secondary signal, since the exponent value for the primary beam is -0.53±0.01 and for the secondary beam is -0.51±0.05. The directionality pattern, shown in Fig. 3.27, is the best proof of the parametric effect for the secondary beam since both beams have similar directivities. The directionality obtained with the primary beam is a FWHM of 8° and for the secondary beam is an FWHM of 15°.

The results obtained with the large-tube transducer validated satisfactorily the parametric generation with both signals the sine sweep and the bipolar pulse. The non-linearity effect of the parametric signal was appreciated in the studies performed. The secondary beam showed higher amplitude evolution and narrower directionality pattern than in the linear range. Moreover, the signal reproduction of the acoustic neutrino-like signals generation by using the parametric technique was achieved. However, in the case of the small-tube transducer, the results obtained in the directionality study with the secondary beam does not show an evidence of the parametric effect as the directionality pattern of the beam is similar to the one obtained at low frequency in the non-linear range (right panel of Fig. 3.8). Since the directionality pattern of the secondary beam is the best indicator for proving the parametric generation and one of the goals in the emission of the bipolar pulse is to achieve a very directional beam, the small transducer was rejected for the design of the neutrino´s array calibrator. The efficiency obtained of the parametric signal was very similar with both transducers, as well as, the TVR.

According to the results, the large tube ceramic designed with aluminium backing and matching layer of polyurethane EL241F showed the best acoustic characteristics in the non-linear range. Therefore, it was the selected transducer for the multi-element array calibrator. The next section describes the final calibrator design as a multi-emitter array.

3.5 Design of the multi-element transducer array calibrator

After the design of the single transducer and its validation with the parametric generation of the bipolar pulse signal, the design of the complete array system composed of few units of the developed transducer was performed. The array design was performed to obtain a more energetic and directional bipolar pulse, this caused by the interaction, at long distances, of the parametric beam generated for each array element.

3.5.1 Simulation

The first step was simulating the opening angle of the bipolar pulse signal at 1 km from the emission of three and five elements of the array considering an element separation of 5 cm and 10 cm. Fig. 3.28 show the results of the calculations performed by summing the contributions of the different sensors at different angles. The results of this simulation helped to select an appropriate array configuration for achieving the ‘pancake’ directionality (with an opening angle close to 1°). From the results, a linear array of three or five elements separated from 10 cm to 15 cm could be enough to obtain an opening angle of about 1º. The signal used for the simulation was the original received signal from the single element emission of the bipolar pulse carrier signal at 400 kHz, shown in the right panel of Fig. 3.25, in blue colour. Following the same procedure of section 3.1.3.3, the signal received at 20 cm (V[t]) was converted into spectral pressure components (P[f]), using the receiver sensitivity, and propagated until 1 km of distance. The propagation was performed taking into account the loss from the medium absorption coefficient (under the conditions of the KM3NeT telescope) and the spherical divergence.

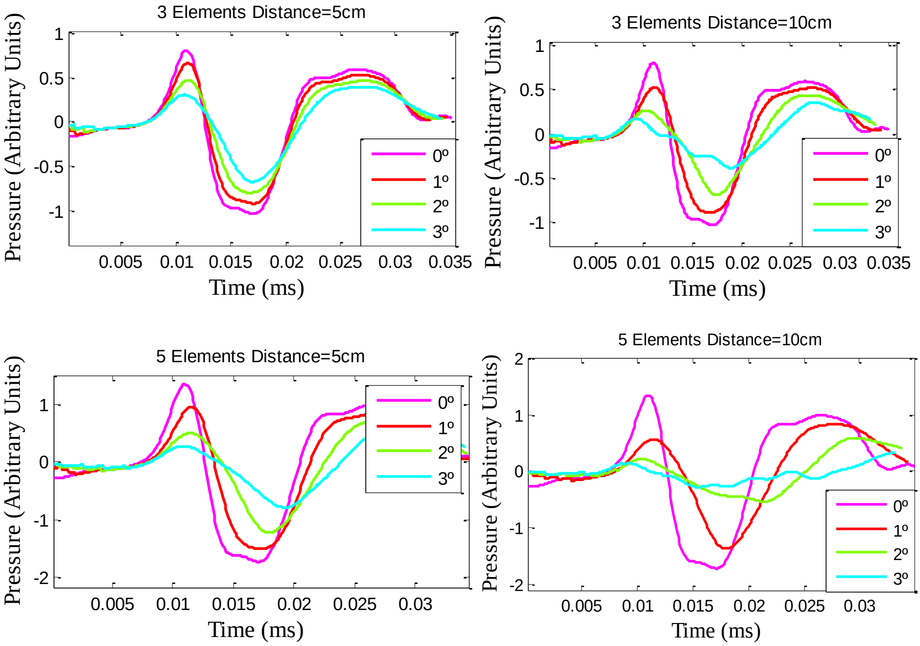

Fig 3.28. Acoustic pressure obtained by the propagation of the emitted wave to distances of 1 km. Notice that received and propagated signal are shown in different units.

With this, an optimal array configurations for the generation of the bipolar pulse with higher directionality (opening angle ~1º), was determined for both the based on three transducers and on five transducers separated 14 cm.

3.5.2 Mechanics

The next step was designing the structure for holding the transducers in a linear array shape. In this stage, it was decided, to create a flexible design which allowed to change easily the distance between two consecutives emitters, in order to study the two interesting array configurations and being able to optimise the distance experimentally afterwards. Therefore, the selected design was composed of a straight aluminium bar and the transducers introduced in the bar through their hole perforation in the transducer backing with the same diameter as the bar diameter (ϕ= 1 cm), as it is shown in Fig. 3.29 and Fig. 3.30. The purpose of using the bar as fixed structure is to maintain the linear array shape and the transducers orientation. The transducers were fixed in the bar through aluminium screws. Finally, to monitor the handling of the line-array, a U-shaped mechanical structure attached to the bar was designed (Fig. 3.31). The mechanical structure had a junction to join with the positioning system of the laboratory pool where the measures and test of characterization were performed.

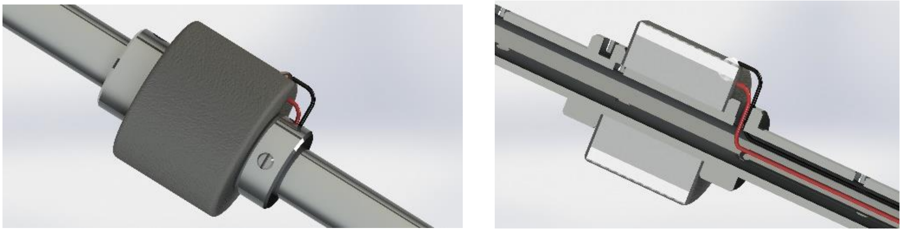

Fig 3.29. Layout of a single transducer introduced in the array bar. On the left image; detail of the transducer holding through screws. The right figure show the detail of the ceramic cable connection and its itinerary through the bar.

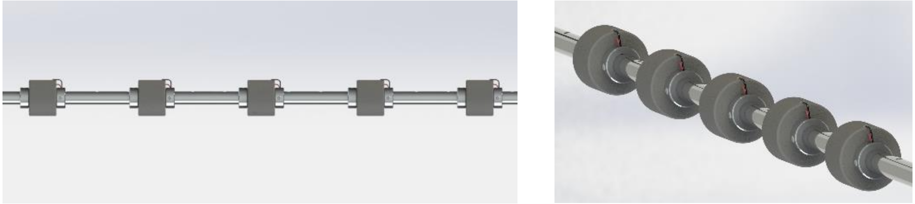

Fig 3.30. Layout of the transducers line array configuration introduced in the aluminium bar.

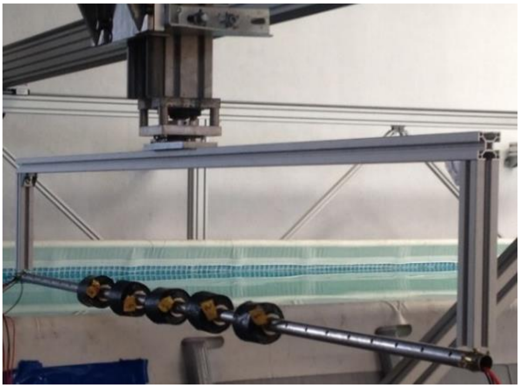

Fig. 3.31. Picture of the transducers line array configuration joined to the U-shaped mechanical structure attached at the positioning system of the laboratory pool.

3.5.3 Test of the transducer line-array

The line-array calibrator was characterized for one of the optimal configurations obtained in the previous simulation, the one based on three emitter transducers separated 14 cm. Simulation and experimental test for the linear and non-linear (parametric) range generation were performed in order to understand and check its functionality. Firstly, every array element was characterized and in a second phase the array with three active elements was calibrated, all in terms of TVR and directionality. The last step for the array calibration was testing it for the parametric generation. The parametric signal generation for the low frequency sine sweep signal and the bipolar like-pulse signal was measured in order to validate the parametric array emission.

3.5.3.1 Experimental Test setup

The multi-element array transducer was characterized in the laboratory pool of Campus de Gandia (at Gandia's harbour) which is 6.3 m length, 3.6 m width and 1.5 m depth. A precise positioning system integrated in the pool synchronized with the generation and acquisition through a Red Pitaya system. The line array emitter and the hydrophone were placed in different structure arms from the positioning system in order to control independently their movement and position during the measures (see Fig. 3.33). The array transducers were parallel connected to the output of a linear RF amplifier 1040L (55 dB, ENI©) which, at the same time, the input was connected to the Red Pitaya waveform generator card. The signal output voltage from the amplifier to the each transducer was identical, while the intensity was equitably shared to each element due to the parallel connection of the transducers respect to the signal amplifier. The receiver hydrophone used for these measurements was the model RESON-TC4034 which was connected to the digitizer card of the Red Pitaya, through which received signals were acquired. The generation and acquisition processes were controlled and managed through the software Matlab. Fig 3.32 show the diagram of the experimental set-up connection performed during the array calibration measurements.

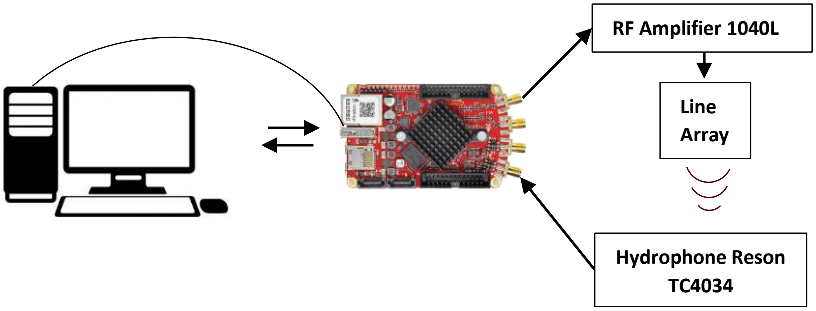

Fig. 3.32. Block diagram of the calibration experimental set-up connection.

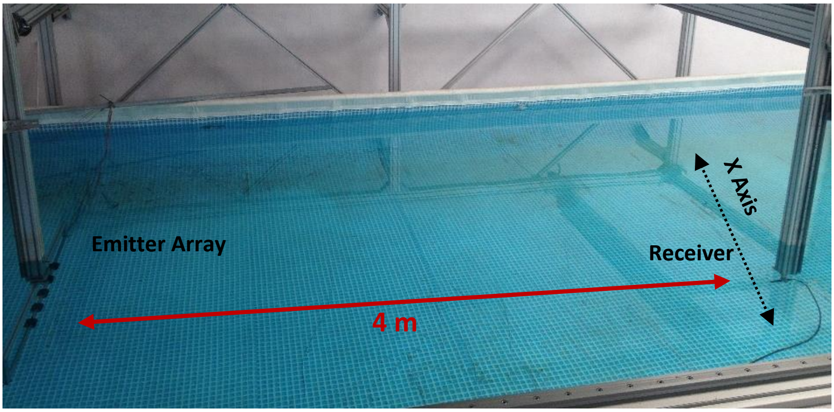

Fig. 3.33. Calibration of the experimental set-up, line-array and hydrophone placed on the positioning system arms.

3.5.3.2 Array characterization. Primary beam.

Firstly, the calibration of each array element, in the frequency range close to the resonance, was performed in order to check the functionality of the transducers. The calibration was performed in terms of TVR, using tone bursts at different frequencies. The distance between the array emitter and the hydrophone was 1 meter. The measured frequencies were from 350 kHz to 500 kHz in steps of 5 kHz. The TVR was measured individually for the three centred elements of the emitter array, indicated in Fig. 3.34. Secondly, the TVR of the three-element centred array emitting simultaneously was measured. For this, the transducers were connected in parallel to the output of the amplifier. Fig. 3.35 shows the TVR results obtained. The maximum TVR values are comprised between 163 dB – 166 dB re µPa/V at 1 m. The maximum values obtained in each transducer are located in different frequencies between 375 kHz – 410 kHz. The fact that the maximum values are not the same for each transducer was due to the ceramics could have little differences in their properties, and that, the mouldings have an error of ±0.1 mm in their thickness, and this could affect to it as well. Besides, for the parametric emission measurements, the frequency of 400 kHz was selected for the modulation, which for the three transducers measured there was a sensitivity close to 162 dB re µPa/V at 1 m.

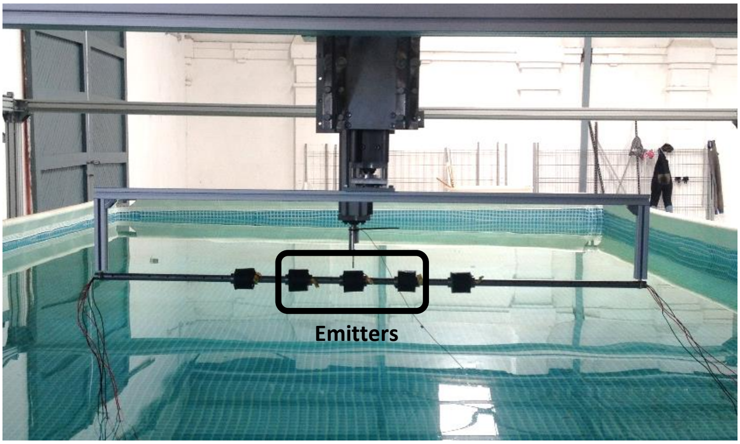

Fig. 3.34. Picture of the line-array transducer in the positioning system, indicating the three-element centred array.

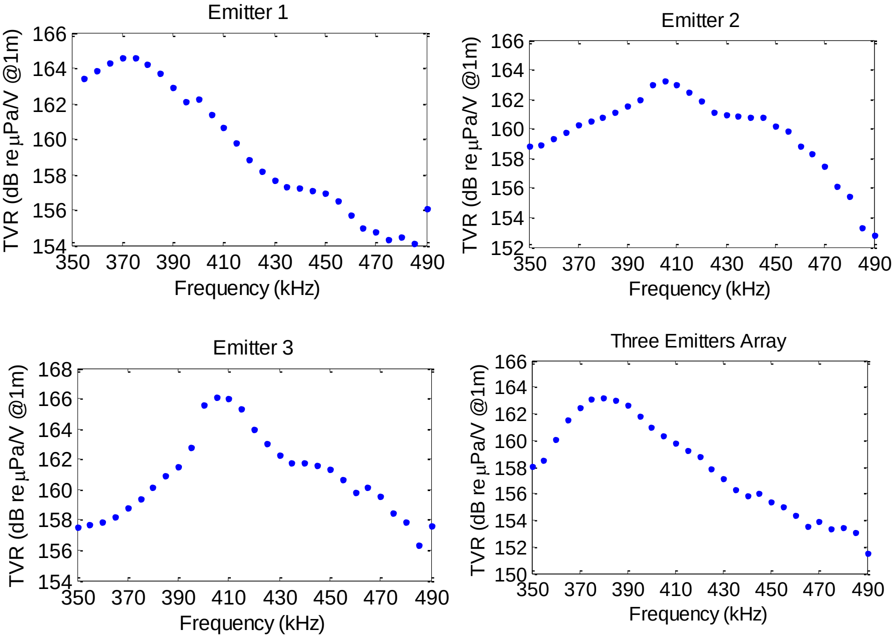

Fig. 3.35. TVR of each element of three-transducer centred of the array (top and bottom left) and TVR or the three transducers emitting simultaneously (bottom right).

3.5.3.3 Array characterization. Parametric (secondary) beam.

The next step was performing the parametric characterization of the line-array using the same procedure as the one used with the single transducer, emitting the signal for the parametric generation with three elements that emit acoustic waves at the same time. The carrier signals for the parametric generation were implemented in this case, at 400 kHz. The parametric acoustic source technique was evaluated for the sine sweep signal and for the bipolar pulse signal by means of the low frequency-parametric generation. The experiment was performed following the same experimental setup described in section 4.3.1 with the addition of a charge amplifier CCA 1000 (Teledyne RESON) connected to the hydrophone, before the input of the signal acquisition system, for amplifying the received signal, especially the low frequency signals. The line-array was configured with three active element (emitters) and it was 3.70 m apart from the hydrophone for the measurements.

The first study was performed with the sine sweep signal generation from 20 kHz to 50 kHz, the carrier signal (emitted) was designed with a carrier frequency of 400 kHz. The emitted signal was configured to start after 4.25 ms from the beginning of the signal emission, left panel of Fig. 3.38 show the emitted signal. The first study performed, for observing the non-linear effect of the low-frequency sine sweep signal received, was comparing the amplitude of primary and secondary beams by starting from low amplitude emission and increasing it to high amplitude (where the parametric effect is noticeable). The second study was measuring the directionality patterns of both beams, in order to check if the parametric low-frequency signal (secondary beam) had an opening angle similar to the one at high frequency. The methodology used for the data processing with the sine sweep signal was using the cross-correlation with the expected signal which allows to recognize easier the parametric signal. The right panel of Fig. 3.36 show one received signal correlated with the secondary beam. The analyses were obtained by taking the amplitude value of the received signal correlation with the primary beam signal for high frequency and with the expected secondary beam signal for the low frequency parametric beam.

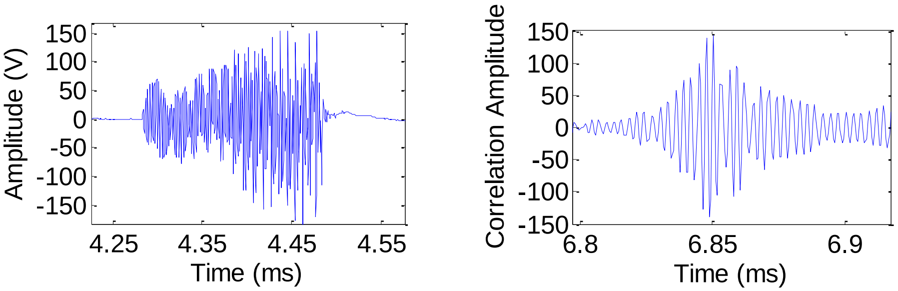

Fig. 3.36 Emitted signal for sine sweep (20 kHz – 50 kHz) generation (left) and cross-correlation of the original received signal with the expected secondary beam (right).

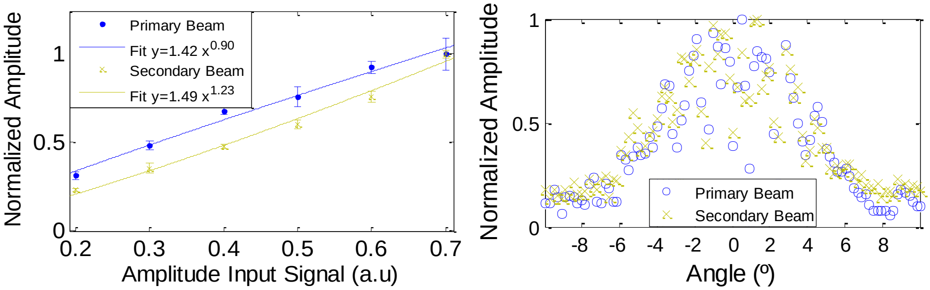

Fig.3.37 Parametric results with the Sine sweep signal; correlation amplitude of the received signal with the primary beam (blue) and the secondary beam (yellow) as a function of the input signal amplitude (left) and directionality pattern of both beams (right).

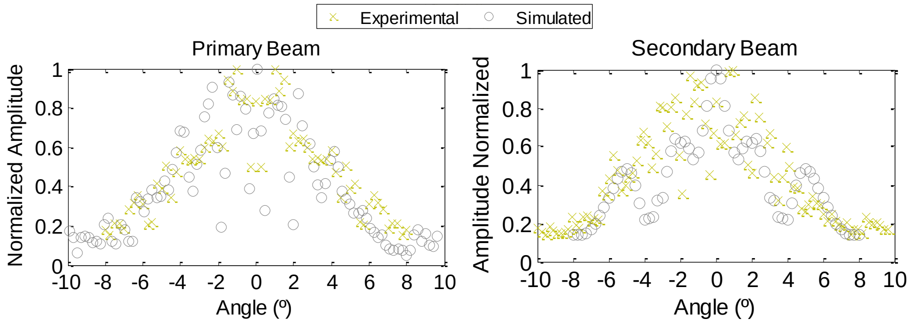

Fig.3.38 Comparison of the directionality pattern obtained with the experimental and simulated results for the parametric sweep signal generation with the array of three elements separated 14 cm: for the primary beams in the left and for the secondary beam on the right.

The left graphic of Fig. 3.37 shows the amplitude behaviour of the received signal correlated with the primary beam and with the secondary beam as a function of the input signal amplitude. The data fitting to parameterizations showed that the exponent for the secondary beam is larger than that of the primary beam, which is an evidence of the non-linear effect. The exponent value of the primary beam is 0.87 ± 0.07 and for the secondary beam is 1.25 ± 0.09. The exponent of the primary beam is slightly lower than one due to saturation effects of the amplifier. For the secondary beam, the exponent was expected to be twice the primary beam exponent, however the results showed it was a bit lower. The directionality patterns for the primary and secondary beam are obtained with the sine sweep signal are shown in the right graphic of Fig. 3.37. Some fluctuations are observed in the directionality patterns of both beams due to the effect of the received signals interference from the emission of the three transducers of the array to the receiver at 4m. The simulations performed, shown in Fig. 3.38, confirm this effect. The simulation uses the same configuration as in the measures in terms of distances array (14 cm of distance between elements and 4 m from the centred emitter to the receiver in 0º) and the signal used in simulations is the experimental one registered with one element at a few centimetres from emitter and extrapolated 4 m. The emitted signal of each element to the receiver position is obtained taking into account the attenuation due to propagation (travel distance) and transducer directionality, and the travel delay of the signal arrival. In this way, the three signals coming from each element contribute to the arrival signal to the receiver. Both experimental and simulation results show the interferences between the three element array and the generation of the parametric low frequency sine sweep signal with a similar directionality to the one of the primary beam. Moreover, it is much more directional than the ceramic directly fed at low frequency which had a FWHM between 40º-80° for the range of 20 kHz to 50 kHz. The FWHM obtained with the simultaneous emission of the line-array with three active elements is 8º (σ=3.4º) for both the primary beam and the secondary beam. This value can be compared with the directionality obtained emitting with a single transducer which had an opening angle for secondary beam of 16.6º FWHM (σ=7º) which corresponds to a reduction of 1/2 on the opening angle with the emission of the three elements in the line array.

The next study was performed with the generation of the bipolar-shape pulse signal, the emitted signal was designed by using a carrier signal at 400 kHz. The emitted signal was configured to start after 4.22 ms from the beginning of the signal emission, left panel of Fig. 3.39 shows the emitted signal. The right panel of Fig. 3.39 shows the original received signal, which corresponds to the primary beam at 400 kHz, and the secondary beam, which is the received signal filtered at low frequency with a band pass filter ([5 - 80] kHz). The secondary beam (bipolar pulse) is multiplied by a factor of 100 in order to be visible together with the original received signal (non-filtered). As expected, the secondary beam has a bipolar pulse-shape. A peak after the bipolar pulse is appreciated. This effect is due to the signal response of the transducer. The analysis of the different parametric studies with this signal were obtained by taking the amplitude value of the signal in volts peak to peak (V_{pp}) received at high frequency (primary beam) and of the bipolar pulse signal (secondary beam).

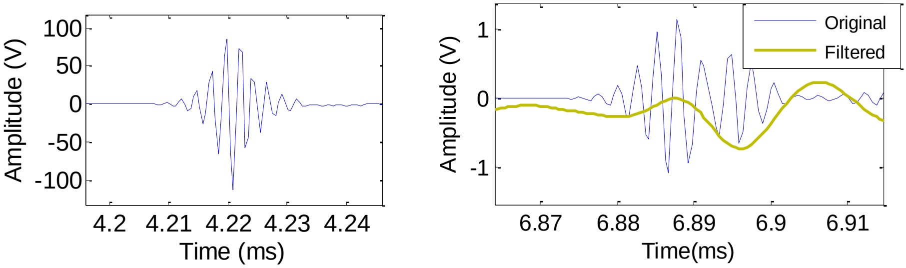

Fig. 3.39 Received signal, in blue, and bipolar signal obtained after applying a band-pass filter, in yellow. (multiplied by a factor of 100 in order to be visible).

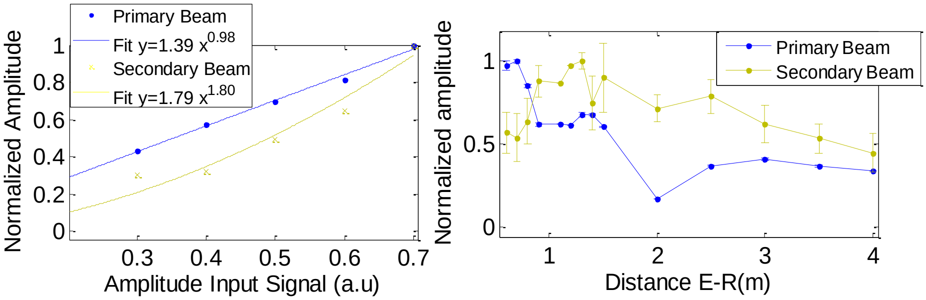

Fig. 3.40 Parametric results with the bipolar pulse signal generation; amplitude of the received signal with the primary beam (blue) and the secondary beam (yellow) as a function of the input signal amplitude (left) and amplitude of the original received signal (primary beam, in blue) and of the low-frequency filtered received signal (secondary beam in yellow) as a function of the distance between emitter and receiver (right).

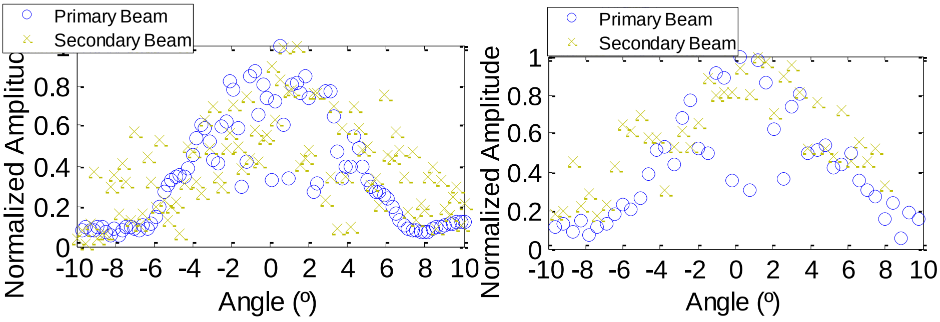

Fig. 3.41 Directionality pattern of both beams emitting with the carrier signal (primary beam, in blue) for the bipolar pulse generation (secondary beam, in yellow), measured experimentally. The left graphic shows the results obtained with the measures where the receiver was moved in the X axis line and the right graphic panning the emitter rotating in the horizontal axis.

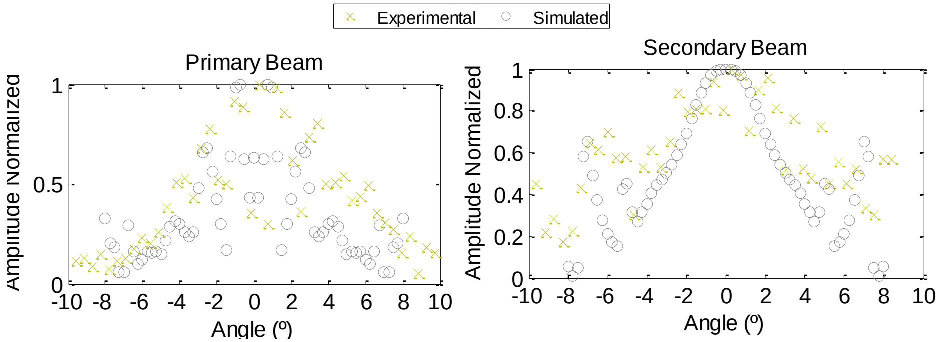

Fig.3.42 Comparison of the directionality pattern obtained with the experimental (panning measures) and simulated results for the parametric bipolar signal generation with the array of three elements separated 14 cm: for the primary beam in the left and for the secondary beam on the right.

The left panel of Fig 3.40 shows the amplitude behaviour of the received signal, without filtering (original) and with the band-pass filtering (the parametric bipolar signal) as function of input signal amplitude. The fitting data to parameterizations showed that the exponent for the secondary beam is twice the exponent of the primary beam, representing the non-linear effect. The exponent value of the primary beam is 0.98±0.08 and for the secondary beam is 1.80±0.45.

The directionality pattern is shown in Fig 3.41, the figure shows the results obtained experimentally for the primary and secondary beam with the bipolar pulse signal for the measures performed with movement of the receiver along the X axis line (left graphic) and with the panning of the emitter in the horizontal axis (right graphic). Also, some fluctuations are observed in the directionality patterns due to the effect of interference from the emission of the three transducers of the array to the receiver position at 4m. In order to check this effect simulations were performed using the same configuration. For the simulations, the same procedure as in the case of sine sweep has been used. The final results are shown in Fig 3.42. The directionality obtained with both beams experimentally and through simulation present a similar pattern tendency, showing a clear correspondence between simulations and experimental results. The opening angle FWHM obtained with the simultaneous emission of the line-array with three active elements is 8.0º (σ=3.4º) for the primary beam and approximately the same for the secondary beam. These values compared with the directionality obtained emitting with a single transducer, FWHM=15º (σ=6.4º) for the secondary beam showed a considerable reduction, almost one half of the opening angle for the secondary beam due to the effect of the emission of three elements in the line array.

The right graphic of Fig. 3.40 shows the evolution of both beams with the distance from 0.5 m until 4 m. The behaviour as a function of the distance is complex because we have the interaction and interferences between the three elements, furthermore if there might be some misalignment in the measurement axis. Anyway, for the secondary beam it was observed that the amplitude increases until 1.3 m and from that distance the beam amplitude started to decrease with distance. This behaviour seems to indicate the secondary beam signal interaction from each element emission was increasing up to 1.3 m. In order to better understand this study, the experimental results were compared to the simulation ones for both beams. The simulation was performed assuming a perfect alignment (0º) between the central emitter of the array and the receiver in all distances, and for misalignments of 3º and 6º at the receiver distance of 4 m being aligned at 2 m of distance and misalignment of 1.5º and 3º, respectively, at 1 m of distance. The left graphic of Fig. 3.43 shows the simulation and experimental results of the primary beam evolution with distance from 1 m to 4 m. The right graphic of Fig. 3.43 shows the same study for the secondary beam. Relative values between the secondary beam and the primary beam are shown in Fig. 3.44.

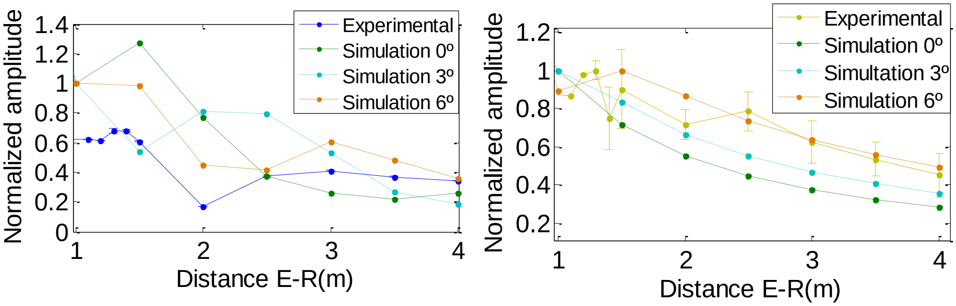

Fig. 3.43 Amplitude of the received signal as a function of the distance between emitter and receiver, for the experimental signal and the simulated for 0º, 3º and 6 º misalignment. The left graphic shows the results for the primary beam with the experimental results shown in blue. The right graphic shows the results for the secondary beam with the experimental results shown in yellow

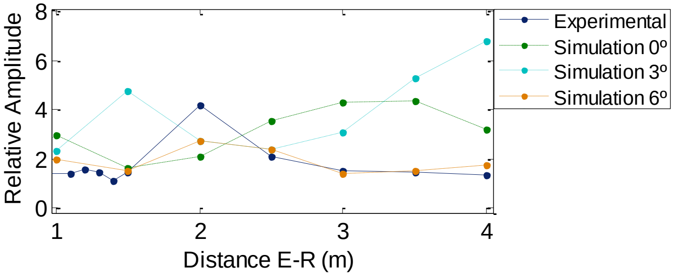

Fig. 3.44 Relative amplitude between secondary beam and primary beam as function of the distance between emitter and receiver for the experiment (in grey) and simulations with 0º, 3º and 6 º misalignment.

The simulations show that the misalignment corresponding to 6º fits rather well with the experimental data, proving that the signal interaction from the array emission could be influenced by the parametric signal formation of each element emission and a misalignment between the emitter and the receiver.

In order to study the parametric bipolar signal generation with the array emission over longer distances and to know what to expect from it, simulations for obtaining the estimated directionality have been performed. The simulations are performed following the same procedure as described in section 3.5.1. The study has been performed first with the array of three elements with a distance of 14 cm between them. Simulations of the propagated bipolar pulse signal (secondary beam) have been performed propagated to distances of 4 m to compare with the experimental measures, 100 m and 1 km, usual distances for the future in situ measures of neutrino acoustic detection calibration. The directivities obtained for each of these distances are shown in Fig. 3.45. The results show the directionality lobe is reduced as the distance between array and receiver is increased from 4 m to 100 m and 1 km of from a FWHM of 7º (σ=3.0º) to a FWHM of 4º (σ=1.7º). On the other hand, the average and the standard deviation of every three consecutive measures for both beams show that the opening angle of the experimental results are about 1º higher than the simulation at 4 m of distance from the array, though they have the same tendency and can be considered quite similar. For the simulation performed with the emission of the five element array with a distance of 14 cm between them, the directionality pattern obtained is shown in Fig. 3.46. The expected directionality at 1 km from the array emission of five elements is 3º FWHM (σ=1.3º).

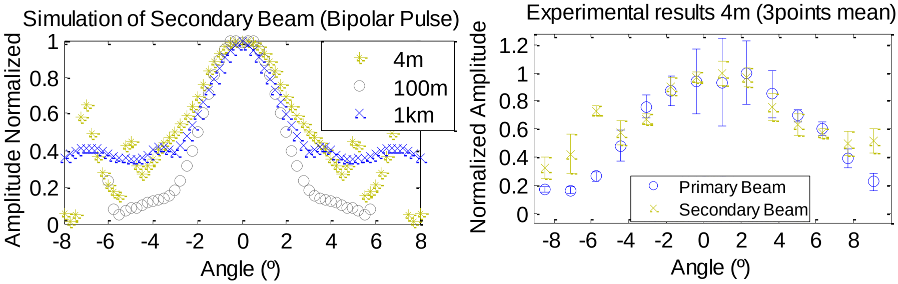

Fig. 3.45 Left: Directionality obtained through simulation at 4 m, 100 m and 1 km by propagating the emitted signal for the bipolar pulse generation with the three element array. Right: Experimental directionality obtained with the bipolar pulse generation with the array of three elements for both the primary and secondary beam by averaging every three measures in order to smooth the interference effect.

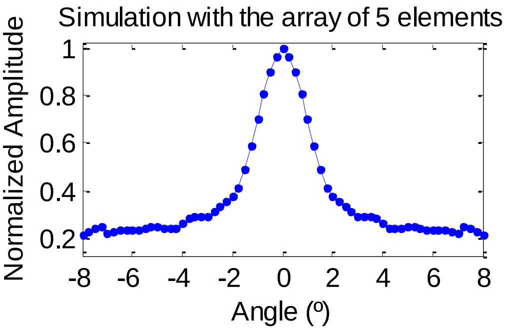

Fig. 3.46. Directionality obtained through simulations for a bipolar signal emitted with the five element array measured at a distance of 1 km.

Then, in order to estimate the acoustic pressure in the media at 1 km with the array emission for three and five elements, the pressure values of the propagated bipolar pulse signal are determined. The signal used for the simulation was the original received signal from the single element and emitted by each element of the array, obtaining the signal at 1 km formed from the contributions of the different sensors. Following the same procedure of section 3.5.1., the signal received at 20 cm (V[t]) is converted into spectral pressure components (P[f]), using the receiver sensitivity, and propagated until 1 km distance. The propagation was performed taking into account the loss from the medium absorption coefficient (for the conditions of the KM3NeT telescope) and the spherical divergence. The signal used for the simulation was the original received signal from the single element emission of the bipolar pulse with carrier signal at 400 kHz, shown in the right panel of Fig. 3.25 in blue colour. Fig 3.47

shows the bipolar signal pressure pulses obtained at 1 km from the simulation performed by summing the contributions of three sensors for the angles from the 0º to 4º. The results show that a pressure bipolar pulse of 1.1 mPa at 0º is obtained at 1km with the three element array fed with 200 Vpp (the potential used for Fig 3.25). Fig 3.48 shows the bipolar signal pressure pulse obtained at 1km for the five element array. A pressure bipolar pulse of 1.8 mPa at 0º is obtained at 1km from the array. With this, the needed input voltage of every array transducer for obtaining a good signal to noise ratio of the bipolar pulse at 1km can be estimated. Since a signal pressure of 20 mPa (rms) can be detected by the detector sensors under good sea conditions, an amplitude of 50 mPa (peak to peak) of pressure for the bipolar pulse can be considered as good representative case. In order to reach this value of 50 mPa, we need approximately 50 times more amplitude for the three element array that could be obtained with seven times more input voltage (~1400Vpp) since the secondary beam scales as the square of the feeding voltage. For the array system with five active elements, each transducer will need around five times more input voltage in order to obtain a bipolar pulse of around 50 mPa (~1000Vpp).

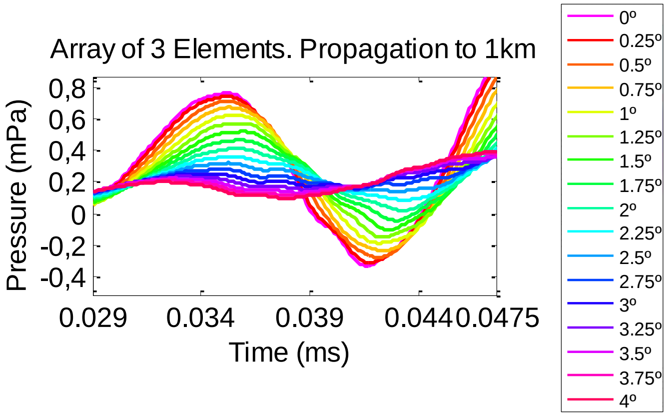

Fig. 3.47. Signal obtained through the simulation by propagating the emitted bipolar signal with the three element array to a distance of 1 km.

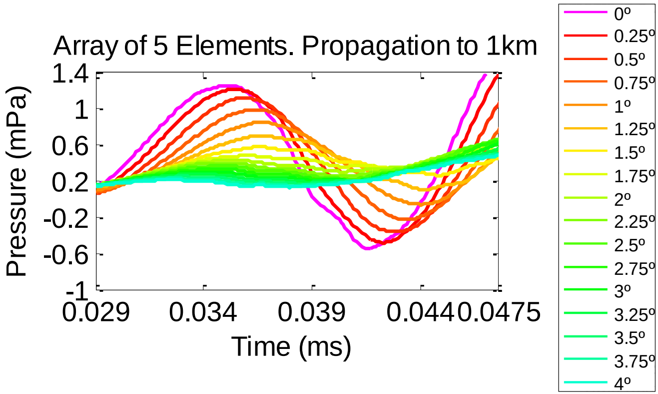

Fig. 3.48. Signal obtained through the simulation by propagating the emitted bipolar signal with the five element array to a distance of 1 km.

The conclusion of the parametric array characterization is that the results validated satisfactorily the parametric generation with the line-array emitting with three transducers for both signals the sine sweep and the bipolar pulse. The signal reproduction of the acoustic neutrino-like signals generation with the array by using the parametric technique was achieved. The parametric directionality studies with the array emission show favourable results since it was achieved almost one half reduction on the opening angle for the secondary beam angle in comparison to the single transducer. The results from the emission of the line-array with three emitters, showed a bipolar pulse generated with an opening angle FWHM of 7º (σ=3º) at 4 m. The simulations show that the opening angle is reduced at longer distances, estimating a FWHM of 4º (σ=1.7º). Since the opening angle of the acoustic neutrino signal at 1 km is ~ 1º, we could consider it as a good approximation for calibration of neutrino-like signals. The simulations performed for the array with five active elements show the directionality is reduced, estimating a FWHM of 3º (σ=1.3º).

As future work there is the array characterization for different number of elements and distances. With the five-element array, a more reduced opening angle in the directionality is expected to be obtained. Following this work, the next step will be completing the array-calibrator system by designing the electronics adapted to the array transducers in order to achieve the required power emission able to produce a detectable parametric signal. The electronics will incorporate the functionalities for communication, configuration, control, and amplification of the signal. The new electronics will be based on the same philosophy as the prototype electronic board designed previously (Llorens et al. 2012) (Adrian-Martínez et al. 2013), while adapted to the particularities of the new array transducer and application. The idea is to design independent boards for every single transducer to emit synchronously. This will allow to simplify the design and to provide more amplification to the emitted signal. Once the electronics will be designed, the complete array characterization, including the electronics, will be performed and tested over longer distances. Finally, the calibrator will be used either in sea campaigns for emissions from a vessel, or incorporated in the KM3NeT deep-sea neutrino telescope infrastructure, in order to performing the calibration tests of the acoustic telescope systems.

Summary and Conclusions

The thesis aimed and achieved two different goals related to the design and development of underwater acoustic emitters in the frame of the deep-sea KM3NeT neutrino telescope: an Acoustic Beacon (AB) as the emitter of the Acoustic Positioning System (APS) of KM3NeT and a transducer compact array for calibrating the acoustic neutrino detection technique.

The first topic of the thesis is focused on the design, development and characterization of the AB for the APS. Firstly, the *in situ* tests performed with the previous AB prototype were processed and analysed. Signal processing techniques with broadband ultrasound signals, such as advanced cross-correlation methods and filtering, were developed for optimizing the acoustic emission and position detection which concluded with relevant signal processing techniques useful for the APS data analysis. The results obtained also validated the beacon prototype operation and helped to define the improvements needed for the final AB version. Simulations of propagation of acoustic waves emitted with the prototype in the same conditions of the test were performed. They showed that they could be detected up to 2 km with good accuracy, which can be considered as a favourable reach for a large telescope such as KM3NeT. Some modifications in the design were performed for the final AB since the requirements and conditions imposed were slightly different. One of the conditions imposed was that the emitter should be a single unit containing the electronics and the transducer. This was achieved by using a robust vessel where the electronics are housed and connected to the transducer located in the external part of the vessel. Another point of improvement was related to the power emission which should be increased 10 dB in order to achieve a level of 180 dB re 1 µPa/Volt @ 1 m. The different studies made for the AB system and the work done for a precise laboratory test allowed us to design appropriately the AB. The test results assured the AB satisfying all the requirements for the APS of KM3NeT. The SPL obtained with the final AB goes from 174 dB to194 dB for the 20 kHz to 50 kHz frequency range, respectively. A total of eighteen units of the AB were designed and calibrated in cooperation with MSM SLL. They were provided to KM3NeT project in 2015. By the end of 2015, two units of the AB were integrated at ARCA detector and they were tested showing good agreement with the expected power emission of the acoustic waves and general functionality. However, the time synchronization functionality could not be tested due to a DAQ system problem at that time. Additionally, simulation studies for the optimal positions selection of ABs in the APS of both ARCA and ORCA detectors were performed. The final solution obtained with the study showed an equitable spreading of the sound pressure in the field of DU receivers. The KM3NeT project will use this study for the integration of the next ABs in the APS.

The second topic of the thesis has been dedicated to the design and development of a parametric transducer array able to mimic the acoustic signal generated by Ultra-High Energy (UHE) neutrino interaction in water. Firstly, a single transducer design was developed as unit element for the final array calibrator. The complete transducer was constituted by the piezo ceramic with a backing and heading material that increased the TVR 9 dB at resonance frequency in comparison with the bare ceramic. The single transducer designed had a resonance frequency at about 450 kHz with 169 dB re μPa/V at 1 m TVR and 10° (FWHM in amplitude) directionality. The parametric emission with the single transducer was validated with two different signals at low frequency-parametric, a sine sweep signal and a bipolar shape pulse signal. The non-linearity effect of the parametric signal was appreciated in the studies performed. The secondary beam showed higher amplitude evolution and narrower directionality pattern than in the linear range. Therefore, the signal reproduction of the acoustic neutrino-like signals generation by using the parametric technique was achieved. Then, in order to obtain a more energetic and directional bipolar pulse the array of transducers was designed. The selection of the optimal design configurations of the complete array system for three and five units was achieved through simulations. A flexible design which allowed to change the distance between emitters was developed to test different interesting array configurations and being able to optimise the distance experimentally. The line-array calibrator was characterized for one of the optimal configurations obtained in the previous simulation, the one based on three emitter transducers separated 14 cm. The last step for the array calibrator was characterizing it for the parametric generation. For this, measurements in a pool were made and compared with simulations. Although for the distances of the pool, the effect of the interference between the different transducers of the array were observed, by combining experiment and simulations we could understand and disentangle the effect and evidence the parametric signal generation for the low frequency of the sine sweep signal and the bipolar like-pulse signal. A similar directionality was obtained for both primary and secondary beams, reaching the goal of having a final directionality of a few degrees (FWHM in amplitude) for the bipolar pulse.

All this work and results have been presented in different ANTARES and KM3NeT collaboration meetings, and conferences (BIENAL, 2013; UIA, 2014; MARSS, 2014; VLVnT, 2015; ICRC, 2015; EUROREGIO, 2015) and published in refereed journals (Adrián-Martínez, S. et al., 2015; Viola, S. et al. 2015, Saldaña, M. et al. 2015, Saldaña, M. et al. 2016).

Bibliography

Aartsen et al., M.G., 2014. Observation of High-Energy Astrophysical Neutrinos in Three Years of IceCube Data. *Physical Review Letters*, 113.

Abdou et al., Y., 2012. Design and performance of the South Pole acoustic test setup. *Nucl. Instrum. Methods Phys. Res. Sect. A*, 683, pp.78–90.

Adrián-Martínez et al., S., 2013a. A versatile compact array calibrator for UHE neutrino acoustic detection. In *AIP (American Institute of Physics)*.

Adrián-Martínez et al., S., 2015. Acoustic signal detection through the cross-correlation method in experiments with different signal to noise ratio and reverberation conditions. *Lect. Notes Comput. Sci*, 8629, pp.66–79.

Adrián-Martínez, S. et al., 2013b. A compact acoustic calibrator for ultra-high energy neutrino detection. *Nuclear Instruments and Methods in Physics Research, Section A: Accelerators, Spectrometers, Detectors and Associated Equipment*, 725, pp.219–222.

Adrián-Martínez, S., 2015. Design and Development of an Acoustic Calibrator for Deep-Sea Neutrino Telescopes and First Search for Secluded Dark Matter with ANTARES. *PhD thesis.*

Adrian-Martinez, S. et al., 2016. Letter of intent for KM3NeT 2.0. *Phys. G: Nucl. Part. Phys*, 43.

Ageron et al., M., 2008. KM3NeT: Conceptual Design for a Deep Sea Research Infrastructure Incorporating a Very Large Volume Neutrino Telescope in the Mediterranean Sea.

Ageron, M. et al., 2011. ANTARES: The first undersea neutrino telescope. *Nuclear Instruments and Methods in Physics Research A*, 656, pp.11–38.

Aguilar, J.., 2011. AMADEUS – The Acoustic Neutrino Detection Test System of the ANTARES Deep-Sea Neutrino. *Nuclear Instruments and Methods in Physics Research Section A*, 626-627, pp.128–143.

Ainslie, M.A. & McColm, J.G., 1998. A simplified formula for viscous and chemical absorption in seawater. In *Journal of the Acoustical Society of America*. pp. 1671–1672.

Amore, I., 2009. First results from the NEMO Phase-1 experiment. *Nucl. Instr. and Meth. in Phys. Res. A*, 602, pp.68–71.

An, F.P. et al., 2012. Observation of electron-antineutrino disappearance at Daya Bay. *Phys. Rev. Lett.*, 108.

Andrés, E. et al., 2001. Observation of high-energy neutrinos using Cherenkov detectors embedded deep in Antarctic ice. *Nature*, 410, pp.441–443.

Ardid, M. et al., 2012. Acoustic transmitters for underwater neutrino telescopes. *Sensors*, 12(4), pp.4113–4132.

Ardid, M., 2009. An Underwater Network of Sensors for Neutrino Astronomy and Deep-Sea Research. *Ad Hoc & Sensor Wireless Networks*, 8, pp.21–34.

Ardid, M., 2009. Calibration in acoustic detection of neutrinos. *Nucl. Instrum. Methods Phys. Res.*, 604, pp.S203–S207.

Ardid, M. et al., 2007. Calibration of sensors for acoustic detection of neutrinos. *Journal of Physics: Conference Series*, 81.

Askaryan, G.., 1957. Hydrodynamical emission of tracks of ionising particles in stable liquids. *Sov. J. At. Energy*, 3, pp.921–923.

Aynutdinov, V. et al., 2008. The Baikal neutrino experiment: Status, selected physics results, and perspectives. *Nucl. Instrum. Methods Phys. Res.*, 588, pp.99–106.

Belolaptikov, I.A. et al., 1997. The Baikal Experiment: Status Report. , 95, pp.1–7.

Bevan, S. et al., 2007. Simulation of Ultra High Energy Neutrino Interactions in Ice and Water. *Cross Sections*, pp.366–379.

Bevan, S. et al., 2009. Study of the acoustic signature of UHE neutrino interactions in water and ice. *Nuclear Instruments and Methods in Physics Research, Section A: Accelerators, Spectrometers, Detectors and Associated Equipment*, 607(2), pp.398–411.

Beyer, R.T., 1975. Nonlinear Acoustics, *U S Government Printing Office.*

Bosetti, P.., 1988. DUMAND II Proposal.

Bou-Cabo, M., Ardid, M. & Felis, I., 2013. Acoustic studies for alpha background rejection in dark matter bubble chamber detectors. *AIP Conference Proceedings*, 1549, pp.142–147.

Chiarusi, T., 2014. Status and first results of the NEMO Phase-2 tower. *Journal of Instrumentation (JINST)*, 9.

Close, F., 2010. Neutrino, *Oxford University Press.*

Danaher et al., S., 2007. First Data from ACoRNE and Signal Processing Techniques. *Journal of Physics: Conference Series*, 81, pp.1–8.

Francois, R.E. & Garrison, G.R., 1982. Sound absorption based on ocean measurements. Part I: Pure water and magnesium sulphate contributions. Part II: Boric acid contribution and equation for total absorption. *Journal of the Acoustical Society of AmericaAcoustical Society of America*, 72, pp.896–907, 1879–1890.

Graf, K., 2013. Acoustic neutrino detection in sea water: Technical aspects. *AIP Conference Proceedings*, 169(1).

Hodges, R.P., 2010. Underwater acoustics: analysis, design and performance of sonar, *John Wiley & Sons, Ltd.*

Ho-Kim, Q. & Pham, X.-Y., 1998. Elementary Particles and Their Interactions: Concepts and Phenomena, *Springer.*

Icecube Collaboration, 2013. Evidence for high-energy extraterrestrial neutrinos at the IceCube detector. *Science*, 342.

International Marine Contractors Association (IMCA), 2009. Deep Water Acoustic Positioning. *IMCA M 200, IMCA S 013*. Available at: www.imca-int.com.

Kinsler, L.R. et al, 1999. Fundamentals of Acoustics. *4th editio., John Wiley & Sons,Inc.*

KM3NeT Collaboration, 2011. KM3NeT: Technical Design Report for a Deep-Sea Research Infrastructure in the Mediterranean Sea Incorporating a Very Large Volume Neutrino Telescope.

KM3NeT Project Website, www.km3net.org.

Kossof, G., 1966. The effects of backing and matching on the performance of piezoelectric ceramic transducers. *IEEE Trans. Sonics Ultrason*, 13, pp.20–30.

Kuttruff, H., 2006. Acoustics an Introduction, *Taylor & Francis.*

Larosa, G., 2012. Design and Development of an acoustic positioning system for a cubic kilometre underwater neutrino telescope. *PhD thesis.*

Larosa, G. & Ardid, M., 2013. Acoustic position calibration of the KM3NeT neutrino telescope. *Nucl. Instr. and Meth. A*, 725, pp.215–218.

Larosa, G., Ardid, M. & Llorens, C.D., 2012. Development of an acoustic transceiver for the KM3NeT positioning system. *Instrumentation and Methods for Astrophysics*, pp.1–4.

Learned, J.G., 1979. Acoustic radiation by charged atomic particles in liquids: An analysis. *Phys.Rev*, D19, p.3293.

Li, H. et al., 2012. Design parameters of a miniaturized piezoelectric underwater acoustic transmitter. *Sensors (Switzerland)*, 12(7), pp.9098–9109.

Lieberman, L.N., 1948. The Origin of Sound Absorption in Water and in Sea Water. *The Journal of the Acoustical Society of America*, 20(6)(868-873).

Linkwitz Lab Website, http://www.linkwitzlab.com/models.htm.

Llorens, C.D. et al., 2012. The sound emission board of the KM3NeT acoustic positioning system. *Journal of Instrumentation, 7(01)*

Lurton, X., 2010. An Introduction to Underwater Acoustics: Principles and

Applications XXXVI., *Springer.*

Migneco, E., 2006. Status of NEMO. *Nucl. Instr. and Meth. A*, 567, pp.444–451.

Moffett, M.B.; Mello, P., 1979. Parametric acoustic sources of transient signals. *J. Acoust. Soc. Am*, 66, pp.1182–1187.

Moisey Alexandrovich, M., 1960. High-energy Neutrino Physics.

Neff et al, M., 2013. Simulation Chain for Acoustic Ultra-high Energy Neutrino Detectors. *AIP Conf.Proc*, 204.

NESTOR Collaboration, 2006. NESTOR Deep Sea Neutrino Telescope: Deployment and results. *Elsevier*, 151(1), pp.279–286.

Niess, V. & Bertin, V., 2006. Underwater acoustic detection of ultrahigh energy neutrinos. *Astropart.Phys.*, 26(243-256).

Ooppakaew, W., 2012. Advanced Signal Processing Techniques for Underwater Acoustic Transmission using Steerable Transducer Arrays. *PhD thesis.*

Picão, J. et al., 2010. USBL positioning system - Implementation and tests at sea. *9th Portuguese Conference on Automatic Control CONTROLO'2010*.

Reines, F. & L.Cowan, C., 1956. The Neutrino Nature. *Nature*, 178(446).

Riccobene, G. et al., 2005. Online monitoring of underwater acoustic background at 2000 m depth. *29th International Cosmic Ray Conference Pune*, 9, pp.287–290.

Richardt, C., Anton, G. & Graf, K., 2014. Reconstruction methods for acoustic particle detection in the deep sea using clusters of hydrophones. *AStroparticle Physics, Elsevier*, 31(1), pp.19–23.

Rossi, B., 1964. Cosmic Rays, *New York: Mc Graw-Hill.*

Saldaña et al., M., 2015. Ultrasonic transmitter for positioning of the large underwater neutrino telescope KM3NeT . *Physics Procedia*, 63, pp.195–200. Available at: http://dx.doi.org/10.1016/j.phpro.2015.03.032.

Saldaña, M. et al., 2016. Transducer Development and Characterization for Underwater Acoustic Neutrino Detection Calibration. *Sensors*, 16(8).

Saldaña, M. et al., 2011. Acoustic Array Calibration and Signal Processing for UHE Neutrinos Generation. *Mobile Ad-Hoc and Sensor Systems, IEEE International Conference on*, 00, pp.910–915.

Sapienza, P., 2006. Status of the NEMO Project.

Seon-Hee, S. et al., 2014. New Results from RENO. In *Proceedings of XVth International Workshop on Neutrino Telescopes*. Physics.

Sherman, C.H. & Butler, J.L., 2007. Transducers and Arrays for Underwater Sound, *Springer.*

Simeone, F., 2008. Detection of underwater acoustic signals induced by ultra-high energy neutrinos interactions. *PhD thesis.*

SLAC National Accelerator Laboratory website, SLAC National Accelerator Laboratory website. Available at: http://www2.slac.stanford.edu/vvc/theory/fundamental.html.

Sulak, L.., 1978. Studies of a Detector to Test for Baryon Stability to a Lifetime of 1033 Years. In *Proceedings of the Seminar on Proton Stability,*.

Thompson, L.F. & Perkin, J.D., 2008. The ACORNE project. *J. Phys. Conf. Ser.*, 136.

Tomczak, A., 2011. Modern Methods of Underwater Positioning Applied in Subsea Mining. , pp.381–394.

Uchino, K., 2003. Introduction to Piezoelectric Actuators and Transducers. *International Conference on Intelligent Materials (5th) (Smart Systems & Nanotechnology)*, p.40.

Vandenbroucke, J. et al., 2005. Experimental study of acoustic ultra-high-energy neutrino detection. *Astrophys. J.*, 621, pp.301–312.

Viola, S. et al., 2015. Acoustic positioning system for KM3NeT. *Proceedings of Science ICRC2015*, 1169.

Viola, S. et al., 2013. NEMO-SMO acoustic array: A deep-sea test of a novel acoustic positioning system for a km 3-scale underwater neutrino telescope. *Nucl. Instrum. Methods Phys. Res.*, 725, pp.207–210.

Wenz, G.M., 1962. Acoustic ambient noise in the ocean: spectra and sources. *J. Acoust. Soc. Amer*, 34, pp.1936–56.

Acknowledgements

Firstly, I would like to express my sincere gratitude to Miquel Ardid, who is my principal supervisor, for giving me the opportunity to develop the thesis, for his excellent academic support and guidance during all the thesis process and for helped me to grow in knowledge and perspective. I especially thank my second supervision Joan Martínez-Mora, for his support and guidance during the thesis and for his academic and personal advices.

I would like to thank to my thesis team partner Ivan Felis for his presence and friendship, for his knowledge, and for his academic and moral support during all these years. It has been a pleasure and a present to share part of this phase of life with him.

And also I want to thanks all the people from the physics department of the EPSG, specially, to the colleagues from the room D-203 for sharing the work time together, and all the good moments shared, also at the cafeteria during the lunch time.

My special thanks to Patricia Ordóñez, who is one of my partners of life and who I call my ‘guru’. She has always been there for listening, helping and supporting me, specially, in a personal level, and also, academically. Thanks for giving me love and strength when I most needed, I feel eternally grateful for that my friend. In the same sense, I thanks Nuria and Alvarico, for giving me also their support, sweetness and love during all this phase. And to all the friends who were and are close to me, as part of my life too.

I would like to express my gratitude to my family, my parents, my brother and my cousins, for taking care of me, for supporting me, for being always there, for growing together.

Love you all.

I feel very grateful for what this life phase has giving me, it has driven me to grow very much, to understand more and expand in love.

My special thanks also go to the ANTARES and KM3NeT collaboration, especially to the acoustics and calibration team.

I would like to express my gratitude toward the UPV for giving me the opportunity and support throughout my PhD course.

And finally, my acknowledge to the financial support of Plan Estatal de Investigación, ref. FPA2015-65150-C3-2-P (MINECO/FEDER), and Consolider MultiDark CSD2009-00064 (MINECO) and of the Generalitat Valenciana, Grants ACOMP/2015/175 and PrometeoII/2014/079.

Table List

Figure List

Acronyms

AB	Acoustic Beacons
ACORNE	Acoustic Cosmic Ray Neutrino Experiment
ADC	Analog to Digital Converter
AMADEUS	ANTARES Modules for the Acoustic DEtection Under the Sea
AMANDA	Antarctic Muon And Neutrino Detector Array
ANTARES	Astronomy with a Neutrino Telescope and Abyss environmental
APS	Acoustic Positioning System
ARCA	Astroparticle Research with Cosmics in the Abyss
AUV	Autonomous Underwater Vehicles
BPC	Beam Pattern Correction
CB	Calibration unit Base
CLB	Central Logic Board
CRLB	Cramer Rao Lower Bound
CTD	Conductivity Temperature and Depth probes
CU	Calibration Units
DAR	Digital Acoustic Receiver
DIT	Digital Interface Transmitter
DOM	Digital Optical Modules
DU	Detection Unit
DUMAND	Deep Underwater Muon and Neutrino Detection
FFR	Free Flooded Ring
FPGA	Field Programmable Gate Array
FWHM	Full Width Half Maximum
HTI	High Tech, Inc
IGIC	Instituto de Investigación para la Gestión Integrada de Zonas Costeras
IU	Instrumentation Line
JB	Junction Box
KM3NET	Cubic Kilometre Neutrino Telescope
LBL	Long Base Line
LVDS	Low-Voltage differential signaling
MLS	Maximum Length Sequence
MRA	Maximum Response Axis
MSM	Mediterráneo Señales Marítimas
NEMO	Neutrino Ettore Majorana Observatory
NESTOR	Neutrino Extended Submarine Telescope with Oceanographic Research
OM	Optical Modules
ORCA	Oscillation Research with Cosmics in the Abyss
PMT	Photomultiplier Tubes
PSD	Position Sensitive Detector
PWM	Pulse Width Modulation

RAMSES	Radioprotection et Mesures Environnementales RESearch
ROV	Remotely Operated Underwater Vehicle
ROV	Remotely Operated Vehicles
RVR	Receiving Voltage Response
SAUND	Study of Acoustic Ultra-high energy Neutrino Detection
SEB	Sound Emission Board
SPATS	South Pole Acoustic Test Setup
SVP	Sound Velocity Profile
TDoA	Time Difference of Arrival
ToA	Time of Arrival
ToF	Time of Flight
TVR	Transmitting Voltage Response
UHE	Ultra High Energy
UPV	Universitat Politècnica de València
USBL	Ultra-short Baseline